SOLAR LIGHT HARVESTING BY ZnO BASED MATERIALS

A THESIS SUBMITTED TO THE

SAVITRIBAI PHULE PUNE UNIVERSITY

FOR THE DEGREE OF

DOCTOR OF PHILOSOPHY

IN CHEMISTRY

BY

S. RAJA AMBAL

(RESEARCH GUIDE)

Dr. CHINNAKONDA S. GOPINATH

CATALYSIS DIVISION

CSIR-NATIONAL CHEMICAL LABORATORY

PUNE 411 008

INDIA

MARCH 2015

DECLARATION BY RESEARCH SCHOLAR

I hereby declare that the thesis "**Solar Light Harvesting by ZnO based Materials**" submitted for the degree of Doctor of Philosophy to the Savitribai Phule Pune University, has been carried out by me at the Catalysis and Inorganic Chemistry Division, National Chemical Laboratory, Pune – 411008, India, under the supervision of Dr. Chinnakonda S. Gopinath. Such materials as obtained from other sources have been duly acknowledged in the thesis.

I declare that the present work or any part thereof has not been submitted to any other University for the award of any other degree or diploma.

S. Raja Ambal

March 2015

Catalysis and Inorganic Chemistry Division,
National Chemical Laboratory,
Pune 411 008,
Maharashtra,
India.

हीरक जयन्ती वर्ष 2009-10

राष्ट्रीय रासायनिक प्रयोगशाला
(वैज्ञानिक तथा औद्योगिक अनुसंधान परिषद)
डॉ. होमी भाभा मार्ग, पुणे - 411 008. भारत

NATIONAL CHEMICAL LABORATORY
(Council of Scientific & Industrial Research)
Dr. Homi Bhabha Road, Pune - 411 008. India.

CERTIFICATE BY RESEARCH GUIDE

This is to certify that the work incorporated in the thesis entitled, "**Solar Light Harvesting by ZnO based Materials**" submitted by **S. Raja Ambal**, for the Degree of Doctor of Philosophy, was carried out by the candidate under my supervision in the Catalysis and Inorganic Chemistry Division, National Chemical Laboratory, Pune – 411 008, India. Such materials as obtained from other sources have been duly acknowledged in the thesis. To the best of my knowledge, the present work or any part thereof has not been submitted to any other University for the award of any other degree or diploma.

C. S. Gopinath

Dr. C. S. Gopinath
(Research Supervisor)

March 2015,
Catalysis and Inorganic Chemistry Division,
National Chemical Laboratory,
Pune - 411 008,
Maharashtra,
India.

Communication Channels

☎
NCL Level DID : 2590
NCL Board No. : +91-20-25902000
EPABX : +91-20-25893300
+91-20-25893400

FAX
Director's Office : +91-20-25902601
COA's Office : +91-20-25902660
COS&P's Office : +91-20-25902664

WEBSITE
www.ncl-india.org

DEDICATED TO.....

MY PARENTS, KARTHICK AND (LIFE-PARTNER) SENTHILKUMAR

Acknowledgement

To begin with, I dedicate my soulful thanks to almighty and Girisen, late grand-father, for blessing me the higher level of education in midst of chaos of life.

I take this fruitful opportunity to revere my supervisor Dr. Chinnakonda. S. Gopinath for guiding my research work. I must remember his generosity and support in helping me to get through tough phases of failures.

I thank CSIR-NCL for granting me research fellowship and Dr. Sourav Pal, Director of NCL, for bringing splendid infrastructure for peaceful stay. I devote my thanks to Dr. A. P. singh, head of the catalysis division to impart necessary facilities. I take immense pleasure to salute Dr. Srinivas, Dr. Satyanarayana, and Dr. C.P. Vinod for useful scientific discussions. I devote my respect to Dr. Sreekumar, Dr. M. Jayakannan and Dr. K. Krishnamoorthy for granting me instrument facility and my research collaborator, Dr. D. Bhattacharyya for introducing me EXAFS analytical research. I render my sincere thanks to Dr. S. K. Asha for her encouragement bringing me sprits.

I thank all my labmates Dr. Maitri Mapa, Dr. Nagarajan, Dr. Thushara, Dr. Edwin, Dr. K. Sivaranjani, Dr. Ashwin and his wife Dr. Bhavna, Dr. Anand, Kanak, Devaraj, Sanjay, Anjani, Kshirodra, Pradnya, Ruchi, Manoj Kumar, Prabhakar and Kavya for earnest help throughout my Ph. D phase. It is pleasure to mention Anuj, Bhogeshwar, Joby, Unnikrishnan, Devadutt, Mehajabeen, Chitra and Sagar for the cheerful environment in the lab work place.

I would like to solicit my special thanks to my wonderful friends Sujit Sarkar *(Suji)*, Sandip, Anand Raj, Manik, Prajitha, Chinmay, Saibal, Shekar, Kaushal, Nagesh, Sandeep, Sarabjoth, Aarthy, Monalisa and her family, Periyasamy, Ashok, Manikandan, RamSundar, Arul Kashmir, Manisha, Manik, Raja Perumal, and Bhagyashree for their care and affection showering memorable evergreen moments.

I am rendering my deepest gratitude to my parents who endured struggles to bring up me in life. My cutest brother, Karthick who shares beautiful days, is the pleasant gift from god.

My most indebted thanks dedicated to my *life partner*, SenthilKumar *(M.Sc Classmate),* who motivated me to do Ph.D. His constant pillar support and academic assistance drive me to accomplish Ph.D successfully. His company with utmost care, unconditional love and ever-springing affection had built self- esteem and confidence within me to tackle the realities and challenges in every walk of my life.

Raja Ambal. S

Table of contents

Chapter 1: Introduction

Chapter 2: Experimental Methods

ABBREVATIONS

AAS	Atomic Absorption Spectroscopy
BE	Binding Energy
BET	Braunauer-Emmett-Teller
CB	Conduction Band
CVD	Chemical Vapor Deposition
DTA	Differential Thermal Analysis
ECR	Electron Cyclotron Resonance
EDAX	Energy Dispersive Analysis of X-rays
EXAFS	Extended X-ray Absorption fine structure
GC	Gas Chromatography
HR-TEM	High Resolution Transmission Electron Microscopy
ICP	Inductive Coupled Plasma Spectroscopy
IR	Infra-red
LRS	Laser Raman Spectroscopy
LSV	Linear Sweep Voltammetry
MBE	Molecular-Beam Epitaxy
MOCVD	Metal Organic Chemical Vapour Deposition
PLD	Pulsed Laser Deposition
PL	Photoluminescence
PVD	Physical Vapor Deposition
SAED	Selective Area (electron) Diffraction
SEM	Scanning Electron Microscopy

SIMS	Secondary Ion Mass Spectrometry
SCM	Solution Combustion Method
TCD	Thermal Current Detector
TG	Thermo Gravimetry
UV-Visible	Ultra Violet- Visible
VB	Valence Band
WSR	Water Splitting Reaction
XRD	X-ray Diffraction
XPS	X-ray Photoelectron Spectroscopy

Introduction

1. Introduction

1.1 General Background

Catalysis plays a vital role in day-to-day life since the nature bestowed the phenomenon of enzyme catalysis. Enzymes take part in catalyzing the infinite number of reactions for the physiological functioning for life. In the year of 1835, Berzilius was the first scientist one who elaborated the concept of catalysis and coined the term 'Catalysis'. He described the catalysis as "A power of substances that enables to awaken the affinities, which are asleep at reaction temperature by their mere presence and not by their own affinity". The above definition demonstrates the fact that the use of catalyst speed up the reaction time along with increment in the yield of the product. Ostwald had experimentally proven that kinetics of the reaction is only changed by the use of catalyst without any change in the free energy of the reactant and products and his contribution was awarded with Nobel Prize in 1909.

The catalyst does not undergo any chemical change or in composition during the course of the reaction. It involves in altering the pathway of the reaction by decreasing the value of threshold activation energy. The principle on catalysis is schematically represented in Figure 1.

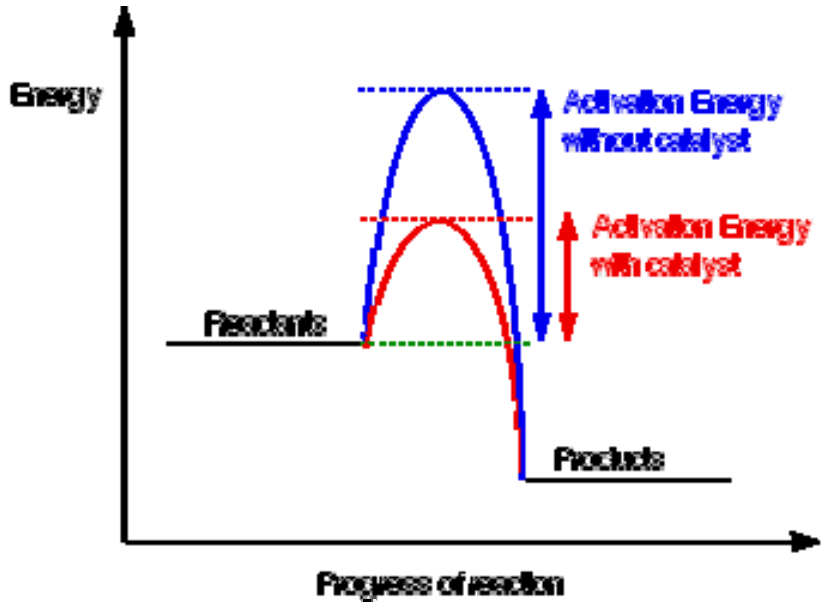

Figure 1. Schematic representation of the role of catalyst in kinetics

The free energy of the reactants as well as products is not changed in the presence of the catalyst. The formation of the activated transient state complex between the catalyst and the reactants is advantageous in lowering the activation energy. Thereby the reaction is accelerated in short time scale and also the turn over number of the reaction is also increased.
Broadly, catalysis can be divided into two categories based on the phases of the reaction.

i. Homogeneous Catalysis

ii. Heterogeneous Catalysis

i. Homogeneous Catalysis

When the catalyst is in same phase with that of reactants and products, the type of catalysis is homogenous catalysis. The attractive features of this type of catalysis are high selectivity, conversion, and yield at ambient reaction conditions. The poor recovery and the use of noble metal catalysts remain as disadvantages. This is in practice for the production of fine chemicals, exotic products and coupling reactions.

ii. Heterogeneous Catalysis

When the physical state of catalyst is in different phase from that of reactants and products, the type of catalysis is called as heterogeneous catalysis. Generally, this type of catalysis demands harsh conditions of temperature and pressure. The easy recovery of the catalyst and recyclability for several times are the salient features of this type of catalysis. It is highly practiced in industries for the production of petroleum products, large scale of organic chemicals, biomass conversion and automobile industries. Heterogeneous semiconductor photocatalysis for hydrogen evolution from water using solar energy attracts high research interest in the last few decades. This protocol is viable to conduct at ambient conditions rather than harsh treatments as required in other heterogeneous catalysis protocols.

1.2 Solar Harvesting – Need of the Hour

Depletion of conventional energy resources, particularly petroleum oil, increases the energy demand at global level. Hubert demonstrated the availability of conventional resources over the period of time.[1] It is observed from the curve that the energy sources start to deplete in this decade and the condition will become worse in the near future. Therefore, it is high time to search alternate energy resources. Although shale gas is available aplenty in the recent times and hence the oil price is tumbling down, in our opinion, sustainable and renewable energy sources will be the permanent solutions. Solar energy is the naturally available energy on everyday basis without the need of human effort. Besides the fact of availability, the power of solar energy also adds value to its potentiality. The solar energy that reaches the earth one day is equivalent to the chemical energy that can be obtained from 800 trillion barrels of oil. Since the global requirement of petroleum energy annually is only 100 barrels of oil. Therefore 0.01% recovery of solar energy is sufficient to meet our global demand.[2] Solar energy is the diffuse form of energy that covers widespread area on the surface of the earth. Therefore, it is feasible to avail the solar energy in most parts of the world. The solar spectrum spans over entire visible region and the regime of 525 nm wavelength is in greater proportion among other wavelengths. This regime of solar spectrum is useful for performing photosynthesis in plants that supply our daily food. The natural architecture of the leaf structure is constructed in such a way to absorb and to allow the penetration of the sunlight. The function of plants in light harvesting can serve as model for the recovery of solar energy as an alternate energy resource. The essentiality of solar light harvesting is schematically depicted in **Figure 2**. Using semiconductor materials, hydrogen generation from pure water under sunlight is often referred as “Artificial Photosynthesis”.

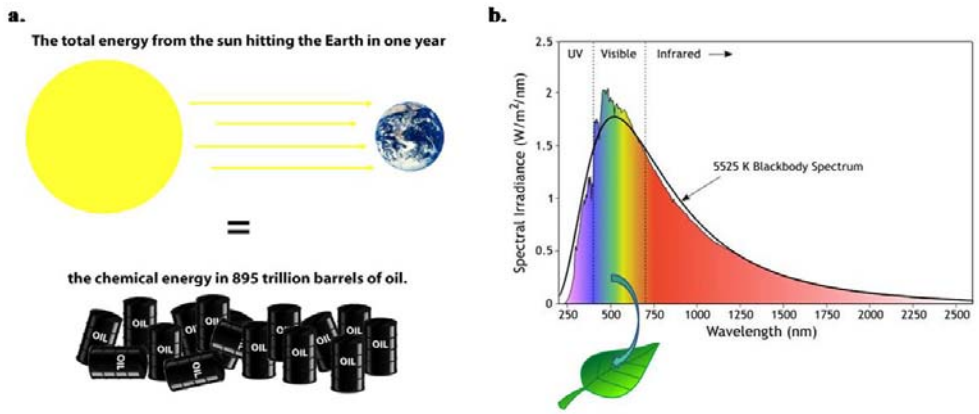

Figure 2. Abundance of solar energy (left) and solar spectrum (right): the useful visible light regime for photosynthesis by leaf.

1.3. Heterogeneous Semiconductor Photocatalysis

Photocatalysis is acclaimed as one of the viable routes to harvest sunlight and to convert into useful forms of chemical energy. The necessary features that are expected in a photocatalyst are the following: a. photofunctionality, b. Catalytic potentiality and c. Stability. The feature of photofunctionality, that is absorption of sunlight, is the highlight expected in a photocatalyst. The absorbed light energy is utilized for activating the reactants to form the desired products. In that aspect, the catalytic potentiality of the reactants is of high importance. The photocatalysts acts as platform for the surface adsorption of the reactants and the absorbed light energy is transferred to the reactants. Under light irradiation for prolonged period of time, the photocatalyst has to remain stable or otherwise leaching of the structural constituents of the catalyst seriously hinders the sustainability of the catalytic process. The photocatalyst that has possessed all the three features would be highly desirable for various photocatalytic reactions.

All the three classes of materials namely metals, semiconductors and insulators are explored as photocatalyst for different purposes. Among all the three classes, semiconductors materials are suitable to perform both reduction and oxidation reactions at same time and in addition relatively lesser energy is needed to excite the band gap of the semiconductor. Therefore semiconductors are used as main photocatalyst while metals serve

as cocatalyst to assist/increase the activity of the main photocatalyst. Since the insulators demand extremely high energy (or $\lambda \leq 350$ nm) light radiation for the purpose of activation, that class is relatively less explored. In some cases, the insulators are used as protective coats for metals to avoid leaching and also as supports to increase the dispersion of semiconductor nanostructures. The schematic representation of the experimental process of heterogeneous semiconductor photo catalysis is given in Figure 3a. The powder semiconductor material is suspended in the reactants containing solution and it is kept under constant stirring and direct light irradiation for required period of time. After the completion of required time, the products are collected from the reactor system and analyzed. This process is highly acclaimed for its viability and simplicity. The stepwise description on the mechanistic principles of semiconductor photocatalysis is described as follows. **Figure 3b** furnishes the schematic representation on the mechanism of photocatalysis.

Step 1: The photon of having energy greater than the band gap of the semiconductor material is absorbed by the material. The reduction potential of the photogenerated electron depends on the potential of the conduction band (CB) minimum (CB_{Min}) and the oxidation potential of the hole depends on the potential of the upper edge of the valence band (VB) known as VB_{Max}. The absorbed photon is utilized in exciting the electron from the VB to the CB of the semiconductor and thus a hole is created in the VB.

Step 2: The photogenerated charge carriers are diffused from the bulk of the photocatalyst to the surface active site of the catalyst.

Step 3: The reactants are adsorbed on the surface of the catalyst. Depending upon the potentials, the photogenerated charge carriers that are transported from the bulk to the surface involve in the redox reactions of the reactants and form the respective products. The cocatalysts are also loaded on the surface of the catalyst that provides additional active sites for a particular photocatalytic reaction. The cocatalysts act as sink for the photogenerated charge carriers and further reaction either i.e. reduction or oxidation are takes

place based on the nature of the cocatalyst. Finally, the products are desorbed from the surface of the catalyst.

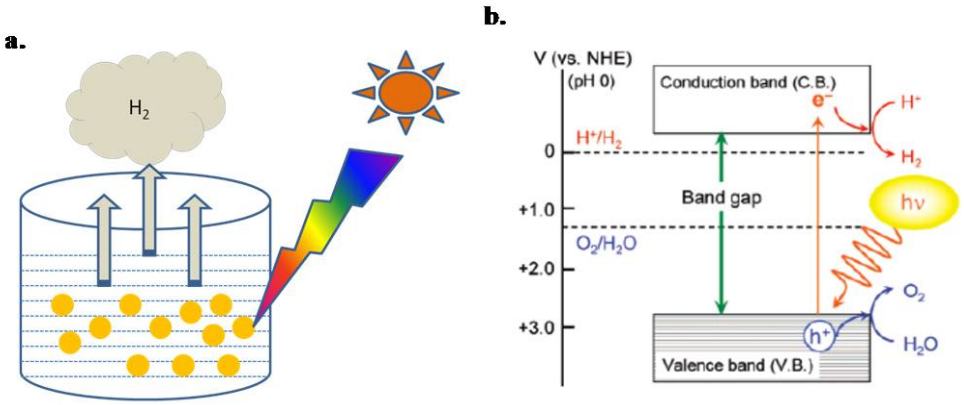

Figure 3. a. Schematic representation of heterogeneous semiconductor photocatalysis and b. Band structure correlation of photocatalysis.

Aforementioned mechanistic aspects are schematically represented in the semiconductor particle and accompanying competing reactions are also indicated in **figure 3.** The recombination of photogenerated charge carriers is the notorious competing reaction that decreases the population of free charge carriers and in turn reduces yield of the reaction. The diffusion of the charge carriers throughout the photocatalyst is another challenge. The structure of the photocatalyst has to be constructed in such a way to promote the mobility of photogenerated charge carriers. The lifetime of the charge carriers also play a deciding factor in the yield of the reaction. When the lifetime of the charge carriers is higher, it increases the probability for the availability to the reactants. On the whole, light harvesting and charge carrier utilization are the two principle determining factors in the heterogeneous semiconductor photocatalysis. There are four major ways of applying photocatalysis in the conversion of solar energy into other useful energy forms. The ways are listed along with respective brief outline on the processes as follows.

a. Degradation of Pollutants into Less Toxic Forms

Organic dyes, waste chemicals released from industries are highly toxic water pollutants and they are essentially to be eradicated. Simply dumping the waste chemicals cannot be a solution and it should be converted into

harmless products. Degrading the pollutants into least toxic forms can alone be a suitable remedy. The photogenerated charge carriers in the photocatalyst involve in the oxidation and reduction of the dye products into water and carbon dioxide.

b. Organic Conversions

Most of the organic chemicals serve as raw materials and intermediates in various drugs, cosmetic products and value added chemicals. Traditional organic synthetic procedures are laborious and also at small scale of production. The photocatalytic method of synthesis can provide ample opportunities in large scale of simple synthesis of organic chemicals thereby abundant basic chemicals are converted into value added chemicals.

c. Hydrogen Generation from Water

Hydrogen is an attractive fuel for fuel cells. There are many research methodologies such as steam reforming of alcohols, electrolysis of water has been practiced for the generation of hydrogen. Comparing to other methods, photocatalytic hydrogen generation is more viable method because of the factors of cheap reactant (water) source and ambient reaction conditions. Another advantage is that chemical nature of the catalyst will remain stable. However, water splitting has thermodynamical constraints with uphill free energy of $\Delta G = 237$ KJ/mol.[3] Therefore it is necessary to approach the reaction by changing the kinetics. The adsorption of water on the catalyst lead to formation of hydroxyl radical that is further undergoes into bond breaking of O-H bond. Water oxidation is the rate determining step in the overall water splitting.

d. Photocurrent Generation

Electrical energy is the utmost need in a standard lifestyle. Conventionally electrical energy is generated using coal, oil, river sources and nuclear energy. At present the conventional routes are not cost effective and nuclear energy source had imposed a threat to humankind. Using photocatalysts, conversion of solar energy into electrical energy is the commendable approach. The photocatalyst material is used as working electrode in the

conventional electrochemical set up. The absorbed photon is converted into charge carriers that further involve in the current generation. The current generation is possible only under light irradiation of the photocatalyst. There are different chemical classes of semiconductors materials such as metal oxides, metal nitrides, metal sulphides, metal carbides and metal phosphates etc. Among all the classes of semiconductors, metal oxides attract great research interest in the field of photocatalysis.[4-7]

1.4 Metal Oxides Based Photocatalysts

Most of the metals invariably show highest affinity for oxygen due to the fact of high electronegativity of oxygen. The metal oxides have pronounced catalytic potentiality and chemical stability over high temperatures for long hours. The oxide surface exhibits high affinity towards the adsorption of the reactants. The less coordinated surface oxygen atoms on the surface of the metal oxide is hydrophilic in nature that helps in anchoring of water molecules, alcohols, acids via O-H bonds. Anchoring of the reactants on the surface of the catalyst assists in bringing the reactants in close vicinity to the active sites of the catalyst. The photogenerated charge carriers that are diffused from the bulk to the surface can easily involve into reactions with the anchored reactants. If the chances of adsorption are slim, then the carriers will be quenched or recombined on the surface of the catalyst. The factor of chemical stability will help in eliminating the chances of metal leaching under prolonged reaction hours. The metal oxides are inherently having oxygen vacancies in the lattice structure that induces polarity in the material. This is advantageous for interacting with structure directing agents to form diverse nanostructures and porous structures. Such structures are far better than bulk photocatalyst in supporting the mobility of charge carriers to the active sites.

The metal oxides containing metal ions with d^0 and d^{10} configurations such as TiO_2, Ta_2O_5, Nb_2O_5, ZnO, exhibits good photocatalytic activity in UV regime.[8] Titanium dioxide is extensively explored metal oxide in the field of photocatalysis for its versatility and photostability. As a best alternative to TiO_2, ZnO is also explored for its catalytic potentiality;

however, ZnO is far less explored than TiO_2, due to its high photocorrosion properties. Tantalum oxides and Niobium oxides exhibit good degree of crystallinity that could aid in reducing the recombination of charge carriers. The layered metal oxides that are called as pervoskites are showing higher activity particularly in water splitting reactions. This is because of the fact of separate active sites for reduction and oxidation reactions. The layered structure is suitable for inclusion of metal ions as dopants in between the layers.[9] Since most of the metal oxides are wide band gap semiconductors, doping in metal oxide is routinely practiced to reduce the band gap of the semiconductors in order to work under visible light and also to increase the charge carrier utilization.[10-15] Lanthanum doping in metal oxides is known for increasing the lifetime of the charge carriers.[16]

1.5 Zinc Oxide

Zinc Oxide is white color solid powder with least chemical toxicity, extreme chemical stability and cheap availability. It is a direct and wide band gap (3.37 eV) semiconductor[17] possessing wurtzite crystal structure. ZnO has high exciton binding energy of the value of 60 meV even at room temperature that affords good electron conducting properties. It exhibits intense pyro-electric, piezo-electric properties and also the ability to form various nanostructures. The inherent physicochemical and electrochemical properties of ZnO find wide variety applications in mechanical actuators, sensors, Ultra Violet (UV) light emitters, catalysis, panel displays and solar cells.

1.5.1 Physiochemical Properties of ZnO

The crystal structure of ZnO is hexagonal wurtzite with tetrahedral coordination formed by four anions surrounding each cation and vice versa. The alternate planes comprise both oxygen anions and zinc cations along the vertical c-axis and the corresponding representation is given in Figure 4. The tetraherdral coordination is known to have covalent character but there is considerable ionicity in ZnO chemical structure. The space group of wurtzite structure is C_{6V}^4 and the lattice parameters are calculated as a= 3.296 Å and c = 5.20 Å at STP conditions.[18] In case of ZnO semiconductor, there is

deviation of the lattice parameters with the change in the ratio of c/a from the typical wurtzite arrangement. This deviation is the underlying factor for lattice stability as well as ionicity. There is no centro-symmetry in the structure of wurtzite ZnO that arises high degree of electromechanical coupling. Other possible crystal structures are zinc blende and cubic rock salt structure. For ZnO, wurtzite is the stable crystal structure up to 1200 ^{o}C of temperature and after that transition will occur. In that crystal structure, there are formation of tetrahedral voids that are available for interstitial Zn and also inclusion of bigger ions like Indium. The same serves as the reason for antisites formation during doping of heavy group-V elements like antimony and arsenic.

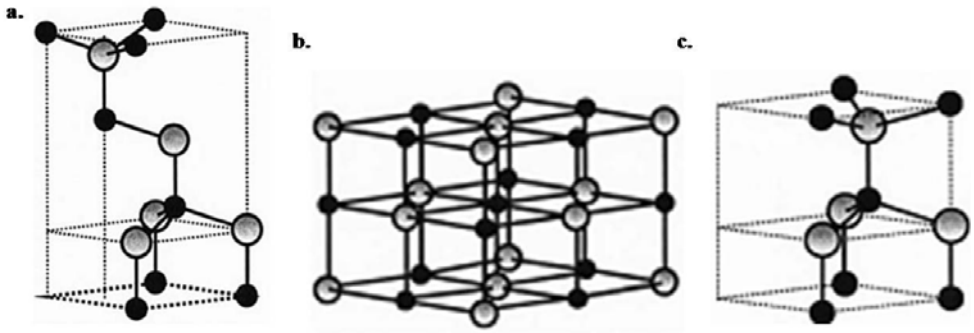

Figure 4. Crystal structural forms of ZnO a. Wurtzite, b. cubic rock and c. cubic zinc blende.

This feature brings the piezo electric and pyro electric properties that allow the use of ZnO crystals as sensing cantilevers in surface microscopy techniques.[19] Some of the planes in ZnO contain either less number of oxygen or more number of Zn atoms occupying interstitial positions arising polarity in the long range order. The commonly occurring polar surface in the basal plane of ZnO is the notable characteristic feature. Usually, polar surfaces have high dipole moment and surface energy that is useful for making strong interactions with the environment. The structural directing agents or capping agents easily bind over the polar surface. The loading of metal atoms on the polar surface is highly feasible due to high surface energy. The polar surfaces in ZnO are mainly responsible for arising variety of nanostructures that can be tunable to desired size and shape. The

following are the examples of noteworthy works on nanostructures of ZnO. ZnO nano rods with uniform size had been prepared using metal organic vapor phase epitaxial (MOVPE) method.[20] The nano rods shows high optical purity with improved cantilever sensitivity. ZnO nano needles were prepared using chemical-vapor deposition (CVD) method for the purpose of field emission applications. Single crystal ZnO nano wires are synthesized by CVD method.[21] When the dimension of the length of the wire increases, the performance of the sensitivity also increases in the same trend. Hexagonal shape tubes of ZnO attract research in the optoelectronics. The assembly of nanostructures had also been successfully attempted by GaO and Wang.[22] The arrays of six blades with triangular shape were self-assembled in the fashion of nanopropellar and these were prepared using the method of solid-vapor deposition process.[23]

1.5.2 Native Defects in ZnO

The lattice structure of ZnO is natively associated with native defects such as oxygen vacancies, interstitial Zn and Zn vacancies. The native defects in ZnO play crucial role in furnishing both advantages and disadvantages. The major advantages are n-type conductivity,[24] green luminescence and antibacterial activity under UV light whereas notorious photocorrosion remains as disadvantage due to native defects. **Figure 5** enumerates the advantages and disadvantages in the schematic presentation panel and in the following points from a-d.

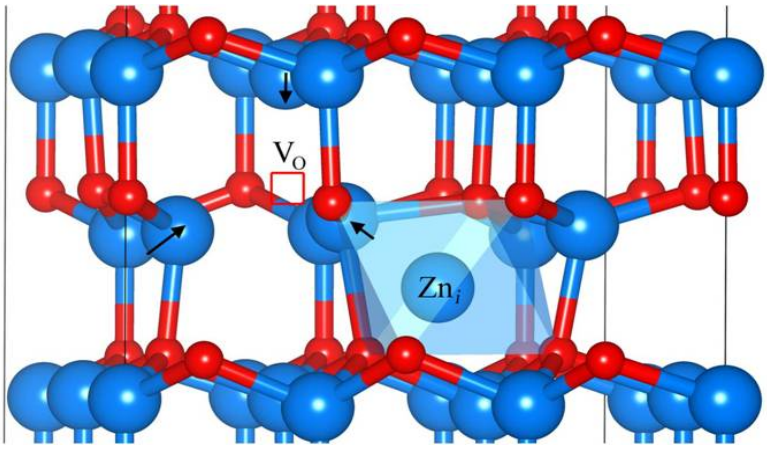

Figure 5. Oxygen vacancies as recombination centers

a. n-type Conductivity

The oxygen vacant sites serves as traps for free negative charge carriers that are released by the structural cations. The trapped free electrons form a donor level just below the CB facilitate easy excitation of charge carriers from the donor level to the CB even at room temperature. The hopping of electrons is also supported in the wurtzite structure.

b. Green Luminescence

ZnO nanocrystals are widely used for green LEDs taking the advantage of inherent green luminescence appears around 510 nm of wavelength at room temperature.[25] Experimental findings provide strong evidence on the direct interrelationships connecting luminescence, the free charge carrier concentration and paramagnetic oxygen-vacancy density. The oxygen vacancies and interstitial zinc form deep levels at an energy level of 2.54 eV below the CB and the exciton emission occurred from that deep levels is the sole reason for green luminescence.

c. Antibacterial Activity

When ZnO is suspended in the aqueous solution and irradiated under light, the oxygen vacancies in ZnO cause Zn metal leaching into the solution. The mechanism of photocorrosion will be described in coming sub-section. Zn metal ions are seriously toxic to the bacterial wall leading to the disruption of the cell wall of bacteria. This antibacterial photoactivity of ZnO is utilized for sterilization purpose in biomedical applications. The tendency of ZnO for metal leaching under sunlight is exploited for Zn additives to the soil for the growth of plants.

d. Photocorrosion

As mentioned in the latter section, oxygen vacancies are the responsible for deleterious photocorrosion. As per the first two steps in the photocatalysis, absorption of photon generates charge carriers followed by their diffusion to the surface of ZnO. Under prolonged irradiation, Zn metal ion leaching from

the ZnO poses serious limitations over the stability of the catalyst.[26] The details on mechanism of photocorrosion can be explained in sequential steps:

Step 1: Zn interstitial ions give up the valence electrons to maintain charge neutrality.

Step 2: The presence of Zn interstitials left surface oxygen atoms in uncoordinated form. The surface oxide ion involves in the reduction of photogenerated hole. Continuous reduction process leads to the formation of oxygen molecule that detaches from the structure.

Step 3: The detachment of surface oxide ions in form of oxygen atoms/molecules create oxygen vacancies in the lattice. In the site of oxygen vacancies, free as well as photogenerated electrons are trapped. Those trapped sites act as recombination centers for photogenerated holes that reduce the yield of the reaction.

Step 4: Another consequence to the detachment of surface oxide, destabilization and breaking of lattice ZnO bonds will occur leading to explusion of Zn metal ion into solution. The overall reaction can be summed up as photogenerated hole oxidizes ZnO into metal ion and oxygen molecule and corresponding equations of the mechanism of photocorrosion is given below.

1.6 ZnO as Photocatalyst

In the field of photocatalysis, ZnO is considered as the second best alternative to TiO_2 photocaatalyst. The aspect of charge carrier utilization is strongly supported by ZnO photocatalyst by taking advantage of the feature of high exciton binding energy. ZnO has 10 times higher electron mobility than TiO_2 and thus promoting fast diffusion of photogenerated electron from the bulk to the surface. As it is already explained in earlier section, ZnO can able to adopt one dimensional structure such as nano rods, nano wires, nano belts and nano needles that are having remarkable charge carrier transport properties. The fast transport of charge carriers improves the separation of holes and electron thereby outweighs the chances of recombination. ZnO has surface hydrophilicity for adsorption of –OH moieties and thus polar

chemical functionalities can be easily adsorbed on the surface ZnO.[27] The combined operation of fast diffusion of electron and catalytic potentiality produce relatively higher yield in first few hours of the photocatalytic reaction. After prolonged hours of reaction, the rate of reaction yield drops down dramatically due to the problem of photocorrosion. Therefore, suppression of photocorrison is highly emphasized to attain sustainable yield. The methods that are demonstrated for suppressing photocorrosion are discussed in next section.

Another important aspect in the photocatalysis is that light harvesting. Naturally, ZnO is wide band gap semiconductor with the absorption edge onset around 370 nm. The short wavelength absorption edge demonstrates the requirement of UV light for necessary charge carrier generation. To harvest solar energy that reaches the earth, the charge carrier generation is to be effected by absorbing visible light photons. Since ZnO is transparent in visible light regime, advancement of ZnO in solar light harvesting is severely limited. It is necessary to reduce the band gap to bring visible light absorption in ZnO.

1.6.1 Band Gap Engineering in ZnO

Band gap engineering is noted as indispensible approach in bringing visible light absorption in wide band gap semiconductors. The reduced band gap enable the generation of charge carriers with lower incident photon energy like visible light photons. In this context, doping of either cation or anion is widely practiced. The incorporation of foreign elements into metal oxide creates new energy levels into the electronic structure of metal oxide. Depending upon the chemical nature of the incorporated element, the energy levels will be either acceptor levels that is formed on the top of VB or donor level that is formed below CB. When the new energy levels of the incorporated elements are discrete it will act as recombination centers. The formation of continuous bands by the new energy levels at the CB and VB edges is expected to avoid recombination and also furnish continuous absorption spectrum for the photocatalyst. The electronic structure of the

incorporated dopant has to overlap with electronic energy of ZnO. Different strategies on band gap engineering will be discussed in the next section.

a. Anion Doping

In case of metal oxides, like ZnO, containing metal ion with d^{10} configuration, VB is formed by filled oxygen 2p orbitals and CB is formed by vacant Zn 4s, 4p orbitals. According to literature reports, though cation doping imparts visible light absorption, formation of new discrete energy levels increase the recombination center density. The anion doping provide ample opportunites for the formation of continuous bands of new energy levels at the VB edges. The foremost criteria in the selection of dopant, the size of the anion dopant should be close to the size of oxygen. The second criterion is that the bond length of Zn-Anion and Zn-O should also be close values. Because incorporation of dopant should not cause lattice distortion beyond 15% limit so as to avoid destabilization of metal oxide structure.

Nitrogen has similar size and ionization energy as that of oxygen and therefore it is considered to be the suitable candidate among various anions.[28] Another important advantage in doping of nitrogen is that the energy levels of N_{2p} orbital significantly overlap with that of O_{2p} orbital at the top of the valence band resulting in band broadening.[29] The VB edge will be shifted to lower energy and thus visible light absorption is possible due to nitrogen doping in ZnO. Besides the aforementioned advantages, there are difficulties to overcome in nitrogen doping. Reproducibility of the doping method, solubility of nitrogen and poor content of nitrogen doping are crucial problems. Sophisticated techniques such as MOCVD, CVD and Molecular beam epitaxy (MBE) are required to form nitrogen doped ZnO film.[30] However there was only 3% nitrogen doping content in those techniques. Mapa et al synthesized highly reproducible 15% nitrogen doped ZnO with triangular morphology via solution combustion synthesis method.[31] The incorporated nitrogen rises problems in charge compensation and neutrality. The nature of doped nitrogen is expected to be nitride form having higher electron density. This is the crucial factor in forming overlapping N_{2p} energy levels at good extent with O_{2p} orbitals of VB. Nitrogen in nitride form also

assists the suppression of oxygen vacancies that will be discussed in next section.

b. Oxynitride and Solid Solutions

To alleviate the problems such as charge compensation and nitride form of nitrogen doping, codoping of nitrogen affinity metal ions is successfully attempted. The state of nitrogen in nitride form can be easily achieved by codoping of another metal ion and that also involves in charge compensation with nitrogen dopant. Oxynitrides usually exhibit higher visible light absorption than the cases of simple nitrogen doping. However, the lattice stability of oxynitride poses issues over sustainability of ZnO.

Solid Solution is the new class of oxynitrides that had been introduced to overcome the lattice stability problem. It can be defined as homogenous lattice structure comprised with two or more compounds having similar crystal structures with close lattice parameters. The metal belong to group III having strong affinity for nitrogen and at the same instance, the crystal structure of binary semiconductors III-IV is wurtzite as same as that of ZnO. Among group III metals, Ga and In has negative enthalpy of nitride formation. The size of In and Ga can able to stabilize in the lattice structure of ZnO. Domen et al successfully prepared solid solution of GaN:ZnO via conventional nitridation method.[32]

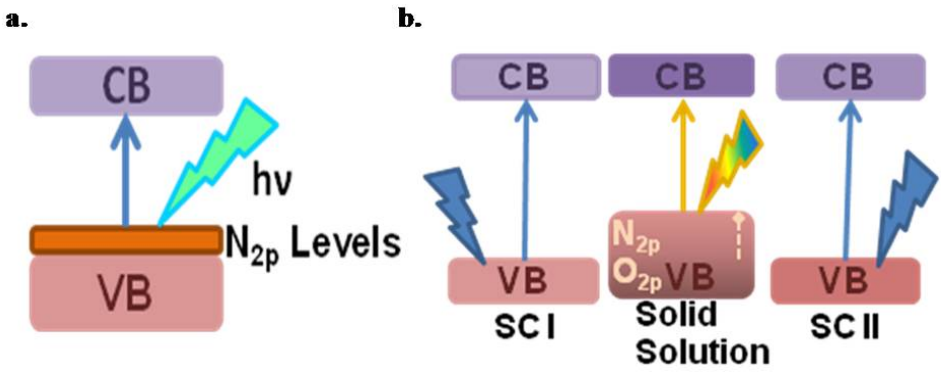

Figure 6. Comparison of electronic structure of N-doped ZnO (a) and Solid solution (b).

Figure 6 shows the comparison of the electronic structure of precursors and the solid solution. The band gap reduction in solid solution is attributed to the valence band broadening due to the overlapping of N_{2p} orbital from GaN with O_{2p} orbital from ZnO. Mapa et al successfully prepared solid solutions of GaN:ZnO and InN: ZnO through solution combustion method.[33] The solid solutions exhibit good extent of visible light absorption onset around 550 nm. There is significant band gap reduction in solid solutions than the parent precursors, particularly GaN and ZnO precursors having wide band gap of 3.4 eV.

c. Integrated Solid Solutions:

To obtain electronic integration along with structural integration in solid solution, the solid solutions are prepared using two compounds with similar crystal structure shares common anion. When the anion is common there are chances of forming continuous linkages of both the compounds or in other words the nanoclusters of one compound is interlinked with the other compound in the neighbour through covalent linkages. This results in formation of continuous bands in the electronic structure of solid solution. There are noteworthy examples for integrated solid solutions: ZnS:CdS solid solution shares the common anion that leads to the formation of quantum dots of CdS in ZnS.[34] InN and GaN shares the common anion of nitrogen with similar crystal wurtzite structure favouring the formation of InGaN quantum dot. We prepared InGaN quantum dots integrated with ZnO. The formation of integrated InGaN quantum dot is favoured in ZnO lattice through the interconnection of Zn-N bonds in the same wurtzite lattice. This is discussed in detail in chapter 4.

1.6.2 Light Harvesting Composites

Composites are multifunctional material exhibiting the properties of functional components.[35] Fabrication of composites by combining ZnO with visible light active materials is an alternate method to band gap engineering method. Such composites serve dual purpose of visible light absorption and charge carrier transport which are the key aspects in solar light harvesting. Integration of ZnO with interesting visible light active material follows any

one of the two principles: a. Physical deposition, and b. Chemical linkages/functionalization. Each of the principle has its own advantages and disadvantages. Noble metal nanoparticles and semiconductor nanostructures are widely used as visible light harvesting components. Few examples of composites made of biomaterials like algae, siderophores as light harvesting components are reported.[36]

a. Noble Metal Nanoparticles as Light Harvesters

Nanoparticles of noble metals such as Au and Ag that are termed as plasmonic nanostructures exhibit visible light absorption due to the phenomenon of surface plasmon resonance (SPR). The SPR activity affords advantage of intense visible light absorption cross-section with three order higher magnitude than dyes.[37] Depending on the size and shape of the metal nanoparticle, absorption maxima is being tuneable. The metal nanostructures can build up of intense field around the surface providing the generation of hot electrons that increases the charge carrier utilization. Large size nanoparticles > 50 nm have poor SPR effect but the scattering effect will be bestowed. The scattering of light increases light penetration and allows several passes of photon into the structure that brings effective utilization of charge carriers.[38]

The metal nanostructures are either directly deposited on the surface of ZnO or linked by using bifunctional moieties. When there is direct loading of metal nanoparticles, the transfer of 'hot' electrons is only through the mechanism of tunnelling in space. In aspect of utilization of charge carriers, this type of direct loading is advantageous but tuneabilty of size and shape remains difficult. High level of dispersion of nanoparticles over the surface of oxide is necessary to achieve good activity. Wet impregnation, CVD and photodeposition are the routine methods for direct loading of nanoparticles. When the metal nanoparticles are attached through linkers, the chemical nature and spacer length of linker are highly important. This method allows tuning of size and shape by changing the capping agents but SPR activity is highly shielded by the capping linkers. To achieve maximum of SPR effect,

the optimum distance between ZnO and metal nanoparticle is to be ~2-5 nm. Suspension of metal oxide in the colloidal solution of metal nanostructures has been carried out for attaching metal nanostructures. The working principle of noble metal nanostructures is described as follows. Under visible light irradiation, plasmonic metal nanostructures absorb light and hot electrons are generated due to SPR effect and the hot electrons are transferred to active sites of ZnO.[39] As the reactants are absorbed on the surface of ZnO, the charge carriers involve in the action.

b. Semiconductor Nanostructures as Light Harvesters

The use of semiconductor nanostructures is cost effective in place of noble metals nanostructures. Semiconductor nanostructures having sizes of around 10 nm are termed as quantum dots (QD). QD are well known for having electron confinement in all three directions and for enhanced stability. Unlike other nanoparticles, the electronic excitation in QD follows the mechanisms as that of semiconductor. The key advantage of QD is having tuneable optical band gap with respect to size and shape.[40] Notably, the inherent feature of multiple exciton generation (MEG) by absorbing single photon in QD is highly useful for increasing the quantum efficiencies[41] whereas in the bulk structures, the energy obtained from MEG had been dissipated in form of heat. The flux of absorption for QD is 1000 times higher than that of organic dyes.

Kamat et al demonstrated that the size difference of even 1 nm influences huge difference in the charge transfer kinetics and also shift the absorption wavelength.[42] Figure 7 shows the comparison of the QD with different sizes.

When the size of the QD decreases, rate constant for transfer also decreases and thus free energy of the process attains negative potential and high spontaneity. When the size of the QD increases, the absorption wavelength also increases from blue to red because the optical band gap decreases. On the other hand, the CB and VB edges shifted towards lower potential and rate of transfer also decreases. Therefore, there should be optimum size to compensate the charge transfer as well as visible light

absorption. Solution processing is the routine method followed for preparing QD structures.[43] QD of cadmium chalcogenides are highly explored for wide

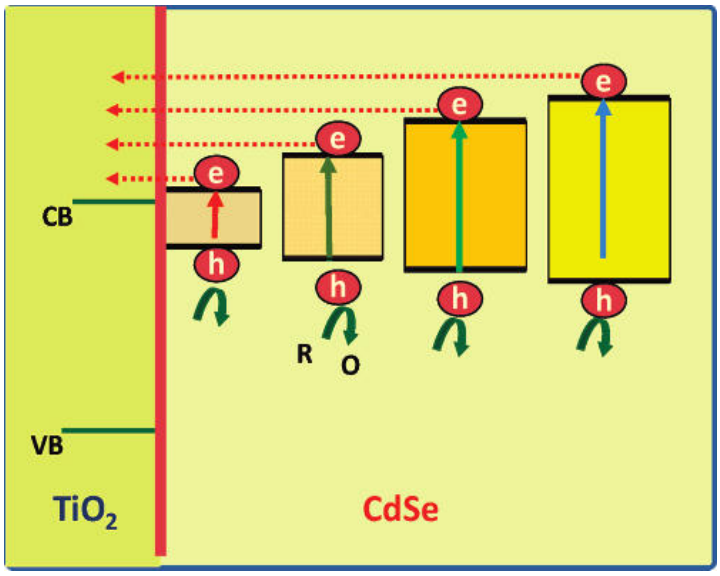

Figure 7. Effect of Size of QD over the conduction band potential

variety of applications.

Figure 8 demonstrates the working principle of the composite of ZnO/Semiconductor nanostructure. QD absorbs the visible light photon followed by excitation of electron from VB to CB. The electron from CB of QD is transferred to CB of ZnO since the edge of CB of QD is higher negative potential than ZnO. The hole generated in VB of QD is utilized for oxidizing the reactant while the electron in CB of ZnO is utilized for reducing the reactant. The accumulation of holes in QD poses serious problems like photocorrosion and self quenching of the quantum dots and this problem is highly pronounced in case of CdSe and CdS QDs.

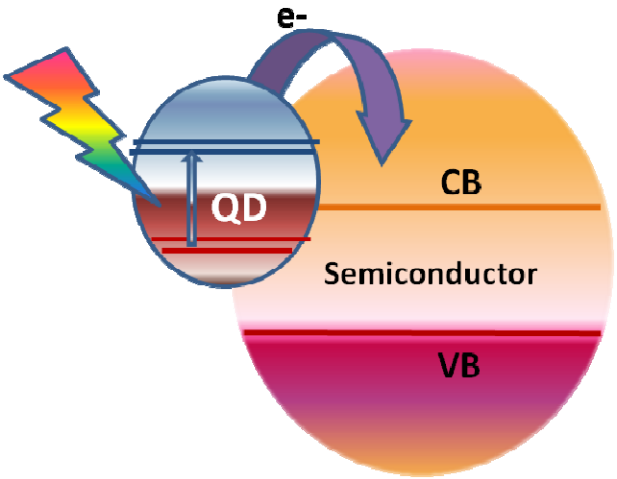

Figure 8. QD sensitized photocatalysis: visible light absorption followed by electron transfer from QD to Semiconductor.

1.6.3 Suppression of Native Defects in ZnO

The ZnO lattice exhibits inherent oxygen vacancies and the density of vacancies increases even with the slight increase in temperature. When ZnO is heated to high temperature, there is a color change observed from white to yellow color due to oxygen vacancies. As discussed in previous section, the oxygen vacancies create problems of photocorrosion which is necessarily to be avoided so as to find application in solar light harvesting.

During the formation of ZnO, there is equilibrium between the level of oxygen vacancies and Zn vacancies. The oxygen vacancies form donor levels arising n-type conductivity while Zn vacancies or interstitial form acceptor levels arising p-type conductivity. To suppress oxygen vacancies, it is essential to bring p-type conductivity which is a bottle neck problem.[44] There were successful attempts in shifting the equilibrium towards Zn vacancies but other compounding problems like lattice distortion were accompanied that decrease lattice stability. Doping of alkali metal ions such as Li and Na, nitrogen, phosphorous and antimony in ZnO is theoretically predicted to form acceptor levels. The shallow acceptor levels, rather than deep aceeptor levels, are effective in achieving p-type conductivity. Among all the candidates, nitrogen in nitride form is selected to be the best candidate

because of the formation of shallow acceptor levels. Another advantage is that nitrogen will not form metastable antisites. Sources of nitrogen in doping conditions play a role in deciding the electronic nature of nitrogen. Besides the formation of acceptor levels above the top of VB, nitride type of nitrogen can occupy the oxygen vacancies thereby the density of oxygen vacancies can be possibly suppressed. Among various sources, namely nitrogen, nitric oxide, ammonia and amines, ammonia is considered to be the suitable source. The flux of gaseous ammonia at high temperatures feasibly interacts with the oxygen vacancies and bond breaking of ammonia molecules into nitride and hydrogen occurs. Hydrogen gas will be evolved while nitride is stabilized in the lattice of ZnO at the expense of oxygen vacancies. The surface structure of ZnO also plays a role in influencing the polar nature as well as photocorrosion. The uncoordinated oxide atoms in the surface also take crucial part in photocorrosion. Functionalization of ZnO using under coordinated oxide atoms will reduce the chances of oxidation of oxide bond by the photogenerated holes and further expulsion of oxygen molecule from the lattice of ZnO. The graphene oxide, fullerenes and dyes were functionalized on the surface of ZnO to passivate the surface of ZnO.[45] The sites of oxygen vacancies are captured by the adsorbants. However, the surface passivation hinders direct interaction between ZnO and the reactants, but also reduces light penetration into ZnO structure.

1.7 Objective of Thesis

Owing to the fast depletion of conventional fuels, there is search for alternate energy resources. Solar energy harvesting seems to be the attractive solution to meet part of the energy demand. Heterogeneous semiconductor photocatalysis provide cost-effective platform for light harvesting and simultaneous conversion to value added chemicals. Several semiconductors and structural modifications of them are extensively explored as photocatalysts for dye degradation, organic chemicals, water splitting and photocurrent generation.

The literature survey on heterogeneous semiconductor photocatalysis enumerates that ZnO is the one of the leading semiconductor. The structure of ZnO affords effective charge carrier utilization and catalytic potentiality with appropriate surface adsorption of reactants. The wide band gap nature limits visible light absorption and native defects such as oxygen vacancies poses difficulties in photostability. To find advancement in solar harvesting applications, imparting visible light absorption and suppression of native defects in ZnO are targeted. Band gap engineering in ZnO through nitrogen doping, oxynitride and solid solution formation are successfully attempted. Solid solutions based on ZnO show visible light absorption extended up to 550 nm with poor absorbance. The portion of visible light at 510 nm is in major proportion in sunlight that reaches the earth and plays vital role in photosynthesis. To harvest sunlight, light absorption by the photocatalyst is necessary to span over entire visible light region and particularly at 510 nm there should be good absorbance. The photocatalytic activity of the bare solid solutions is negligible due to defect densities and there is a serious demand of noble metal cocatalysts to exhibit considerable activity. The suppression of defect densities can alone improve the activity of virgin catalyst.

Besides absorption of visible light, the origin of visible light absorption is earnestly important to understand in the view of development of new photocatalysts. In systems of GaN rich ZnO solid solutions, Zn atom is merely substituted Ga atom forming impure acceptor levels. The energy of those acceptor levels depends on the concentration of Zn atoms. Though these impure discrete levels bring visible light absorption, it increases the defect densities severely limiting the activity. Through local structure analysis of solid solution needs to understand to demonstrate the lattice defects. Density functional calculations reveal that VB_{Max} comprises N_{2p} orbital succeeded by Zn 3d orbital and the O 2p orbital.[10] In that case, p-d repulsion is the sole reason for band gap reduction and in turn visible light absorption. However, this can be applicable only to 1:1 stoichiometric unit cells of GaN and ZnO. GaN is reported to be catalytic inactive and so solid solution with ZnO rich has to be prepared and the electronic structure of the

same will be different from previous case of solid solution. The photocatalytic activity, origin of visible light absorption and structural relationship between the local structure of ZnO rich GaN solid solution with the photocatalytic activity have been left unexplored.

The deposition of semiconductor nanostructures like QD is perceived to be cost-effective approach in place of noble metal loading. This is recently emerged alternative protocol to band gap engineering towards visible light absorption and effective charge carrier utilization. Surface passivation of QDs or through chemical linkages limits the charge transfer from QD to ZnO. Therefore it is necessary to structurally and electronically integrate QD with ZnO. Effective utilization of charge carrier can be accomplished through separation of charge carriers. Development of composites of p-type and n-type materials is to be emphasized in order to realize charge carrier separation for decent photocurrent generation.

In the context of solar light harvesting, systematic approach on understanding the photocatacatalyst and development of new photocatalysts to alleviate the aforementioned issues are the main objectives of this thesis.

- To prepare Zinc oxide rich ZnO-GaN solid solution, which is free from Ga_2O_3 or other oxide impurities, by solution combustion synthesis method. The structure property relationship with photocatalytic activity can be understood through EXAFS study on local structure analysis and photoluminescence study.
- To prepare the photocatalyst that absorbs the entire visible light region. InGaN quantum dots are integrated into ZnO lattice via solution combustion synthesis method.
- To achieve synergistic operation of visible light harvesting and effective charge carrier utilization, direct structural and electronic integration of InGaN QD to ZnO is accomplished. Suppression of oxygen vacancies is also demonstrated.
- To develop integrated composite of ZnO with visible light absorption, ZnO/InGaN QD@ZnO composite is prepared. ZnO as one of the component is prepared using biocompatible glycerol assisted approach.

- To demonstrate composites for charge carrier separation, composites of ZnO(n-type)/p-type NiO and ZnO(n-type)/p-type CuO are prepared through wet impregnation method.

1.8 Outline of Thesis

The thesis deals the synthesis of new photocatalysts, systematic characterization of photocatalysts, and understanding on the structure property relationships, photocatalytic conversion of solar energy into chemical energy, such as alcohol dehydrogenation, hydrogen generation by water splitting and photocurrent generation. There are four systems of photocatalysts elaborated. They are i) ZnO-rich ZnO-GaN solid solution, ii) InGaN(QD) @ ZnO integrated material, iii) biocompatible template assisted synthesis of ZnO/InGaN(QD)@ZnO systems, and iv) Composites of n-type ZnO/p-type NiO and CuO. The description on chapter-wise outline of the thesis is followed below.

Chapter 1 elaborates general introduction on heterogeneous semiconductor photocatalysis for solar light harvesting. It enumerates the contribution of metal oxides, governing principles of photocatalysis. It brings out the traits and limitations of ZnO towards light harvesting. The concepts of the developments of ZnO based photocatalysts are discussed. The objectives and scope of the thesis is also presented in the last section of the chapter.

Chapter 2 presents the aspects of the synthesis protocol of solution combustion synthesis and the synthesis procedure of all the four systems of materials. The theory, experimental set up, inferences on characterization techniques are discussed. The experimental conditions and reactor set up of the photocatalytic conditions are furnished.

Chapter 3 deals with the system of ZnO rich: GaN solid solution. The material is prepared and characterized by relevant structural characterizing techniques. The local structure analysis was carried out for

solid solution by EXAFS technique. The photoluminescence studies are carried out for probing the electronic structure. HRTEM studies on ZnO-rich ZnO-GaN solid solution are carried out for evidencing the formation of solid solution and existence of GaN and ZnO in the same lattice. The photocatalytic activity of the bare materials for hydrogen generation form water without containing sacrificial agents is evaluated. The potentiality of the material for photocurrent generation is also established.

C**hapter 4** describes the system of InGaN(QD)@ZnO. The aspect of structural integration is investigated by using XRD and HRTEM techniques. Critical fragments, such as In-Ga-N, Ga-N, Ga-N-Zn, Zn-N bonds are directly identified using secondary ion mass spectrometry. The electronic integration was evidenced from XPS, Raman, UV-Visible absorption spectroscopy and photoluminescence. The materials are explored for solar light harvesting and the conversion of light energy into chemical and electrical energy. The efficiency of the conversion of bare photocatalysts is determined from incident photon conversion energy IPCE using different cut-off filters of different wavelengths. The response of the materials for photocurrent generation at the longer wavelength of 610 nm underscores the utility of the material.

Chapter 5 includes two systems of composites of ZnO. In the first part, the use of biocompatible templates (Glycerol) for preparing ZnO is described. Using wet impregnation method, the composite of ZnO and InGaN(QD)@ZnO is prepared. The morphology of ZnO nanoparticles and the changes in the morphology of the composite are investigated. The features of structure and visible light absorption are probed by employing relevant techniques. The photocatalytic performance of the materials is evaluated for photocatalytic hydrogen generation and photocurrent generation are evaluated.

In the second part, the material InGaN(QD)@ZnO is loaded with p-type nanoparticles of NiO through incipient wet impregnation method and CuO nanoparticles through microwave assisted method. HRTEM studies on the composites are taken to provide the evidence for the composite

formation. The materials are evaluated for photocatalytic hydrogen generation with pH adjusted to 4.5. The materials exhibit 6 times higher hydrogen generation than InGaN(QD)@ZnO catalysts.

1.9 References:

1. M. K. Hubbert, *Science*, 1949, **109,** 103.

2. P. V. Kamat, *J. Phys. Chem. C.*, 2007, **111,** 2834.

3. K. Bowker, *Green Chem.*, 2011, **13,** 2235-2246.

4. A. Kudo and Y. Miseki, *Chem. Soc. Rev*., 2009, **38,** 253.

5. A. Fujishima and K. Honda, *Nature*, 1972, **238,** 37.

6. V. Chen, S. Shen, L. Guo and S. S. Mao, *Chem. Rev.*, 2010, **110,** 6503.

7. Z. Zou, J. Ye, K. Sayama and H. Arakawa, *Nature*, 2001, **414,** 625.

8. T. Ohno, F. Tanigawa, K. Fujihara, S. Izumi and M. Matsumura, *J. Photochem. Photobiol. A.,* 1999, **127,** 107.

9. S. Zhang, G. Zhang, S. Yu, X. Chen and X. Zhang, *J. Phys. Chem.* C., 2009, **113,** 20029.

10. M. Higashi, R. Abe, T. Takata and K. Domen, *Chem. Mater.*, 2009, **21,** 1543.

11. T. Ohno, F. Tanigawa, K. Fujihara, S. Izumi and M. Matsumura, *J. Photochem. Photobiol. A.,* 1999, **127,** 107.

12. G. Liu, Y. Zhao, C. Sun, F. Li, G. Q. Lu, and H. M. Cheng, *Angew. Chem., Int. Ed.*, 2008, **47,** 4516.

13. R. Asahi, T. Morikawa, T. Ohwaki, K. Aoki, and Y. Taga, *Science,* 2001, **293,** 269.

14. M. Sathish, B. Viswanathan, R. P. Viswanath, and C. S. Gopinath, *Chem. Mater.*, 2005, **17,** 6349.

15. T. Ohno, T. Tsubota, K. Nishijima, and Z. Miyamoto, *Chemistry Letters*, 2004, **33**, 750.

16. K. Ogisu, A. Ishikawa, K. Teramura, K. Toda, Hara and K. Domen, Chem. Lett., 2007, **36,** 854.

17. Ü. Ozgur, Y. I. Alivov, C. Liu, A. Teke, M. A. Reshchikov, S. Dogan, V. Avrutin, S. J. Cho and H. J. Morkoc, *J. Appl. Phys.,* 2005, **98**, 041301.

18. N. J. Renault, P. Pichat, A. Foissay and R. Mercier, *J. Phys. Chem.,* 1986, **90,** 2733.

19. Y. B. Li, Y. Bando and D. Golberg, *Appl. Phys. Lett.,* 2004, **84,** 3603.

20. Z. Fan, D. Wang, P.-C. Chang, W.-Y. Tseng and J. G. Lu, *Appl. Phys. Lett.,* 2004, **85,** 5923.

21. T. Minami, H. Sato, H. Nanto and S. Takata, *Jpn. J. Appl. Phys. Part 2.,* 1985, **24,** L781.

22. (a) S. Y. Myong, S. J. Baik, C. H. Lee, W. Y. Cho and K. S. Lim, *Jpn. J. Appl. Phys. Part 2.,* 1997, **36,** 1078. (b) B. M. Ataev, A. M. Bagamadova, A. M. Djabrailov, V. V. Mamedo and R. A. Rabadanov, *Thin Solid Films*, 1995, **260**, 19.

23. (a) H. J. Ko, Y. F. Chen, S. K. Hong, H. Wenisch, T. Yao and D. C. Look, *Appl. Phys. Lett.,* 2000, **77,** 3761. (b) V. Assuncao, E. Fortunato, A. Marques, H. Aguas, I. Ferreira, M. E. V. Costa and R. Martins, *Thin Solid Films*, 2003, **427,** 401.

24. T. Minami, H. Sato, H. Nanto and S. Takata, Jpn. *J. Appl. Phys. Part 2*., 1985, **24,** L781.

25. K. Vanheusden, W. L. Warren, C. H. Seager, D. R. Tallant, and J. A. Voigt, *J. Appl. Phys.,* 1996, **79,** 10.

26. V. A. Fonoberov, K.A. Alim, A. A. Balandin, F. Xiu, Liu, *J. Phys. Rev. B,* **2006**, *73*, 165317.

27. I. Volintiru, M. Creatore, W. H. van Helvoort, J. L. Linden and M. C. M. van de Sanden, *Appl. Phys. Lett.,* 2006, **89,** 022110.

28. C. C. Lin, S. Y. Chen, S. Y. Cheng and H. Y. Lee, *Appl. Phys. Lett.*, 2004, **84,** 5040.

29. C. L. Perkins, S-H. Lee, X. Li, S. E. Asher and T. J. Coutts, *J. Appl. Phys.*, 2005, **97,** 034907.

30. C. Wang, Z. Ji, K. Liu, Y. Xiang and Z. Ye, *J. Cryst. Growth.,* 2003, **259,** 279.

31. A. Kobayashi, O. F. Sankey and J. D. Dow, *Phys. Rev. B,* 1983, **28,** 946.

32. M. Mapa, K. S. Thushara, B. Saha, P. Chakraborty, C.M. Janet, R. P. Viswanath, C. M. Nair, K. V. G. K. Murty, C. S. Gopinath, *Chem. Mater.,* 2009, ***21,*** 2973.

33. M. Mapa, K. Sivaranjani, D. S. Bhange, B. Saha, P. Chakraborty, A. K. Viswanath, and C. S. Gopinath, *Chem. Mater*., 2010, ***22,*** 565.

34. J. Yu, J. Zhang, and M. Jaroniee, *Green. Chem*., 2010, **12**, 1611.

35. D. Wang, Z. Zhigang Zou, and J. Ye, *Chem. Mater.*, 2005, **17***,* 3255.

36. A. Devaux, G. Calzaferri, P. Belser, P. Cao, D. Bru hwiler and A. Kunzmann *Chem. Mater.*, 2014, **26,** 6878.

37. S. Linic, P. Christopher and D. B. Ingram, *Nat. Mater.*, 2011, **10,** 911.

38. S. C. Waren, and E. Thimsen, *Ener. Environ. Sci*., 2012, **5,** 5133.

39. H. M. Chen, U. K. Chen, Y. Chang, W. S. Chang, and K. H. Chen, *Angew. Chem. Int. Ed*., 2010, **49,** 5966.

40. A. Kongkanand, K. Tvrdy, K. Takechi, M. Kuno, and P. V. Kamat, *J. Am. Chem. Soc*., 2008, **130,** 4007.

41. A. J. Nozik, *Chem. Phys. Lett.*, 2008, **457,** 3.

42. P. V. Kamat, *J. Phys. Chem. C*, 2008, ***112,*** 18737.

43. T. Trindade, P. O'Brian and N. L. Pickett, *Chem. Mater*., 2001, **13,** 3843.

Experimental Methods

2. Experimental Methods

The preparation and characterization methods play an important role in the development of functional catalysts with novel properties. Predominantly, we employed solution combustion method for preparation of solid solution of ZnO-GaN and InGaN(QD)@ZnO systems. To prepare few composites, we used incipient wet impregnation method. In this chapter, aspects of the synthetic methods, details on preparation conditions, reactor designs, studies on photocatalytic activity and description on catalyst characterization techniques such as structural, morphology, spectroscopy methods, surface analytical methods and electrochemical methods are provided.

2.1 Aspects of Synthetic Methods

2.1.1 Solution Combustion Synthesis

Combustion synthesis is a versatile, viable process for synthesizing single phase solid solutions, nanomaterials, porous materials, crystalline oxides, composites as well as complex mixed oxide phases and homogenous doping in metal oxides. The strategy of the technique adopts a self-persistent reaction between an oxidizer and fuels that are dissolved in water medium. Combustion synthesis is broadly classified into two types based on the nature of the reaction state during course of the reaction: (a) solution combustion synthesis, wherein the reactants are in solution state and (b) gel combustion synthesis or pechini process wherein reactants form a polymeric gel state.

Relatively speaking combustion synthesis takes place at rapid kinetics. The combustion synthesis is an energy efficient process and requires simple instrumental facility of muffle furnace. The reaction takes place in a furnace chamber that is preheated to the desired high temperature sufficient for the complete combustion of reactant mixture. At elevated temperature, the water was evaporated first and the mixture becomes thickened followed by a self-ignition route. After the combustion process takes place, the precursor materials are converted into fine crystallites

accompanied with the evolution of plenty of gases. The reaction time and mode takes major role in deciding the growth of the crystallites either into bulk form or nanoparticles form. There are two types of reaction modes: self-propagation mode and voluminous combustion synthesis (VCS).

a. Self-propagation mode: The reaction initiates locally and propagates a wave-like pattern throughout the medium. This type of mode takes longer time for completion. The slow but stepwise heating favours the growth of nanoparticles. The steady evolution of reactant gases produces wormhole mesoporous materials that are acclaimed for having the property of fast diffusion of charge carriers from the bulk to the surface. For an example, mesoporous N-doped TiO_2 is prepared by combustion synthesis via self-propagation mode.[1]

b. **Voluminous combustion mode**: There is uniform heating and concurrent reaction occurs throughout the reaction mixture. This mode is advantageous for producing crystalline materials. The feature of crystallinity in photocatalysts is one of the important factors for reducing recombination centers and in particular catalysts that are involved in water splitting reaction are expected to have good crystallinity. This is fascinating preparation for wide variety of materials with excellent catalaytic activities. The most attractive feature of this preparation method is that there is no need of any purification treatment required as well as high thermally stable catalysts. For an example, ZnO based solid solutions are prepared using this mode.

Achieving single phase structure with homogenous distribution of nitride nanoclusters in ZnO is targeted in our work. Thus, we have exploited voluminous combustion synthesis for the preparation of GaN:ZnO solid solution and InGaN(QD)@ZnO materials. Though the high-temperature process favours thermodynamically stable phases, the strategy of bottom-up approach of molecular to nano clusters growth with plenty of defects in the environment of in-situ generated ammonia (by urea decomposition) helps to introduce nitride in the oxide unit cells. In essence, typical nitridation conditions were simulated with high flux of ammonia while metaloxo nanoclusters grow in size. The nitride phases are highly desired for

optoelectronic applications. Besides the role of the material preparation strategy, the factor of structural similarity between ZnO and nitrides namely GaN, InN, InGaN also assists in stabilizing nitride forms in ZnO lattice.

The choice of fuel and the ratio of fuel to oxidizer are also being deciding factors in formation of phases. Among various fuels that are used, urea attains the center stage for the reason of producing least amount of carbon-di-oxide. The evolution of CO_2 involves in increasing the exothermicity of the reaction that influences the formation of impure phases such as zinc carbonate species. The fuels that based on amino acids will increase the exothermicity of the combustion conditions. The following figure compares the two fuels glycine and urea in increasing the temperature over the range of ratio of fuel/oxidizer. The temperature that was attained by using urea as fuel to metal nitrate ratio of 3 is easily attained by the temperature when glycine was used as fuel to metal nitrate ratio of 1. The temperature rises to certain ratio range (fuel to metal nitrate) and beyond that it is saturated. The stoichiometry of the fuel involved in combustion to produce either oxygen rich or lean conditions depends upon the nature of the metal oxide and the interaction of the decomposition products with the oxide.

We have selected urea as fuel in the synthesis of ZnO rich GaN solid solutions and InGaN(QD)@ZnO materials. During the combustion conditions, urea is decomposed and high flux of in-situ ammonia is produced. Ammonia is proved as the best source of nitrogen doping in metal oxide. The fact is that ammonia can interact with the oxygen vacancies and cleave into nitride and hydrogen. Incorporation of nitride form of nitrogen is alone favorable in forming overlapping energy levels with O_{2p} orbital.

2.1.2 Plausible Mechanism of Nitrogen Doping in ZnO.

Nitrogen incorporation in ZnO is the first and foremost requisite which was followed by further co-incorporation of nitrogen affinity elements like Ga and In. Bottom- approach method was adopted in growing nitrogen doped Zinc oxide. When the homogenous solution mixture containing the

starting materials was inserted in the muffle furnace at 500 ^{o}C, the water was evaporated within first few minutes. The plenty of in-situ ammonia from the combustion of urea as fuel is evolved. In parallel, nascent zinc oxo clusters grow with lot of oxygen vacancies. The ammonia interacts with oxygen vacancies and nitrogen incorporation is accomplished at the expense of oxygen vacancies. The illustration of nitrogen doping in ZnO along with the samples of varying incorporated nitrogen contents is given in Figure 1

The equation for complete combustion is given below the reaction scheme, which does not show any ammonia as it is consumed partially for nitrogen introduction into the ZnO lattice and the rest is oxidized. Ammonia generation and utilization is indicated in the scheme. [2] In case of co-incorporation, the nitrogen affinity elements like In and Ga would be present in gaseous state during the combustions conditions. There are ample of chances for the elements to interact with ammonia and thermodynamically, the formation of nitride is favoured. To compensate charge neutrality, metal ion incorporation is also favoured in form of nitride.

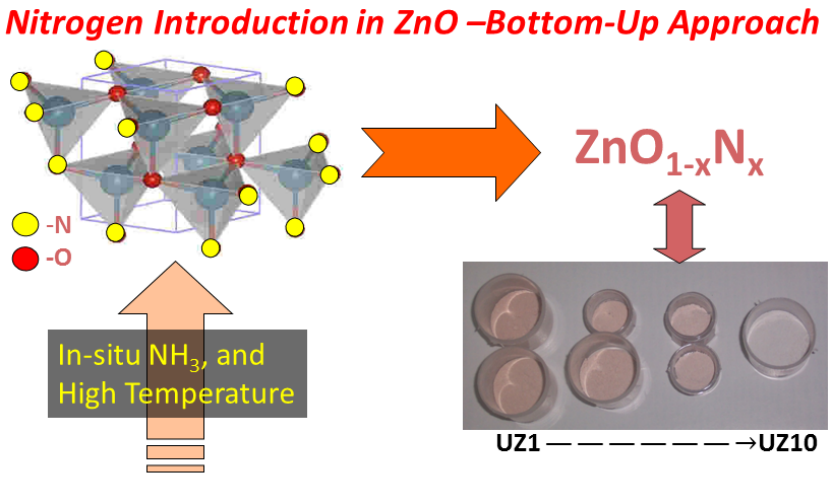

Figure 2.1 Illustration on Nitrogen Incorporaion in ZnO through solution combustion method.

a. GaN:ZnO solid solutions ($Zn_{1-y}Ga_y)(O_{1-z}N_z$)

SCM was adopted wherein urea, as fuel, was used. Gallium nitrate (from Sigma Aldrich), zinc nitrate and urea (both from Merck) were used without further purification. Urea/(Zn+Ga) molar ratio was kept constant at 5. Required amounts of zinc nitrate hexahydrate, gallium nitrate hydrate and urea were dissolved in 10 ml of water and stirred to form homogeneous solution. The homogenous solution was kept inside a muffle furnace, in which temperature was maintained at 500 ^{0}C. The voluminous combustion process occurs, after water boils off in the first few minutes, and leads to $(Zn_{1-y}Ga_y)(O_{1-z}N_z)$. Depending upon the composition, the color of the material varies from bright yellow to dark yellow. The material preparation can be completed within 10 minutes and the same was confirmed for many times in different batches to prove high reproducibility and the same was confirmed at least fifty times. The material remains stable at ambient conditions for a period of about a year in a typical laboratory conditions. The codes of the materials are given as ZGy, Z and G representing zinc and gallium followed by a numeral y indicating Ga content in mol percent. Material prepared without gallium is $ZnO_{0.914}N_{0.086}$ is denoted as UZ5.

b. InGaN Quantum dots @ZnO ($Zn_{1-x-y}In_xGa_y)(O_{1-z}N_z$)

One pot solution combustion synthesis is adopted. Urea to indium + zinc + gallium nitrates molar ratio was kept constant at 5. Required amounts of zinc nitrate hexahydrate, gallium nitrate hydrate, indium nitrate hydrate and urea were dissolved in 10 ml of water and stirred constantly until homogenous solution was formed. Reference ZnO is prepared by evaporating zinc nitrate hexahydrate without using urea. This homogenous solution was kept inside a muffle furnace, which was pre-heated and maintained at 500^{0}C. The voluminous combustion process occurs, after water boils off in the first few minutes, and leads to fine powder of InGaN@ZnO. Depending upon the composition, the colour of the material varies from yellow, dark yellow, deep orange to reddish orange. 2 g of any InGaN@ZnO composition can be prepared easily in a single batch. Examples on specific amounts of the

starting materials along with respective codes are given in Table 1 The material can be prepared within 10 minutes rapidly and reproducibility is confirmed for several times. The material remains stable at ambient conditions for at least 9 months period of time.

Table 1: Starting materials along with respective code and color of the products

Code	$ZnNO_3.6H_2O$ gm	$GaNO_3.H_2O$ gm	$InNO_3.H_2O$ gm	Urea	Colour
I2G2	11.422 g	0.2044 g	0.4812 g	12 g	Deep yellow
I5G2	11.065 g	0.2044 g	0.620 g	12 g	Reddish orange
I5G8	10.352 g	0.8178 g	0.6016 g	12 g	Reddish orange
I3Ga12	10.114 g	1.2265 g	0.361 g	12 g	Deep orange

The materials are designated as IxGy, where x and y are variables and indicating nominal input of In and Ga mol percent respectively. Examples on specific amounts of the starting materials along with respective codes are given in Table 1. In terms of mol content- 0.04 mol is maintained for urea and total 0.04 mol of metal nitrate mixture. Examples on specific amounts of starting materials, color of the product, respective codes, surface area of the product – InGaN quantum dots: ZnO are tabulated. To the best of our knowledge, this is the first report on solid state synthesis of QDs within 10 minutes, distinguished from various solution-based processes dominating till date.

2.1.3 Incipient Wet Impregnation Method

The impregnation method is useful to physically bind two materials. One of the components is taken as major constituent and act as support. There are two types of impregnation methods, namely dry impregnation

method and incipient wet impregnation method. The dry method is that the gaseous vapor of minor component is sprayed over the major component. This method is very fast method and require small amount of components. The disadvantage associated with the method is that the nanomaterials will not be dispersed and the clusters are agglomerated. The interaction of the physical contact remains poor due to poorly embedded minor components on the surface of major component.

The wet impregnation method is that the support material is suspended in aqueous solution of minor component. The selection of solvent is based in such a way that support is to be suspended state and the minor component is to be in well dissolved state. This method is advantageous in better dispersion of nanomaterials over the support and that is expected feature in the photocatalyst for easy light penetration. The nanoparticle of the minor constituent is nucleating and growing into clusters on the support and thus, the nanoparticles is deeply buried into the matrix creating composites with tightly bound components. In this thesis, the composites ZnO/InGaN(QD)@ZnO and InGaN(QD)@ZnO/NiO are prepared by using incipient wet impregnation method.

Composites

a. InGaN(QD)@ZnO/ZnO

ZnO component A is prepared by using biocompatible agents and glycerol is selected for that purpose. Glycerol which is highly viscous solvent is having good solubility in water due to alcoholic –OH groups. The notable property associated with glycerol is that it can form three dimensional (3D) networks by chelating through alcoholic OH groups. Glycerol is dissolved in 100 ml of water and heated the solution to boiling condition for 15 minutes of reaction time. To the boiling solution, zinc nitrate is added with constant stirring and 0.1 M of sodium hydroxide for forming zinc hydroxo species is added. A white milky solution is formed and then the temperature is maintained at 80^{o}C and continued for stirring for 15 minutes. Zinc hydroxo species formed chelates with glycerol and thus there is a formation of 3D network of hydroxo species. The powder of InGaN

(QD)@ZnO of desired proportion of In and Ga is mixed with the growing hydroxo networks. The reactant mixture is kept under stirring for 45 minutes and yellow precipitate was filtered. The precipitate was washed with dilute ethanol solution for several times to remove unreacted hydroxo species. The yellow precipitate is calcined at 300 ^{o}C for 2 hours in open air atmosphere. The resultant orange colour solid is analyzed for structure and activity.

Upon heating, zinc hydroxo species form ZnO along with binding of glycerol. The presence of InGaN(QD)@ZnO (component B) in the growing oxo clusters, there is integration in the composite structure. Component B is highly stable towards heating and basic conditions and therefore further oxidation of nitrides is not possible. When the solid is calcined, the glycerol is converted into carbon-di-oxide and orange coloured solid is obtained. Component B with different proportions of In and Ga are varied and the respective composites are prepared.

For the purpose of comparison, the alternate way of preparation is that component A is formed first and component B is added to the dilute alcoholic solution containing component A.

b. InGaN(QD)@ZnO/NiO

The powder of InGaN(QD)@ZnO of 100 mg is suspended in water of 100 ml of volume and it is kept under stirring for 15 minutes at 80 ^{o}C. To the suspension, nickel nitrate of 10^{3} M is added and 0.001 M of sodium borohydride which is used as reducing agent as well as nucleating agent is added. After it is allowed for stirring for 15 minutes, 0.01 M sodium hydroxide is added and stirring is continued for 3 hours. Sodium hydroxide is used for producing the nickel hydroxo species which is reduced to nickel metal by sodium borohydide. The nucleating nickel metal nanoclusters are subjected to oxidation to nickel oxide under heating in open atmosphere. As per the literature reports, however there will be bilayer of Ni/NiO formation. At the same time, nanoclusters of Ni/NiO are deposited on the suspended InGaN(QD)@ZnO material resulting greenish yellow powder which is filtered and washed with hot water for several times to remove free Na ions. The catalyst is dried at the temperature of 45 ^{o}C in oven for 24 hours.

Composites containing 2 wt% and 4 wt% of Ni/NiO are prepared and the contents of In and Ga is also varied.

2.2 Photocatalytic Activity Studies

The photocatalytic activity of the materials is evaluated by the efficiency of conversion of incident light energy into useful energy forms. The photocatalytic studies for alchol oxidation into ketone, hydrogen generation from water with and without sacrificial agents, effect of pH, electrolytes and photocurrent generation are demonstrated. The descriptions on the reactor designs followed by the details on reaction conditions of catalytic studies are given.

2.2.1 Photocatalytic Reactor

Based on the scale of the reaction and source of irradiation, the photocatalytic reactors are designed. For small scale reaction of volume of 50 ml, direct irradiation is used and for the large scale reactions, the volume of 200 ml, immersion well reactor is used. The reactors are made up of quartz glass reactor that can able to withstand high temperature and long hours of heating. The reactions that are carried out under UV irradiation, borosil glass reactor is to be avoided because of the fact that borosilicate absorbs UV light irradiation. The basic design of the reactor consists of central well portion in which the lamp is inserted. UV light source uses the power supply of 400 watts medium pressure Hg lamp and visible light source uses 125 watts Xenon lamp. The outer jacket of the reactor has the provision for continuous water circulation. In case of immersion well reactor, the second outer double neck jacket will be there in which reactant solution, suspended catalyst is taken and stirred. The openings of the neck are closed properly and one neck is closed with septum. The products are periodically withdrawn and analyzed by GC.

To perform reactions under sunlight, one sun condition was simulated with solar simulator (standard source of Oriel 300 watts). The cut-off filters of different wavelengths are used to determine the conversion efficiency over

the range of visible wavelengths. There is attachment of clamp with shutter on/off system that allows the light to pass for direct irradiation purpose. The reactants and suspended powder are taken in round bottom flask of 50 ml volume and it is kept under stirring for required time. Below is the photograph of the solar simulator reactor system.

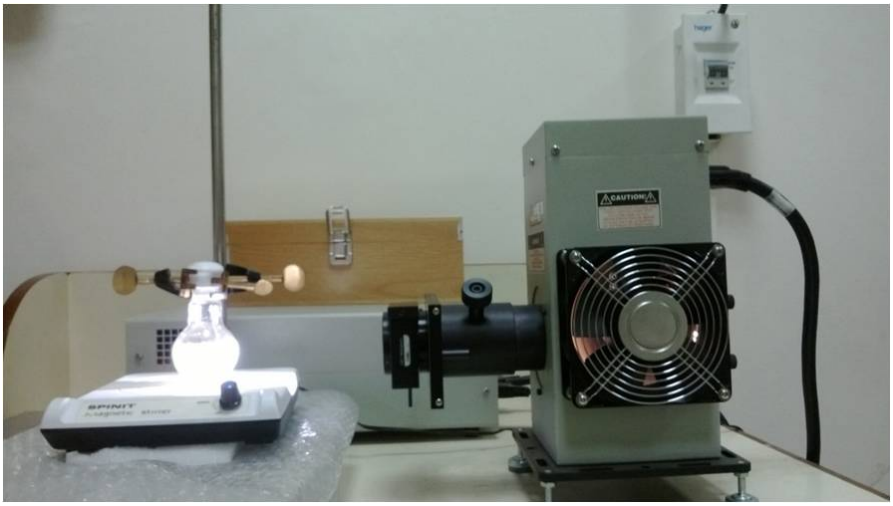

Figure 2.2. Photocatalytic reaction set up using solar simulator source

2.2.2 Photoelectrochemical Set-up

The conversion of light energy into current is measured through photoelectrochemical set-up. Conventional three-electrode set up with potentiostat is used in which the working electrode is catalyst deposited FTO plate. The reference electrode is the platinum foil of 1 mm diameter which is stabilized by using ferrocene in conventional method. The reference potential is also compared with Ag/AgCl electrode and the counter electrode is used as platinum wire. 0.05 M of lithium per chlorate at neutral pH is used as solution electrolyte for all the samples.

2.2.3 2-butanol Dehydrogenation

Ethyl methyl ketone is industrially important raw material for variety of products such as varnishes, cosmetics and key intermediate in organic compounds. Photocatalytic conversion of 2-butanol to 2-butanone in water is

cost effective viable approach. In this work, 30 mg of desired InGaN(QD)@ZnO composition was suspended in 20 ml of reactant solution comprising 4 ml of 2-butanol and 16 ml of water. The suspended solution taken in air tight 50 ml round bottom flask and irradiated for 2.5 h under visible light source of 125 watts. $NaNO_2$ solution was employed as cut-off filter to remove any UV photons below $\lambda \leq 420$ nm. Cold water circulation in the outer jacket of the lamp was carried out to maintain constant temperature (22 ^{0}C) during irradiation. After 2.5 h the solution was filtered and the filtrate was subjected to product analysis. Indeed from the complete miscible solution to immiscible organic layer formation after irradiation demonstrates a formation of hydrophobic organic compound. The product is separated by separating funnel. On product analysis it was confirmed that the organic layer contains 2-butanone.

2.2.4 Hydrogen Evolution - Water Splitting

Photocatalytic generation of hydrogen was measured by overall water splitting and without using any sacrificial agent , with methanol as sacrificial agent. Water splitting was also measured with different cut-off filters, so that light with different range of wave length was incident.

a. Hydrogen Evolution from Water with pH Adjustment: 40 mg of InGaN(QD)@ZnO was suspended in 40 ml of reactant aqueous solution adjusted to pH 4.5 containing H_2SO_4. The suspended solution was taken in an air tight 50 ml volume round bottom flask and irradiated for 4 h with visible light irradiation. An Oriel instruments solar simulator equipped with a 300 W xenon arc lamp system with an AM1.5 cut-off filter as irradiation source was employed. Cool air circulation was employed to maintain a constant temperature (27 °C) during irradiation. After 4 h, gas analysis was carried out by an online GC equipped with a TCD detector (Agilent 7890) for quantitative analysis. In this experiment, sacrificial agent was not added and the bare catalyst is used without the loading of any noble metal nanoparticle. The experiments are analyzed with varying the proportions of

In and Ga in InGaN(QD)@ZnO. Using area integration under the curve, the rate of hydrogen evolution per hour is obtained

b. Hydrogen Evolution from Water Containing Sacrificial Agent: 40 mg of InGaN(QD)@ZnO was suspended in 40 ml aqueous methanol solution (25 % v/v) containing methanol as sacrificial agent. Other conditions are maintained as given in sec. 2.2. The bare catalyst is used as such without assistance of any noble metal nanoparticle. The catalysts with different proportions of In and Ga are evaluated for this experiment and the value of hydrogen evolution for different catalyst for the period of 1 h and per gram is calculated.

c. Effect of Incident Wavelength: Among the catalysts that are evaluated for above experiments, the best catalyst is probed for the effect of incident wavelength. The efficacy of the catalyst to convert absorbed light energy for hydrogen generation at different wavelengths using cut-off filters of **410** nm, **455** nm, **515** nm, **550** nm and **610** nm is demonstrated using same reaction conditions. The use of visible light cut-off filters particularly cut-off filter of 515 nm which is essential for photosynthesis is highly emphasized. In addition, the catalyst exhibits absorption extended around 670 nm of wavelength the activity evaluation is done using 610 cut-off filter.

d. Effect of Electrolyte: The availability of sea water is much higher than the pure water. The presence of electrolytes makes the difference between the nature of sea water and pure water. Thus artificial sea water that is made by dissolving the mixture of following electrolytes:

a. **Mild Sea Water**: relatively mild Sea water proportions in 40 ml of the volume NaCl; 0.285 g, $MgSO_4$; 0.0682 g, $MgCl_2$; 0.0516 g, $CaCl_2$; 0.0147g, KI; 0.001 g

b. **Hard 'sea water'** proportions; 4 times to mild sea water.

NaCl ; 1 g, $MgSO_4$; 0.290 g, $MgCl_2$; 0.260 g, $CaCl_2$; 0.189g, KI ; 0.004 g

Using the above mixture as reactant, the photocatalytic hydrogen generation by the best working catalyst is demonstrated with the same the reaction conditions.

2.2.5 Photocurrent Generation

Photocurrent generation using semiconductor materials as working electrode is of great interest.[3] PEC studies on the new materials were carried out using Gamry 3000 potentiostat/Galvanostat/ZRA in a conventional three-electrode test cell with platinum wire and a platinum foil as the reference and counter electrodes, respectively, in 0.5M lithium percolate solution at ambient conditions maintaining 0 V potential constantly. Maintaining 0 V potential is of prime importance to represent open short circuit current density of the materials. InGaN(QD)@ZnO coated on FTO plate was used as the working electrode. FTO plates were cleaned thoroughly and the powder slurry made by 5 mg of powder in 1 ml of isopropanol was drop casted on the electrode surface and dried at room temperature. This electrode was used as the working electrode for all the electrochemical studies. Irradiation source is Oriel instruments 300 watts Xenon arc lamp adapted with various filters such as A.M 1.5 filter, broad-band pass filter allowing wavelengths from 380 nm to 770 nm and other cut-off filters at specific wavelengths 455 nm, 515 nm, 550 nm and 610 nm is used as irradiation source.

Liner Sweep Voltametry (LSV) messurements were recorded under continuous light irradiation with broad-band pass filter having 80% transmittance in the spectral range from 380 nm wavelength to 770 nm wavelength at the scan rate of 10 mV/s in the potential sweep from -0.5 to 0.5 V, and the same conditions under dark also. This voltage range is followed because of the reason of material stability. The irradiance power with use of filters is checked by LUX meter.

Chronoamperometry measurments were recorded at 0V using the same irradiation source and with filters mentioned above. When the shutter is opened the current rises and when the shutter is closed, current drops immediately. The immediate response highlights the photofunctional behaviour of the material. Over the entire peiod of time of shutter opening the current remains constant demonstrating the current production is exclusively due to photoresponse of InGaN@ZnO.

The solar energy conversion efficiency for the materials was evaluated using the conventional formula given as follows:

$$IPCE = (1240 \times ImA\ cm^{-2}) / (\text{cut-off } \lambda\ nm \times J\ mW\ cm^{-2})$$

where I denotes the current density at 0 V in the chrono-amperometry measurements with respect to the incident wave-length.

2.3 Physicochemical Characterization

2.3.1 Introduction

To understand any catalytic material, thorough physicochemical characterization using relevant techniques is a necessary prerequisite. Routine techniques such as X-ray diffraction, UV-visible absorption spectroscopy, Raman spectroscopy, X-ray photoelectron spectroscopy, microscopy, surface analytical techniques and thermo gravimetric analysis are adopted in order to obtain information on chemical composition, morphology, active sites, surface structure, particle size, photofunctional features and chemical nature of incorporated elements. Local structure analysis is done by using EXAFS studies. The fragments on the surface of the matrix are mapped and analyzed using secondary ion mass spectroscopy. Recyclability and effect of photocorrosion in the catalyst are also tested. The techniques that are used for evaluating photocatalytic activity are also explained. Instrument used for some of the standard or routine measurements are mentioned in the following. Some of the special or rarely used experimental methods are provided in detail.

2.3.2 Experimental Methods

XRD patterns were recorded on a Philips X'Pert Pro powder X-ray diffractometer using Cu K_α radiation (l = 1.5418 Å) with a flat sample stage in the Bragg–Brentano geometry.[3, 4] The diffractometer was equipped with a Ni filter and X'celerator as detector. The samples were scanned in the range $2\theta = 5–75^o$ and the scans were collected.

Extended X-ray Absorption Fine Structure Analysis (EXAFS)

The presence of minor impure phases in the lattice can act as recombination centers in a photocatalyst and also bring serious changes in the electronic structure of the material. Therefore it is necessary to probe the local structure of the material and thus we had demonstrated the EXAFS studies on ZnO rich: GaN solid solutions with varying contents of Ga element. The EXAFS measurements were carried out under the dispersive EXAFS beamline (BL-8) in transmission mode at the INDUS-2 Synchrotron Source (2.5 GeV, 100 mA) at Raja Ramanna Centre for Advanced Technology (RRCAT), Indore, India. The beamline uses a 460 mm long Si(111) crystal having 2d value equal to 6.2709 Å, mounted on an elliptical bender, which can bend the crystal to take the shape of an ellipse.[5-7] The radiation transmitted through the sample was detected by a position-sensitive CCD detector with 2048 x 2048 pixels. A plot of the absorption versus photon energy was obtained by recording the intensities I_0 and I_T, as the CCD outputs, with and without the sample, respectively. The absorption coefficient was obtained using the following relation:

$$I_T=I_0e^{-\mu x}$$

where axis the thickness of the absorber. Samples of appropriate weight, estimated to obtain a reasonable edge jump, were taken in powder form and thoroughly mixed with cellulose powder to obtain a total weight of 100 mg and homogenous pellets of 15 mm diameter were prepared using an electrically operated hydraulic press. The Zn K-edge and Ga K-edge XAS measurements were performed. For the present measurement, a Si(111) crystal was set at an appropriate Bragg angle to obtain a band of energy around 9659 or 10 367 eV at Zn K-edge or Ga K-edge, respectively for the EXAFS measurements. Zn and Ga filters were used for the calibration of CCD channels for the Zn K-edge measurements, while for the Ga K-edge measurements, Ga and Ge filters were used. To control the oscillations in the absorption spectra, m(E) was converted to absorption function w(E) defined as follows:

$$\chi(E) = \frac{\mu(E) - \mu_0(E)}{\Delta\mu_0(E_0)}$$

Where E_0 absorption edge energy, $\mu_0(E_0)$ is the bare atom background and $\Delta\mu_0(E_0)$ is the step in $\mu(E)$ value at the absorption edge. The energy dependent absorption coefficient $\chi(E)$ has been converted to the wave number dependent absorption coefficient $\chi(k)$ using relation,

$$K = \sqrt{\frac{2m(E - E_0)}{\hbar^2}}$$

where m is the electron mass. $\chi(k)$ is weighted by k^2 to amplify the oscillation at high k and the $\chi(k)k^2$ functions are fourier transformed in R space to generate the $\chi(R)$ versus R spectra in terms of the real distances from the center of the absorbing atom. The set of EXAFS data analysis available in within IFEFFIT software package have been used for EXAFS data analysis [9]. This includes background reduction and Fourier transform to derive the $\chi(R)$ versus R spectra from the absorption spectra (using ATHENA software), generation of the theoretical EXAFS spectra starting from an assumed crystallographic structure and finally fitting of experimental data with the theoretical spectra using ARTEMIS software.[7-12]

Secondary Ion Mass Spectrometry (SIMS)

The composition of the surface and deep layers up to 10μm is analyzed using SIMS technique that operates on the principle of sputtering the ion using molecular ion beam with energy of 1-30 KeV and the sputtered ions are analyzed in coupled mass spectroscopy. In this work, the chemical composition of the fragments are mapped using Bi3+ ion in a local point on the matrix before sputtering process. The pixels of the fragments and color profiles are the relative measure of the intensity of the particular fragment in that local point. In our work, Bi^{3+} primary ion source is utilized for adopting well distinguished fragmentation and the sputtered fragments are identified by coupled mass spectrometer.[13] The numerical scales given in range of

colours against every image refer to the intensity of particular fragment in that location in the sample matrix.

The surface area of the catalysts was determined by the Brunauer–Emmett–Teller (BET) method via nitrogen adsorption on NOVA 1200 Quanta Chrome Equipment. Thermal analyses of these adducts were recorded by Perkin–Elmer Diamond's thermogravimetry (TG) and differential thermal analysis (DTA) with alumina as the internal standard. UV-Visible absorption for solutions was collected in the same instrument with water as reference.[14]

Photoluminescence spectroscopy is a complimentary technique to UV-Visible spectroscopy that gives information on the electronic structure from the emission process (fluorescence) of the excited electron to the ground state. Photoluminiscence (PL) measurements were performed using Photon Technology International spectrophotometer equipped with Hg-Cd source at room temperature under the excitation light of 330 nm. The conditions are maintained to compare the photocatalytic conditions.[15] Raman spectra were recorded on a Horiba JY Lab RAM HR 800 spectrometer excited with 633 nm lasers.[16] Diffuse reflectance UV-Vis measurements were performed on a spectrophotometer (Shimadzu, Model UV-2550) with spectral grade $BaSO_4$as the reference material.

XPS measurement has been made using a custom built ambient pressure XPS system from Prevac, Poland, and equipped with VG Scienta SAX 100 emission controller monochromator using AlKα anode (1486.6 eV) in transmission lens mode. The photoelectrons are energy analyzed using VG Scienta's R3000 differentially pumped analyzer. The spectra were recorded at a pass energy of 50 eV. [17]

The gas products are collected and injected into GC(online) equipped with TCD detector (Agilent 7890) through the gas tight septum valve. The morphology of the catalyst was examined by environmental scanning electron microscopy (E-SEM).[18] EDAX measurements described in this thesis were performed on a Leica Stereoscan-440 scanning electron microscope instrument equipped with a Phoenix EDAX attachment. Elemental mapping was carried out in above mentioned SEM system with recently equipped with an EDAX analyzer (Bruker, D451-10C Quantax 200

with X-flash detector) attachment. X-flash 4010 detector was employed for fast and high resolution real time spectrometry and elemental mapping. EDAX spectra were recorded in the spot-profile mode by focusing the electron beam onto specific regions of the sample. However, materials composition reported is based on the data collected over large areas (>300 μm^2). Chemical analysis of solid materials and for Zn-leaching due to photocorrosion was measured by inductively couple plasma (ICP) instrument with atomic absorption analyzer of model WFX-320 AAS model designed with Argon as carrier gas.

Linear Sweep Voltammetry (LSV)

To monitor the change in current, this technique is used using the principle of voltammetric method in a conventional three electrode immersed in the electrolyte bath system. The current of the working electrode is measured while the potential between reference electrode and counter electrode are sweeping from positive potential to negative potential. Linear sweep voltammogram is the half the cycle of the cyclic voltammetry and redox potential of the elements in the catalyst can be identified. In case of photocurrent generation experiment, the catalyst should not be allowed to undergo both oxidation and reduction reactions because faradiac current should not be confused with the current generated by the conversion of light energy absorbed into excited electron/hole carriers. The window of the potential sweep is to maintain in the range that does not cause corrosion of the catalyst.

Chronoamperometry

This technique is used to analyze the sustainability of the current generation over a period of time. In case of electrochemical applications, the change concentration of electroactive species with respect to time or in other words, the reaction kinetics is monitored using chronoamperometry technique. However, in case of photocatalytic applications, the photocurrent generation is expected only due to the photofunctional behaviour not the

faradiac process. In that case, the plot of current Vs time is done along with the light irradiating shutter on/off operations. When the shutter for light irradiation is opened, current rises and maintains at the same value. The value of current generation drops on closing of the shutter.

2.4 Conclusions

The aspects of preparation methods, reaction conditions, experimental reactor set up are explained in detail. The plausible mechanism for the formation of the product is also described with suitable illustration. The characterization methods which are adopted in thesis chapters are summarised along with instrumental conditions.

2.4 References:

1. K. Sivaranjani and C. S. Gopinath, *J. Mater. Chem*., 2011, **21**, 2639.
2. M. Mapa, S. RajaAmbal and C. S. Gopinath, *Trans. Mater. Res. Soc. Jpn*., 2013, **38**, 145.
3. H. P. Klug and L. E. Alexander, X-Ray Diffraction Procedures: For Polycrystalline and Amorphous Materials, 1974, 618 John Wiley and Sons, New York.
4. B. D. Cullity and S. R. Stock, Elementsof X-ray Diffraction, 2001, Prentice Hall, Upper Saddle River, NJ 07458, 3rd edition.
5. D. Bhattacharyya, A.K. Poswal, S.N. Jha, Sangeeta and S.C. Sabharwal, *Nuclear Instruments Method. in Phys. Res. A,* 2009, **609,** 286.
6. D. Joseph, S. Basu, S.N. Jha and D.Bhattacharyya, *Nuclear Inst. and Methods in Physics Research B,* 2012, **274,** 126.
7. I. Neetika, A. Das, I. Dhiman, A. K. Nigam, A. K. Yadav, D. Bhattacharyya and S. S. Meena*, J. Appl. Phys.* 2012, **112** 123913.

8. S. Basu, Salil Varma, A. N. Shirsat, B. N. Wani, S. R. Bharadwaj, A. Chakrabarti, S. N. Jha and D. Bhattacharyya, *J. Appl. Phys.* 2012, **111,** 053532.

8. S. Basu, B. S. Naidu, M. Pandey, V. Sudarsan, S. N. Jha, D. Bhattacharyya, R. K.Vatsa and R. J. Kshirsagar, *Chem. Phys. Lett.* 2012, **528,** 25.

9. D.C. Konigsberger and R. Prince, *X-Ray Absorption: Principles, Applications, Techniques of EXAFS, SEXAFS and XANES,* 1988, Wiley publications, New York.

10. M. Newville, B. Ravel, D. Haskel, J. J. Rehr, E. A. Stern and Y. Yacoby, *Physica B* **154,** 1995, 208.

11. E. H. Kisi and M. M. Elcombe, *Acta Cryst.*, 1989, C45.

12. A. Benninghoven, F. G. Rüdenauer and H. W. Werner, Secondary Ion Mass Spectrometry: Basic Concepts, Instrumental Aspects, Applications and Trends. 1987, Wiley publications, New York.

13. B. C. Lippens and J. H. de Boer, *J. Catal.* 1965, **4**, 319.

14. R. C. Denney and R. Sinclair, Visible and Ultraviolet Spectroscopy Analytical Chemistry by open learning series, John Wiley and Sons, USA.

15. C. N. Banwell and E. M. McCash, Fundamentals of Molecular Spectroscopy Fourth Edition ed. Tata Mc-Graw-Hill Publishing Company limited.

16. D. Briggs and M. P. Seah, Practical Surface Analysis, Vol. 1: Auger and X-ray Photoelectron Spectroscopy, 2nd ed., Eds., 1990.Wiley, New York,

17. http://en.wikipedia.org/wiki/Scanning_electron_microscope#cite_ref-7.

Electronic structure aspects of $(Zn_{1-y}Ga_y)(O_{1-z}N_z)$ and its correlation to solar light driven photocatalytic activity

3.1 Introduction

Development of visible light active photocatalytic systems is at the centre stage in the field of semiconductor photocatalysis towards solar harvesting.[1] Generally, light absorption in the whole of visible light range and effective utilization of photogenerated charge carriers are the prime features expected in a desired photocatalyst for most of the photocatalytic applications. In this scenario, imparting visible light absorption in catalytically potent wide band gap semiconductors such as TiO_2, ZnO, TaO_2 and ZrO_2 received wide research interest.[2] Band gap engineering is considered to be indispensible way to bring extended visible light absorption in wide band gap semiconductors, leading to new hybrid materials namely oxynitrides, oxysulphides, solid solutions, quantum dot integrated materials.[3-6] Among all class of hybrid materials, solid solutions are ideal for structural and electronic integration of active components. The integration aspect of solid solutions allows the advantages of composition tuneable absorption,[7] least defect densities, long standing stability,[8] easy flow of charge carriers[6] that are necessary requisites for solar harvesting.

Solid solutions comprised of metal oxides and metal nitrides as integral structural parts finding great interest for photocatalytic water splitting as well as H_2 generation applications. Domen et al developed GaN:ZnO solid solution, with predominant Ga-content, exhibiting visible light absorption in difference with respect to precursors (GaN or ZnO).[9] The absorption features and cooperative performance of the solid solution with cocatalyst for visible light driven photocatalytic H_2 generation motivate research interest in developing solid solutions, such as (GaN:ZnO),[9-11] (ZnO:InN),[12] (ZnO:GeN).[13]

In this report, we demonstrate $(Zn_{1-y}Ga_y)(O_{1-z}N_z)$ solid solution as visible light photocatalyst and investigated the bulk structure-property relationship for evolving virgin photocatalytic activity and/or photocurrent generation. Solution combustion method (SCM) was employed for the synthesis of solid solutions. The adopted method affords rapid synthesis, viability, effective nitridation conditions and high degree of reproducibility. To realize effective charge utilization, structures

promoting fast conduction of photogenerated charge carriers and catalytic active sites are necessary. ZnO which is well known for fast electron conduction and catalytic potential has preferably chosen to be major structural part and GaN as the minor structural part. Taking into advantage of similar lattice structure and matching lattice parameters, formation of solid solution is favoured. $(Zn_{1-y}Ga_y)(O_{1-z}N_z)$ solid solutions with varying Ga and N concentrations are prepared and all the compositions show visible light absorption extended up to 550 nm. Despite the salient features of precursors, ZnO and GaN, the advancement is severely hindered by native defects as oxygen/nitrogen vacancies causing detrimental effects on photostability and sustainable performance. According to literature reports, diffusion of Ga from bulk to surface under ambient conditions lead to formation of impure phases as recombination centres. Therefore it is essential to understand the local structure of Zn and Ga, chemical environment of nitrogen and oxygen in the present solid solution. Investigation on bulk structure property relationship is of prime importance so as to address and to alleviate the limiting factors for developing new photocatalysts.[14-18]

To demonstrate the photoconversion efficiency of virgin solid solution, we carried out photoelectrochemical (PEC) water splitting and solar hydrogen generation without any cocatalyst. $(Zn_{1-y}\ Ga_y)(O_{1-z}N_z)$ solid solution exhibits promising current generation at 0 V under simulated sunlight with AM1.5 filter. It also shows reasonable photocatalytic activity towards visible light driven hydrogen evolution.

3.2. Results and Discussions

3.2.1. X-ray Diffraction Analysis

XRD diffraction pattern of ZGy materials along with reference ZnO is shown in Figure 3.1. The codes of the materials are given as ZGy, Z and G representing zinc and gallium followed by a numeral y indicating Ga content in mol percent and the material prepared without gallium is denoted as UZ5 wherein 5 indicates the fuel to metal nitrate ratio.[5] The XRD patterns of the materials showed similarity with that of the precursor ZnO, indicating the retention of the wurtzite structure. The sharp feature of the peak represents

the high crystallinity of the materials. No peak was observed for Ga_2O_3 or other carbonate species. However, a marginal peak shift to a higher angle was observed for all diffraction features with the incorporation of Ga and N. The inset in Figure 3.1 shows a shift in the (101) diffraction feature. The observation of a peak shift to a higher angle without an impure phase is indicative of solid solution formation and marginal lattice contraction.

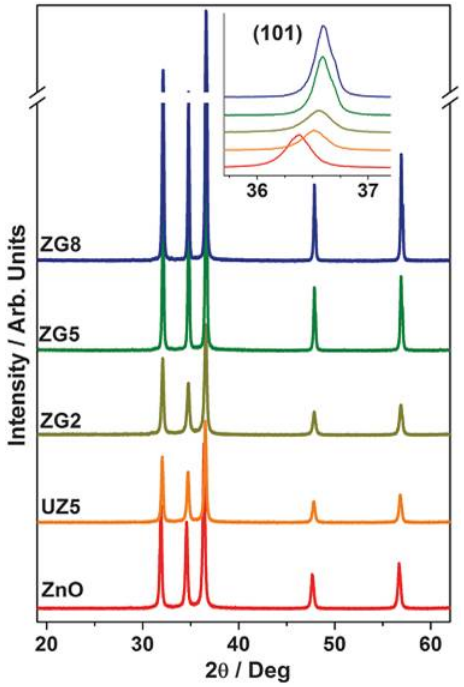

Figure 3.1 XRD patterns of ZGy materials along with the comparison of ZnO and UZ5.

3.2.2. EXAFS Studies:

To understand the local structure of Ga K edge and Zn K edge, EXAFS measurements are performed on UZ5 and ZGy materials with different Ga content. EXAFS near absorption edge study is characteristic of the oxidation state and coordination geometry of absorbing atom. Figure 3.2 shows the normalized EXAFS spectra for solid solutions as denoted as ZGy, measured at Zn K-edge along with XAFS spectrum of ZnO as reference. Normalized EXAFS spectra measured at Zn K edge for nitrogen doped ZnO ($ZnO_{1-z}N_z$) materials is given in Figure 3.3. In both series of materials, the edge position of lattice Zn shows +2 oxidation state and coordination geometry of wurtzite structure which is identical with respect to bulk ZnO. In the present method

of preparation, nitrogen incorporation is accomplished during the growth of zinc oxo clusters and the same plays key role for Ga co-incorporation.

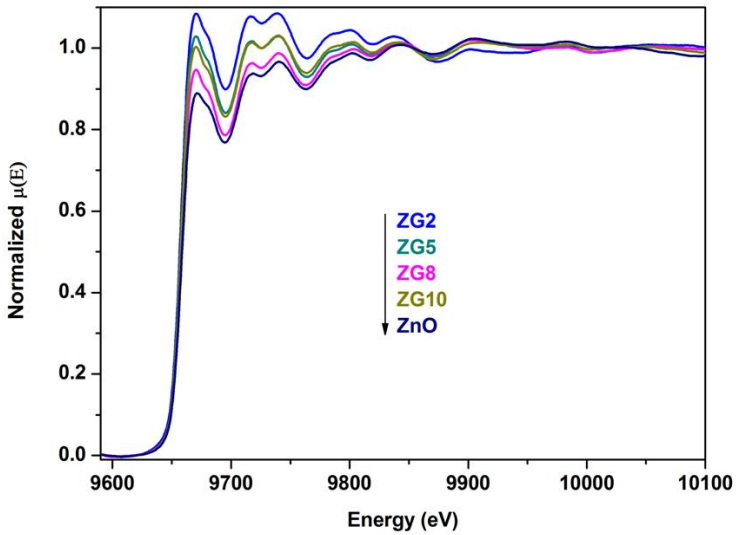

Figure 3.2 Normalised EXAFS spectra of $(Zn_{1-y}Ga_y)(O_{1-z}N_z)$ at Zn K-edge and along with that of ZnO references.

Therefore, the changes in the lattice parameters of N-incorporated ZnO and ZGy, compared to virgin ZnO, are highly expected. To understand the changes in the local environment of lattice Zn, the χ(R) versus *R* spectra; the notations denote Fourier transform in R space in terms of the real distances from the centre of the absorbing atom of nitrogen doped ZnO samples from μ(*E*) versus *E* spectra i.e changes in the absorption edge energy, following the methodology described in Chapter 2, experimental section 2.3.

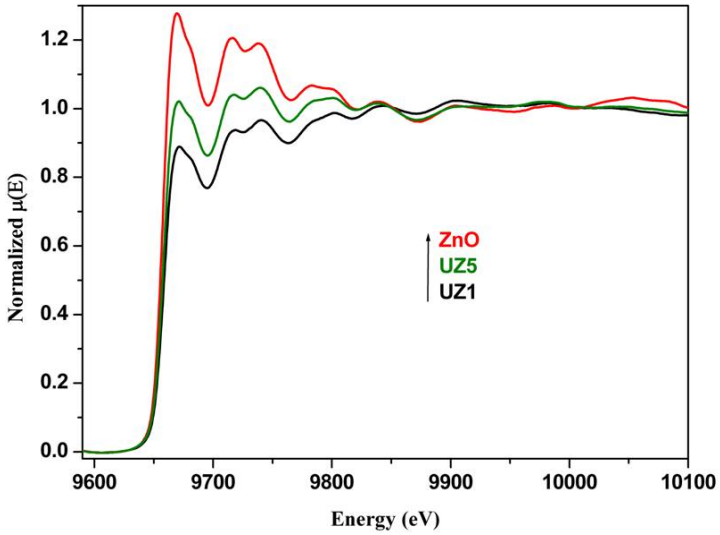

Figure 3.3 EXAFS analysis of nitrogen doped ZnO materials at Zn K edge.

The bond lengths of Zn-O and Zn-Zn second and third shell distances are relatively low in case of nitrogen doped ZnO than that of bulk ZnO. The bond length of Zn-O reduces with the increase in N content in the materials. The above observation agree with the results presented by Mapa et al.,[5] where it has been observed lattice contraction of ZnO upon N doping due to the fact of higher covalency of Zn-N bonds compared to Zn-O bonds. The covalent character increases with increase in N doping concentration and the same result is correlated with our EXAFS result. Another observation is that the coordination of oxygen site decreases whereas that of Zn site increases with N doping. This observation demonstrates nitrogen incorporation at the expense of oxygen vacancies supporting our plausible mechanism on "Bottom-up Approach" for nitrogen doping in growing Zinc oxo clusters[17] (see chapter 2, experimental methods 2.1 for complete explanation). In the case of solid solutions, the local structure analysis of incorporated Ga is also essential as Ga plays major role in stabilizing incorporated N as nitride form.[5, 10] Normalized EXAFS spectra of solid solutions measured at Ga K edge is shown in Figure 3.4 along with Ga_2O_3 as reference.

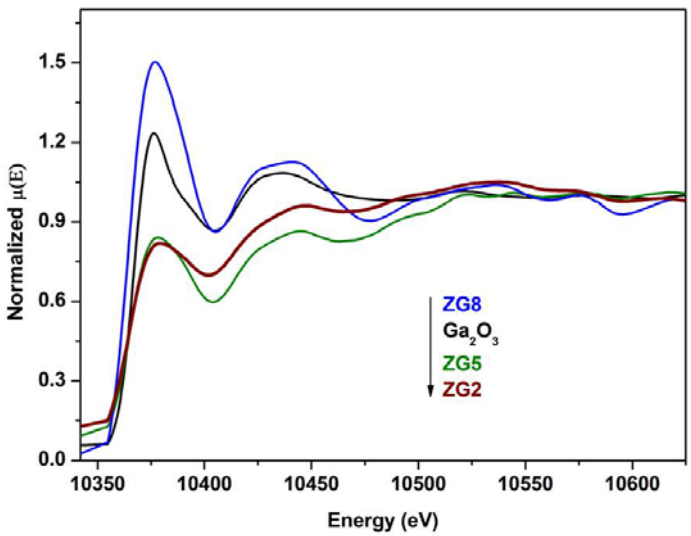

Figure 3.4 Normalised EXAFS spectra of $(Zn_{1-y}Ga_y)(O_{1-z}N_z)$ (ZGy series) at Ga K-edge along with that of Ga_2O_3 reference.

The edge position of incorporated Ga shows +3 oxidation state in the solid solutions. The oxidation state of Ga remains same in both chemical forms: GaN and Ga_2O_3. To confirm the coordination geometry and chemical

environment of Ga in ZnO lattice, structural models of monoclinic Ga_2O_3,[23] hexagonal GaN[23] and ZnO models[23] are used to generate theoretical EXAFS spectra for fitting purpose. The structural parameters (atomic coordination and lattice parameters) of wurtzite ZnO, GaN and Ga_2O_3 used for the simulation of theoretical EXAFS spectra have been obtained from reported values in the literature.[23, 24] It is to be mentioned here that Fourier transformed data upto only 1st shell has been considered. In the first place, simulations of theoretical EXAFS spectra of the materials have been obtained assuming that few Zn atoms in wurtzite ZnO lattice are replaced by Ga atoms. The best fit theoretical $\chi(R)$ versus R spectra using the above models has been shown in Figure 3.5. The best fit is obtained when GaN (Wurtzite) structure is used instead of the other two models. The correlation between theoretical GaN model and experimental result substantiate the presence of GaN form. The co-ordination number of Ga in GaN is 4, whereas the coordination number of Ga in Ga_2O_3 is 6.

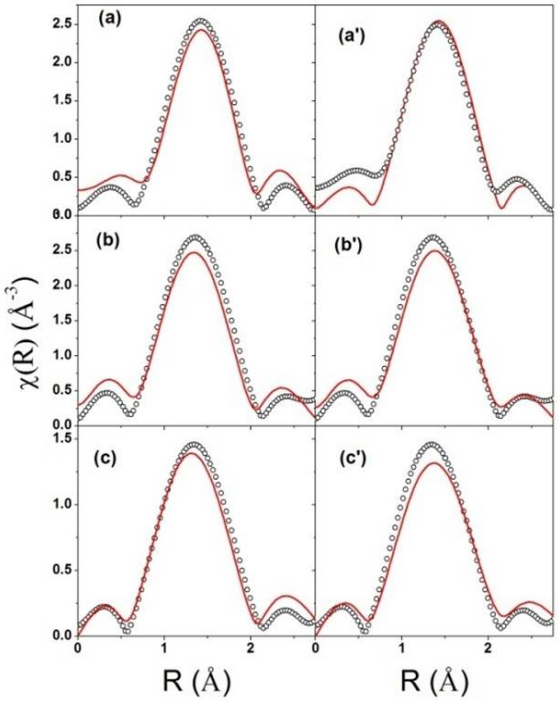

Figure 3.5 Fourier transformed EXAFS spectra of $(Zn_{1-y}Ga_y)(O_{1-z}N_z)$ (ZGy series) at Ga K-edge (Scatter points) and theoretical fit (Solid line). GaN model (left panels) is used as fitting model for (a) ZG5 (b) ZG8 (c) ZG10, whereas right panels show of fitting with Ga_2O_3 model.

As incorporated Ga has the co-ordination number of 4, and hence GaN form in ZnO lattice is evident. The Fourier transform calculation involves the averaging out of the local environments throughout the lattice and thus uniformity in presence of GaN form throughout ZnO lattice is revealed. It is also observed that as Ga and N content increases the central atom (Ga) coordination approach to hexagonal GaN structure. This observation shows good agreement that Ga in the solid solution is present in GaN form. The variation of Zn-O and Zn-Zn bond

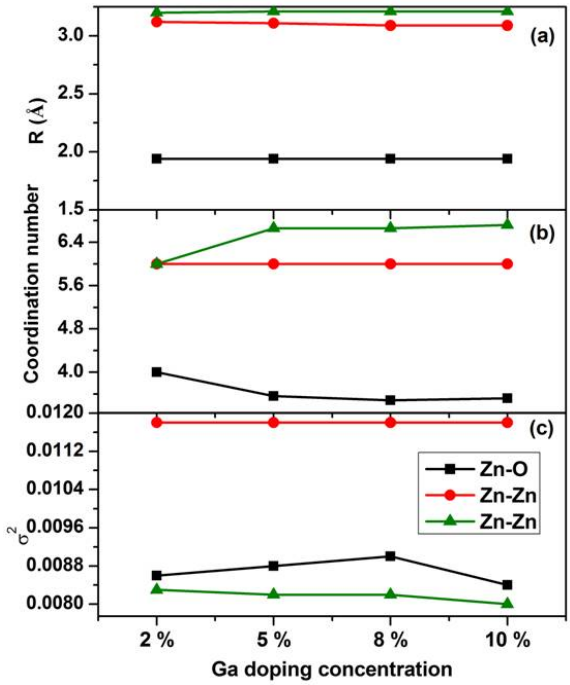

Figure 3.6 Variation of Zn-O and Zn-Zn (a) bond length, (b) co-ordination number, and (c) σ^2 with increasing gallium content in $(Zn_{1-z}Ga_z)(O_{1-x}N_x)$ (ZGy series) samples from EXAFS measurements at Zn K-edge.

lengths, coordination number and disorder (Debye-Waller) factors with respective R-factor, as a function of Ga concentration in the solid solutions from EXAFS measurements at Ga K edge and Zn K edge are given in Table 1 and Figure 3.6, respectively. It has been found that Zn-O bond length for ZGy series of samples are lower than that of bulk ZnO and first and second Zn-Zn/Ga shell bond length indicated in green and red colours, respectively, is found to reduce with increasing Ga content. Similar fit values for UZ5 is also given along with corresponding theoretical values for bulk ZnO. It can

Table-1: Local structural parameters for $(Zn_{1-z}Ga_z)(O_{1-x}N_x)$ (ZGy series) evaluated by EXAFS measurements at Ga K-edge.

Model	Path	Parameters	Theoretical values	ZG5	ZG8	ZG10
ZnO Model[a]	Ga-O	R (Å)	1.91	1.89	1.87	1.86
		N	4	4.4	4.4	4.0
		σ^2		0.001	0.001	0.005
		R-factor		0.01	0.058	0.065
Ga_2O_3 Model	Ga-O1	R (Å)	1.94	1.85	1.86	1.86
		N	3	3	2.76	1.5
		σ^2		0.0041	0.001	0.002
	Ga-O2	R (Å)	2.01	1.91	1.89	1.86
		N	3	2.76	2.955	1.95
		σ^2		0.002	0.0057	0.004
		R-factor		0.02	0.047	0.04
GaN Model	Ga-N	R (Å)	1.94	1.89	1.88	1.87
		N	4	4.8	4.8	4.0
		σ^2		0.001	0.001	0.005
		R-factor		0.01	0.017	0.034

be seen from Figure 3.6 that Zn-O and Zn-Zn bond lengths of ZGy compositions are relatively lower than bulk ZnO. The bond length of Zn-O reduces with increasing nitrogen content. EXAFS result is in agreement with Rietveld refinement study on $(Zn_{1-y}Ga_y)(O_{1-z}N_z)$ materials[10] which revealed a marginal decrease in lattice parameters of solid solutions with respect to ZnO. As the size of the Ga is smaller than Zn, marginal lattice contraction is expected when Ga in the form of GaN is constituted in ZnO lattice. Strong affinity of Ga towards nitrogen and structural similarity between GaN and ZnO facilitates the formation of solid solution.

3.2.3. HRTEM Studies:

HRTEM measurements were carried out for ZGy materials and the representative results are shown in Figure 3.7. This is mainly to explore the homogeneity of solid solutions and the microstructural level as well as the change in morphology. Figure 3.7a shows the morphology of the material for ZG5 composition and lattice planes of the solid solution along with the SAED pattern are given in Figure 3.7.b. Predominant hexagonal structure was observed in TEM results reiterates the hexagonal Wurtzite structure. $(Zn_{1-y}Ga_y)(O_{1-z}N_z)$ possess corrugated structure on the surface, likely, due to the evolution of gases during SCM synthesis. Such surface corrugated structure has been reported to enhance the light scattering[25] and anchoring of the co-catalyst easy.[1,16] Enhancement in light scattering will assist in penetration and interaction of incident photons with the material. Thereby, population of photogenerated charge carriers will be increased.

The intermediate d-spacing values of the materials with respect to parent ZnO and GaN materials demonstrate the solid solution formation. Appearance of uniform lattice fringes without any abrupt interfaces indicates the homogeneity of the solid solution assisting in easy flow of charge carriers. Figure 3.8b shows SAED pattern from which the calculated d-spacing is in good agreement with the earlier calculated value. Homogenous distribution of GaN nanoclusters in ZnO lattice is an essential feature for evolving electronic integration between GaN and ZnO components.

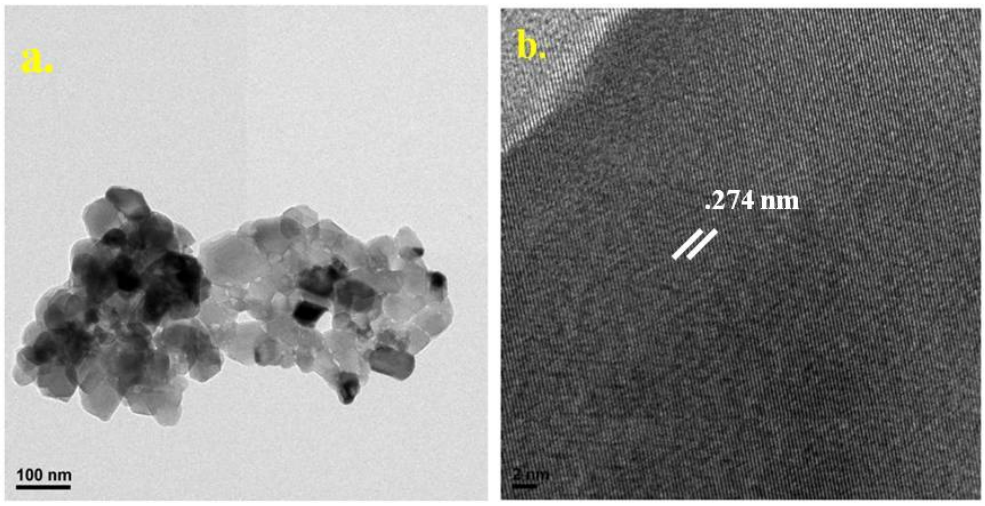

Figure 3.7 HRTEM results obtained for (a–b) ZG5 solid solution. A uniform d100-value, which is in between ZnO (0.282 nm) and GaN (0.277 nm), obtained over large area underscores the solid solution nature.

The lattice planes are analyzed using statistical line profile analysis for calculating interplanar d-spacing value of the solid solutions and corresponding d values are given in the respective image. The d_{100} value of the material is in between that of ZnO (0.282 nm) and GaN (0.275 nm).[6]

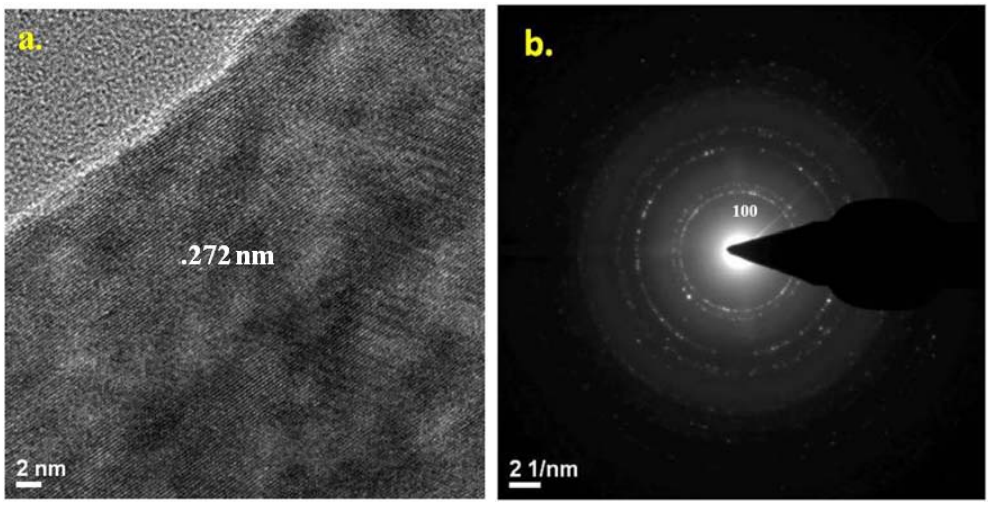

Figure 3.8 HRTEM results obtained for (a-b) ZG8 solid solution. The corrugated structure observed at the edges in panel a, indicates the possibility of easy anchoring of the co-catalysts.

3.2.4. Light Absorption and Emission Studies:

UV-Visible absorption studies were carried out for the solid solutions and the corresponding results are given in Figure 3.9a. The inset in Figure 3.9a shows a digital photograph of the powder form of the solid solutions for the actual colour variations. Upon solid solution formation, the color of the material becomes intense yellow, which is completely different from the colorless ZnO. The absorption spectra of the solid solutions extend into the visible light regime, where the absorption edge onsets between 550 and 600 nm; this is in total contrast to the absorption edge of ZnO precursor at 370 nm. The extended visible light absorption and the bright color associated with the solid solutions indicate the changes in the electronic structure of the solid solutions from that of the parent materials ZnO and GaN.

Room temperature PL studies were performed on the ZGy materials to obtain more information on the electronic structure. Figure 3.9b shows the emission spectra of the solid solutions with different Ga contents along with ZnO (in inset). According to the literature, the near band edge emission of ZnO, which is the precursor of the solid solution appear at 375 nm.[26] In the emission spectra of the ZGy materials, a sharp peak with very low intensity at 375 nm is observed. A decrease in the intensity of the near band edge emission of the materials indicates VB broadening to support the visible light absorption (Figure 3.9a). The phenomenon of VB broadening shifts the VB edge towards lower positive potential (compared to ZnO), resulting in a band gap reduction. Two intense peaks at 420 and 440 nm are observed and those peaks are attributed to the formation of new acceptor levels due to nitride incorporation.[27] This result provides additional supportive evidence for VB broadening, which occurs due to the mixing of N 2p states of nitride with O 2p bands at the top of VB.

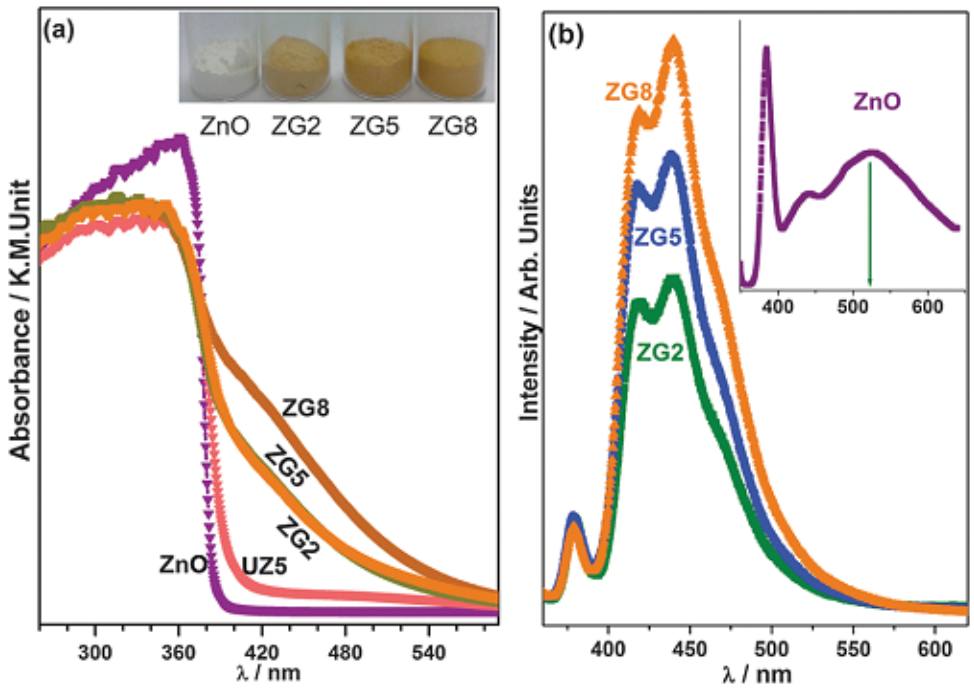

Figure 3.9 Room temperature study of absorption (a), photoluminescence of ZGy with different Ga contents (b).

Another observation from the peaks is that intensity of the peaks at 420 and 440 nm increases with increasing Ga concentration. This indicates that the co incorporation of Ga with N increases the solubility of the latter in the ZnO lattice. Interestingly, the broad emission feature centered on 525 nm in ZnO is completely absent in the case of the ZGy solid solutions. The above emission feature at 525 nm is ascribed to oxygen vacancies, which is responsible for deleterious photocorrosion in ZnO.[28] The absence of broad emission in the green region of the solid solutions highlights the anti-photocorrosive[29] nature of the material with the compensation of oxygen vacancies by effective nitride incorporation.

After corroborating the absorption and emission results, a formation of new energy band overlapping with the top level of the VB was revealed. This phenomenon results in VB broadening, leading notable band gap reduction to 2.4 eV, which results visible light absorption in the material. The schematic representation of VB broadening is illustrated in Figure 3.10

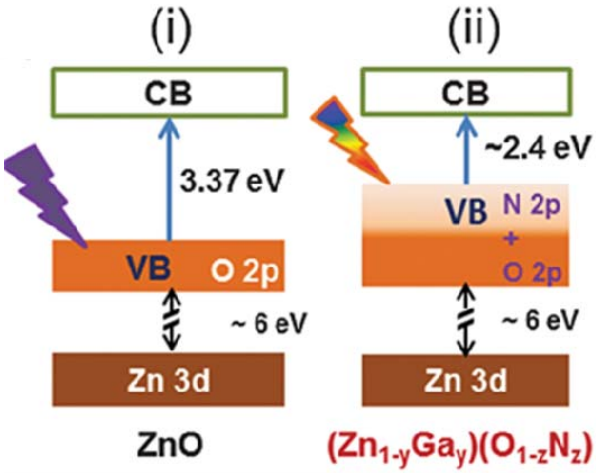

Figure 3.10 Band Structures of (i) ZnO and (ii) solid solutions of ZGy materias are shown. Compared to ZnO, there is possible band-gap reduction in ZGy series to the value of 2.4 eV from 3.37 eV of ZnO is demonstrated with overlapping N 2p states with O 2p band at the top of VB.

that explains the origin of the visible light absorption of the material. It should also be noted that the fully filled Zn 3d band, which is well below the VB in ZnO (by 6 eV), as well as in ZGy, remains at the same energy levels. It is unlikely that Zn 3d bands may have any influence in the VB broadening in ZGy, especially in view of the fully filled orbital.

3.3 Photocatalytic Applications

3.3.1 Photocatalytic Hydrogen Evolution

ZGy materials were evaluated to be a sacrificial agent for visible light ($\lambda \geq$ 400 nm) driven photocatalytic hydrogen generation from aqueous methanol (20%). Experimental conditions for hydrogen evolution are given in the Experimental section, and the corresponding results are tabulated in Table 3. The hydrogen evolution rate increases with increase in the Ga content of the solid solution. This is because visible light absorbance increases to a higher wavelength with increase in the Ga content, and thus the availability and absorption of incident photons increases. When there is more absorption of incident photons with different photon energies, the rate of hydrogen evolution also increases. In contrast, the related solid solution photocatalyst shows negligible activity towards visible light driven hydrogen evolution without a cocatalyst. The use of a noble metal co-catalyst with a

special core–shell morphology increased the activity to 2 mmol/hg of H_2 evolution.[9, 13] The present solid solution enables H_2 evolution without any cocatalyst. The virgin catalyst activity is attributed to the improved catalytic sites with the maximum ZnO content and the suppressed defect densities, such as oxygen vacancies and impure phases.

Table 2: Visible light driven Hydrogen evolution using ZGy materials and ZnO and UZ5 materials for the purpose of comparison

Catalysts	Hydrogen evolution μmol/g h
ZnO	below detection limit
UZ5	below detection limit
ZG2	6
ZG5	12
ZG8	19

ii) Effect of Incident Wavelength:

Among the other compositions, the best working composition of ZGy series is evaluated for the effect of incident wavelength. ZG8 was evaluated for water splitting with different cut off filters to demonstrate the visible light driven photocatalytic activity. Visible band-pass filter (>370 nm), cut-off filters with λ≥400 and ≥455 nm shows hydrogen generation of 19, 16 and 7 μmol/h g, respectively. Although visible light absorption was observed in Figure 3.9 up to 550 nm, no water splitting activity was observed with cut off filter at λ ≥ 500 nm.

3.3.2 Visible Light Driven Photocurrent Generation

The true efficiency of water splitting was further validated by current generation through PEC measurements[30] and PEC studies of $(Zn_{1-y}Ga_y)(O_{1-z}N_z)$ under visible light irradiation were successfully demonstrated. Linear sweep voltammograms (LSV) of the solid solutions with varying Ga concentrations are measured and compared with ZnO bulk as reference in Figure 3.11. There was a marked increase in photocurrent generation from

the solid solutions, about 30 times higher than ZnO, and the current density of the solid solutions increased with increasing Ga content. The enhancement in photocurrent generation was primarily attributed to the effective visible light absorption as well as the utilization of charge carriers towards current generation.

The solid solution with the maximum ZnO and minimum GaN content provides a suitable structure for the fast conduction of photogenerated charge carriers. The presence of the GaN form also plays a pivotal role in suppressing recombination centers, such as oxygen vacancies, and in furnishing the energy overlapping of N 2p with O 2p bands.

Chronoamperometry experiments were carried out at 0 V, using a solar simulator and different cut-off filters (visible band pass filter for 370–770 nm, ≥400, ≥455, and ≥515 nm), and the results are shown in Figure 3.12.

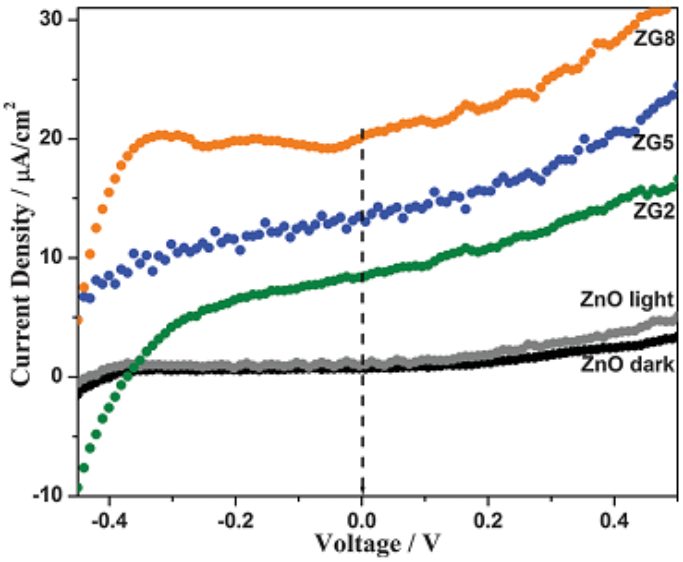

Figure 3.11 LSV of the solid solutions with Ga concentrations ranging from 2% to 8% under visible light irradiation at the scan rate of 10 mV/s.

There is visible light current generation by the solid solution even at longer wavelengths. There is current generation with incident wavelength, particularly ≥510 nm that is useful for photosynthesis and the performance remained sustainable over a period of time in several cycles of the experiment. For shutter opening and closing, the sharp changes in

photocurrent generation demonstrated the photofunctional behaviour of the ZGy solid solutions. The solar energy conversion efficiency for the ZG8, which is calculated as elaborated in experimental section (Chapter 2, sec. 2.5).

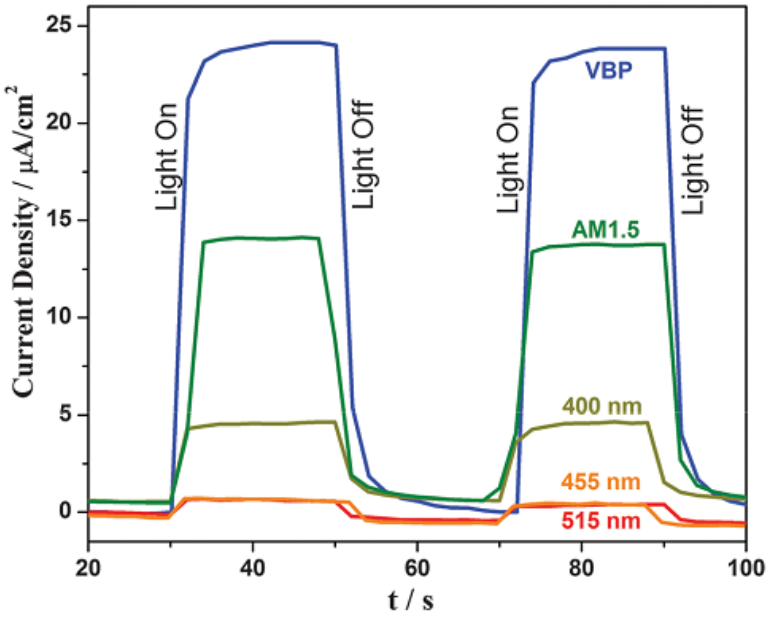

Figure 3.12 Chronoamperometry measurements of the solid solution containing 8% Ga under 300 watts xenon light irradiation using different cut-off filters as indexed.

The calculated incident photon conversion efficiency for ZG8 varied from 4.1% (380 nm), 2.5% (A.M 1.5 filter), 0.84% (400 nm), to 0.41% (455 nm) with different cut-off wavelengths as mentioned in the respective brackets.

3.4 Conclusions

The present work brings out the vital structural features of the solid solution responsible for the photocatalytic activity and photocurrent generation, and in general solar light harvesting.

The SCM preparation method provides effective nitridation conditions by producing a large quantity of in situ ammonia, resembling high flux ammonia conditions, which involved in forming GaN and interacting with the growing zinc oxo nano clusters with oxygen vacancies. The suppression of oxygen vacancies with the incorporation of Ga and N also plays a crucial

role in enhancing the photostability of the material. The EXAFS study revealed the local structure of incorporated Ga in the form of GaN with hexagonal coordination to be homogeneously distributed in ZnO lattice, as evident from HRTEM study. The presence of GaN form assists in minimizing the oxygen vacancies in the ZnO lattice. Light absorption and emission studies support the valence band broadening for being the prime reason for the visible light absorption by the ZGy solid solutions. Homogeneity in the solid solution structure plays a major role in exhibiting promising visible light absorption, photocurrent generation and virgin catalytic activity for hydrogen generation.

3.5 References:

1. A. Kudo and Y. Miseki, *Chem. Soc. Rev*., 2009, **38**, 253.
2. X. Chen, S. Shen, L. Guo and S. S. Mao, *Chem. Rev*., 2010, **110***,* 6503.
3. K. Maeda and K. Domen, *J. Phys. Chem. C,* 2007, **111**, 7851.
4. (a) Z. Li, T. Dong, Y. Zhang, L.Wu, J. Li, X. Wang and X. Fu, *J. Phys. Chem. C*, 2007, **111**, 4727. (b) B. Naik, K. M. Parida, and C. S. Gopinath, *J. Phys. Chem. C*, 2010, **114**, 19473.
5. M. Mapa, and C. S. Gopinath, *Chem. Mater*., 2009, **21**, 351.
6. S. Rajaambal, M. Mapa, C. S. Gopinath, *Dalton Trans*., 2014, **43**, 12546.
7. K. Zhang, D. Jing, C. Xing and L. Guo, *Int. J. Hyd. Energy,* 2007, **32**, 4685.
8. J. Yu, J. Zhang and M. Jaroniee, *Green. Chem*., 2010, **12**, 1611.
9. K. Maeda, T. Takata, M. Hara, N. Saito, Y. Inoue, H. Kobayashi and Domen, K. *J. Am. Chem. Soc*., 2005, **127**, 8286.
10. M. Mapa, K. S. Thushara, B. Saha, P. Chakraborty, C. M. Janet, R. P. Viswanath, C. M. Nair, K. V. G. K. Murty and C. S. Gopinath, *Chem. Mater*., 2009, **21**, 2973.

11. K. Maeda and K. Domen, Chem. Mater., 2010, 22, 612.

12. M. Mapa, K. Sivaranjani, D. S. Bhange, B. Saha, P. Chakraborty, A. K. Viswanath and C. S. Gopinath, *Chem. Mater*., 2010, **22,** 565.

13. Y. Lee, H. Terashima, Y. Shimodaira, K. Teramura, M. Hara, H. Kobayashi, K. Domen and M. Yashima, *J. Phys. Chem. C*, 2007, **111**, 1042.

14. H. Wang, H. Y. Li, X. Q. Gong, Y. L. Gao, G. Z. Lu and P.Hu, *Phys. Chem. Chem. Phys*., 2012, **14**, 16521.

15. S. P. Phivilay, C. A. Roberts, A. A. Puretzky, K. Domen and I. E. Wachs, *J. Phys. Chem. Lett.*, 2013, **4**, 3719.

16. (a) K. Sivaranjani, S. Raja Ambal, T. Das, K. Roy, S. Bhattacharyya and C. S. Gopinath, *ChemCatChem*., 2014, **6**, 522. (b) P. Devaraji, N. K. Sathu, and C. S. Gopinath, *ACS Catal*., 2014, **4**, 2844.

17. M. Mapa, S. Raja Ambal and C. S. Gopinath, *Trans. Mater. Res. Soc. Jpn*., 2013, **38**, 145

18. K. Sivaranjani and C.S. Gopinath, *J.Mater.Chem.*, 2011, **21**,2639. (b) K. Sivaranjani, S. Agarkar, S. B. Ogale, and C. S. Gopinath, *J. Phys. Chem. C*, 2012, **116**, 2581.

19. A. Gaur, B. D. Shrivastava, D. C. Gaur, J. Prasad, K. Srivastava, S. N. Jha, D. Bhattacharyya, A. K. Poswal and S. K. Deb, *J. Coord. Chem*., 2011, **64**, 1265.

20. S. Basu, S. Varma, A. N. Shirsat, B. N. Wani, S. R. Bharadwaj, A. Chakrabarti, S. N. Jha and D. Bhattacharyya, *J. Appl. Phys.,* 2012, **111**, 053532.

21. S. Basu, B. S. Naidu, M. Pandey, V. Sudarsan, S. N. Jha, D. Bhattacharyya, R. K.Vatsa and R. J. Kshirsagar, *Chem. Phys. Lett.*, 2012, **528**, 25.

22. X-Ray Absorption: Principles, Applications, Techniques of EXAFS, SEXAFS and XANES, ed, D. C. Konigsberger and R. Prince, Wiley, New York, 1988.

23. M. Newville, B. Ravel, D. Haskel, J. J. Rehr, E. A. Stern and Y. Yacoby, *Physica B*, 1995, **154**, 208.

24. E. H. Kisi and M. M. Elcombe, *Acta Cryst. C* 1989, **45**, 1867.

25. S. Moon, E. Baranoff, S. M. Zakeeruddin, C. Yeh, E. W. Diau, M. Grätzel and Kevin Sivula, *Chem. Commun*., 2011, **47**, 8244.

26. V. A. Fonoberov, K. A. Alim, A. A. Balandin, F. Xiu and J. Liu, *Phys. Rev. B*, 2006, **73**, 165317.

27. M. A. Reshchikov and H. Morkoç. *J. Appl. Phys*., 2005, **97**, 061301.

28. K. Vanheusden, W. L. Warren, C. H. Seager, D. R. Tallant, J. A. Voigt and B. E. Gnade, *J. Appl. Phys*., 1996, **79**, 7983.

29. Z. Chen, N. Zhang and Y. J. Xu, *Cryst. Eng. Comm.*, 2013, **15**, 3022.

30. H. M. Chen, C. K. Chen, Y. C. Chang, C. W. Tsai, R. S. Liu, S. F. Hu, W. S. Chang and K. H. Chen, *Angew. Chem. Int. Ed*., 2010, **49**, 5966.

InGaN(QD)@ZnO: A Quantum Dot Integrated Material for Solar Harvesting

4.1 Introduction

Harvesting abundant solar energy is a possible potential solution for ever growing clean energy/fuel demands.[1-3] Research efforts in utilizing solar energy has increased steadily in the last decade to produce H_2 from water splitting reaction (WSR) and increasing number of review publications is evident for this.[4-6] To begin with, materials with optical band-gap around 1.5–2.0 eV, and appropriate band edge potentials are very important to absorb the entire visible light range (400–700 nm) to tap the sunlight for WSR.[7,8] Upon photon absorption and charge carrier generation, it is essential to separate electrons and holes, and diffuse them to the relevant sites, where it can help to generate H_2 or power. Minimization of defects and extensive electronic integration of active components enhances charge carrier utilization. In that perspective, quantum dots (QDs) emerged as promising candidates[9-12] and celebrated for its inherent advantages, such as high absorption cross section, multiple exciton generation. To realize the above inherent advantages of QDs, it is essential to rationally design the material such that QD and host matrix is integrated for facilitating charge separation and transport.[13]

$In_{1-x}Ga_xN$ (InGaN) fascinates research in optoelectronics field for its defect tolerant nature, photostability with tuneable band-gap from 3.4 to 1.4 eV to absorb entire range of solar spectrum exhibiting potential for rainbow solar cell.[14] Nevertheless, synthesis of InGaN-QDs poses difficulties due to different ionic radius of In^{3+} (0.84 Å) and Ga^{3+} (0.61 Å), and hence large lattice strain of InGaN.[15] Many sophisticated thin film growth techniques have been utilized to grow InGaN,[16-21] and no simple method is available till date. Further, InGaN thin films grown on various substrates demonstrate limited success in practical applications due to detrimental problems associated with the preparation methods and challenges in reproducibility.[22] Recent exploration on thin films of InGaN grown on GaN substrate for water splitting demands the use of noble metal cocatalyst to achieve considerable activity.[23] Large visible light absorption by InGaN alone does not show significant photoresponse, implying the intrinsic nature of poor charge

utilization by InGaN.[24] On the other hand, ZnO is known for fast electron conduction,[25] but its exploration in solar light harvesting hindered due to wide band gap (3.37 eV), limiting its use exclusively in UV light, and deleterious photocorrosion. Solid solution formation of structurally similar GaN[26-29] or InN[30] with ZnO could bring visible light absorption. Nonetheless, an idea to integrate ZnO and InGaN might work to tap the sunlight at the expense of the above shortcomings and it is worth exploring. Despite the efforts attempted so far, there is no report in achieving a solid solution or a thin film growth of an integrated material that consists of ZnO and InGaN. For the first time, we report InGaN-QDs in ZnO (InGaN@ZnO), which is structurally and electronically integrated into a single material and evaluated for solar light harvesting. The material is successfully synthesized by simple solution combustion method (SCM) in 15 minutes. In-situ production of ammonia acts as nitrogen source creating effective reducing environment for forming nitride of In and Ga. Direct evidence on the structural and electronic integration aspects of InGaN@ZnO is provided by XRD, HRTEM, XPS, Raman, absorption and emission spectroscopies, and secondary ion mass spectrometry (SIMS). InGaN@ZnO exhibits entire visible light absorption, and up to 3-4 orders of magnitude higher photostability than that of ZnO. Synergetic operation of light harvesting by InGaN and catalytic and electron conduction components by ZnO in the closest proximity makes InGaN@ZnO a unique material. This aspect is exploited for visible light induced dehydrogenation of 2-butanol, H_2 generation from overall WSR (OWSR) without using any sacrificial agent or co-catalyst and promising solar photocurrent generation at 0 V under illumination of 20 mW/cm^{-2} A.M 1.5G source. To the best of our knowledge, this is the first report on highly reproducible solid state synthesis of QDs within 15 minutes, distinguished from various solution-based processes dominating till date.[9, 31] Present study suggests direct integration of QD with host matrix is a potential method to realize the advantages of and this material can be one of the example for promising rationally designed photocatalytic materials.[32]

4.2 Results and Discussion

4.2.1. Structural and Microstructural Integration Aspects

Investigation on the structural features of InGaN@ZnO was carried out by powder X-ray diffraction (XRD) and the results are compared with that of ZnO (Figure 4.1). Very similar diffraction pattern of hexagonal Wurtzite ZnO was observed for all InGaN@ZnO, without any impurity features. Unless otherwise specified, number followed by I and G in the material code gives the nominal mol percent of In and Ga, respectively. $ZnO_{0.914}N_{0.086}$ (UZ5)[26] show a marginal shift in XRD features to higher angle. However, Figure 1 reveals that there is peak shift to lower angles for all InGaN@ZnO compositions compared to pure ZnO. A dotted line indicates the extent of peak shift to lower angles with different compositions of In and Ga. Irrespective of In and Ga content, a shift to lower angle observed in XRD indicates the dominance of In size effect than Ga. As the ionic radius of In^{3+} is bigger than Zn^{2+} (0.72 Å) or Ga^{3+}, the peak positions shifts increasingly to lower angles on increasing the In-content. It is also to be underscored that the peak shifts to lower angle even with high Ga-content hints the maximum amount of nominal input amount of In is retained in the structure. The simultaneous incorporation of bigger (In^{3+}) and smaller (Ga^{3+}) ions in place of Zn^{2+} in near neighbour lattice sites affords the advantage of compensating effects of lattice expansion and contraction, respectively, with each other, minimizing the lattice distortion in ZnO.

Thus the solubility limit of total dopant (In + Ga) content increases, compared to the solubility limit of individual InN (8 %) and GaN (10 %) in ZnO.[29,30] Up to 8 % In and 15 % Ga, XRD show no features corresponding to In_2O_3 and Ga_2O_3, highlighting the solubility of In and Ga as nitrides in ZnO under combustion synthesis InGaN@ZnO material compositions, especially with In (or Ga) content higher than 8 % (12 %) in Figure 4.2, shows the impurity phases, such as In_2O_3 and Ga_2O_3. This is due to crossing the combined solubility limit. The small peak identified with * symbol refers to the major peak of In_2O_3 impure phase. Majority (≥90%) of In+Ga still forms the InGaN, as denoted by the peak shift

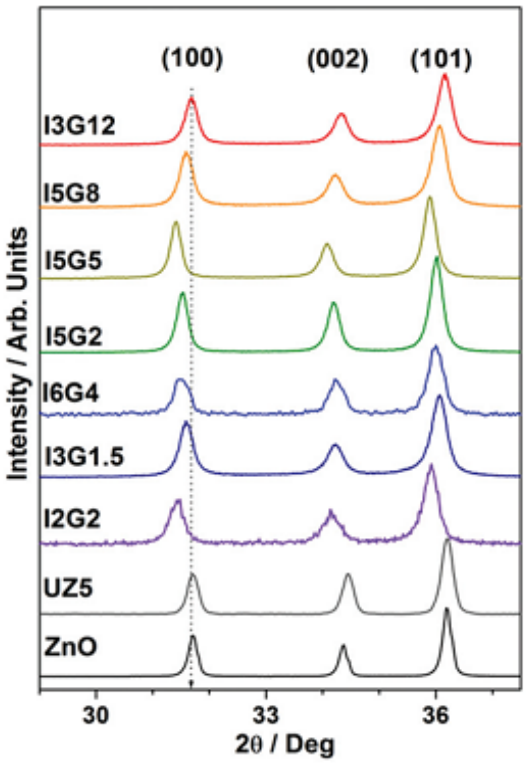

Figure 4.1 X-ray diffraction patterns of different compositions of IxGy series along with ZnO and $ZnO_{0.91}N_{0.09}$ (UZ5).

.

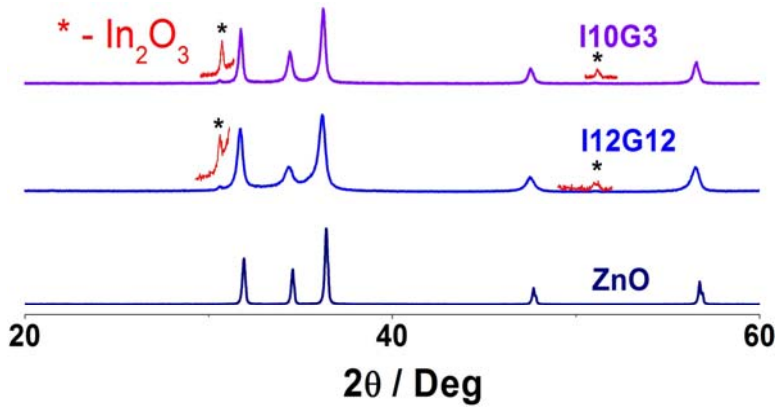

Figure 4.2 XRD pattern of IxGy materials, with In (or Ga) content higher than 8 % (12 %), shows minor In_2O_3 impurity formation in the compositions. *marked peaks could be observed after multiplication by a factor of 15.

The critical and direct microstructural evidence for the formation of InGaN QDs can be found by identification of their characteristic lattice d-spacing in HRTEM analysis. Well resolved high resolution images of lattice planes of I5G8 composition are shown in Figure 4.3.a-b along with the indices of their lattice planes. HRTEM image of the present material

comprises lattice plane with two different contrasts; black contrast area which is encircled with solid square is identified as InGaN with d_{100}-spacing of 0.2998 nm. This is further supported by statistical line profile analysis recorded in the area indicated by InGaN (Figure 4.4); very regular 0.3 nm was observed. In Figure 4.3.b, the encircled portion was enlarged in which the two different contrasts are being continuously formed in the same lattice.

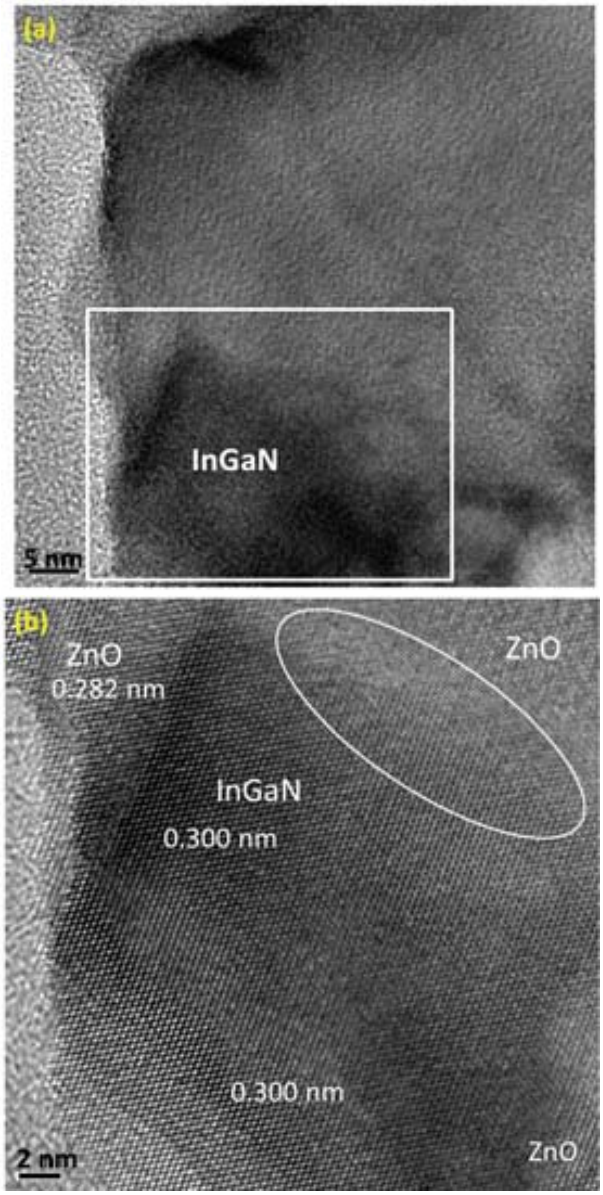

Figure 4.3 (a–b) HRTEM images of (100) lattice planes of InGaN (d≅0.3 nm) (dark portion) and ZnO (d= 0.282 nm) (grey portion) measured from TEM analysis is given for I5G8. The dark portion in the bottom half of (a), indicated by a square, is enlarged in (b).

Nonetheless, d_{100}-value changes, in the nearby area with a grey contrast, to 0.282 nm in the same lattice plane (Figure. 4.4), and this corresponds to ZnO (100) plane and that value corresponds to ZnO. An onset of ZnO penetrating into InGaN region is evident from a gradual increase in d_{100} value from 0.282 nm to higher value of 0.3 nm. Hence the presence of InGaN QDs structurally integrated with ZnO lattice is supported by characteristic changes in d-values.

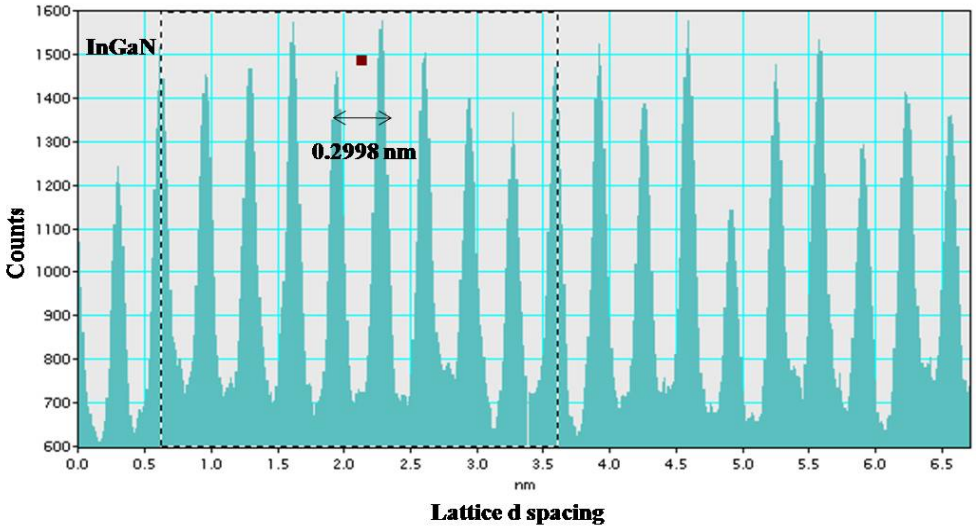

Figure 4.4 Corresponding line profile analysis shows a regular d_{100}-value (0.3 nm) highlighting the InGaN quantum dot regime for InGaN in figure 4.2.3 (b) is given in panels.

The interconnecting lattice between InGaN and ZnO plays the role in transport of the charge carrier diffusion throughout the lattice. Therefore the interpenetrating lattice regime between InGaN and ZnO which was indicated by white oval shape in Figure 4.3a, was explored. There is seamless change from predominant nitride nature at the centre of Figure 4.3b to ZnO at the top right corner without abrupt interface. The same region is analyzed using statistical line profile analysis in Figure 4.5 shows intermediate d-spacing between InGaN and ZnO.

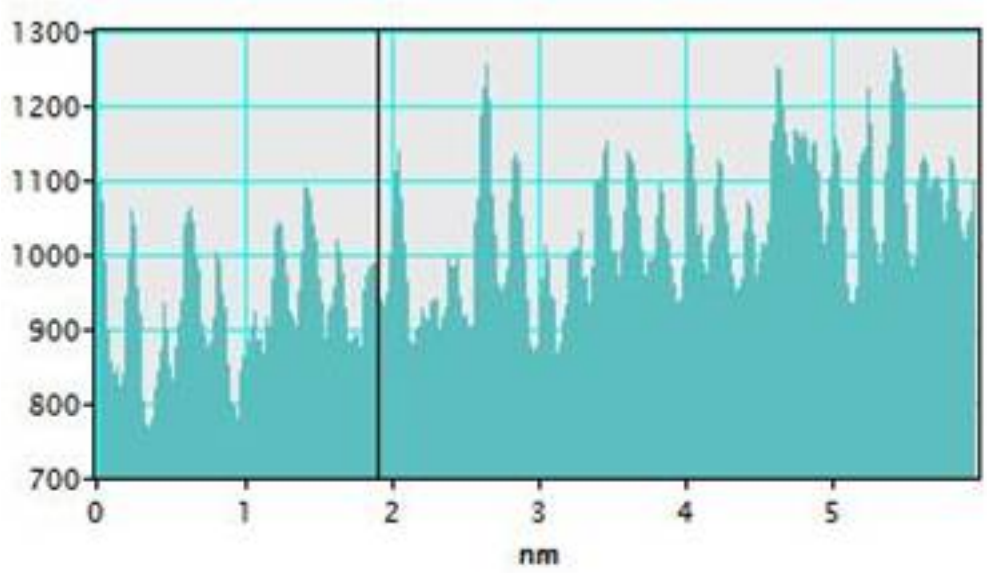

Figure 4.5 The line profile analysis of the interpenetrating junction of ZnO and InGaN which was indicated by oval shape in figure 4.3 b

In some of the regions, two different distinct moieties are formed in such a way that the middle region of lattice becomes right handed helical structure which is given in Figure 4.6a to relieve stress due to interconnection of two different moieties. Analysis on the d spacings of two different planes reveals that InGaN and ZnGaN, are formed in the interconnection region. Corresponding d-spacings of the region: InGaN-0.3 nm, ZnGaN-0.225 nm, are indexed. The outcome of the result indicates the formation of nanojunction ~2x6 nm^2 that can facilitate the charge carrier separation. Another spot of the composition is also given in Figure 4.6.b and that shows hexagonal lattice plane. The whole particles of the representative composition of I5G8 show hexagonal morphology in figure 4.6.c. and the particle size distribution of integrated InGaN measured from TEM images is given in Figure 4.6.d. 25 nm size particles are observed predominantly with size variation between 10 and 35 nm.

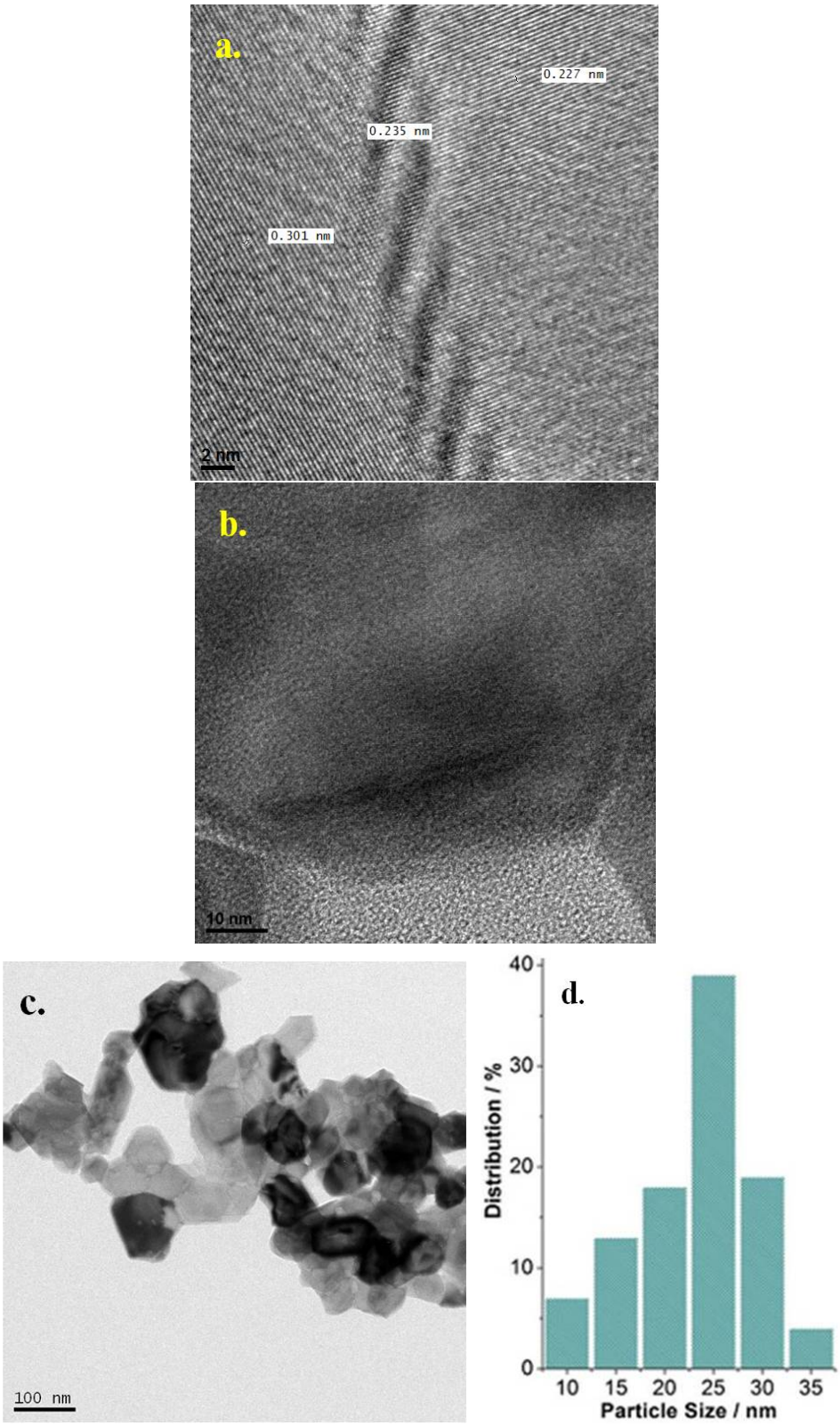

Figure 4.6 a. HRTEM images of lattice planes of the compositions with I5G8 showing 0.3 nm (InN) and 0.23 nm (GaN), **b**. image of I3G2, **c**. morphology of IxGy material and **d.** Particle size distribution of InGaN QDs in ZnO.

It is also to be noted that this size includes the diffused regime of ZnO into InGaN and hence the actual size would be likely to be smaller by 2-5 nm from the values shown in Figure. 4.6.d. Indeed this is also a reason for the significant shift in diffraction features observed in Figure. 4.1. Particle size less than 10 nm cannot be ruled out, but its abundance is very low, for the reason of structural integration aspects.

To establish the existence and mode of distribution of nitride components in ZnO matrix, direct imaging of molecular fragments on the surface of InGaN@ZnO was probed by SIMS analysis after initial sputtering. Figure 4.6 displays the SIMS mapping images of critical fragments of I5G5, namely InGaN, ZnGaN and ZnInN. A fairly homogeneous distribution of the fragments in ZnO matrix could be observed from Figure 4.7a-c. Although, ZnInN also shows a homogeneous distribution Figure 1f, 5-7 times lower counts were observed compared to the other two fragments. These observations are very significant in terms of direct observation of quantum chemical components of the nitride fragments.

Foremost is the presence of InGaN, which is the key evidence for the formation of InGaN@ZnO. About 5 times larger amount of InGaN than ZnInN suggesting the preference of In to Ga, rather than In to Zn; this is

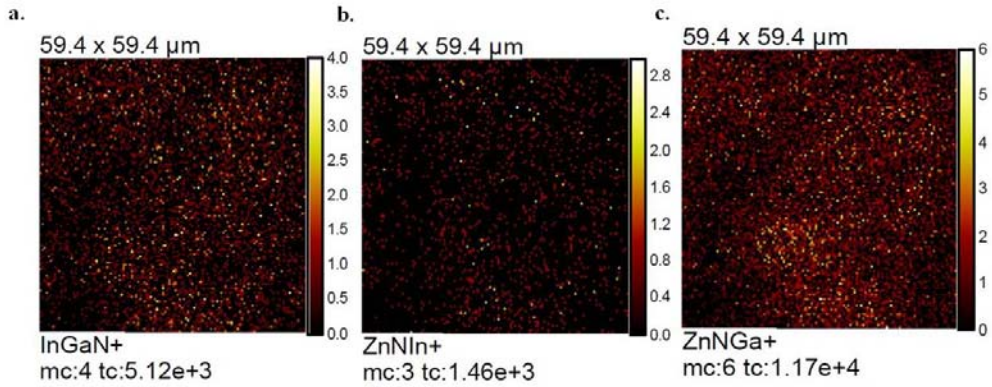

Figure 4.7 Microstructural integration of InGaN quantum dots with ZnO has been demonstrated through SIMS fragment mapping of I5G5 with different mass fragments, given below the image, namely (a) InGaN, (b) ZnNIn and (c) ZnNGa.

expected, as it would reduce the lattice strain of InGaN[15] as well as host ZnO lattice, and facilitates the formation of InGaN@ZnO. Further, highest count observed with ZnGaN hints the preference of Zn towards Ga and presence of GaN is also observed. However, the same argument is not true with InN, since ZnInN shows the least counts.

The composition of I2G2 with relatively lesser In and Ga content, was also analyzed and corresponding results are displayed in Figure 4.8. Intensity trend of various mass fragments follows the same order as that of I2G2; however, the overall fragment intensity decreases due to lower amounts of In and Ga in I2G2 than in I5G5. In general, various nitride containing fragments mapping hints the InGaN QDs are structurally embedded into the ZnO matrix. These observations suggest the nitrogen from nitride is the key component that integrates InGaN with ZnO. Confirmatory results from XRD, HRTEM and SIMS suggest structural integration evolves single phase nature of InGaN@ZnO formation that shows the features that are required for optoelectronic and photocatalysis applications, especially to harvest solar light.

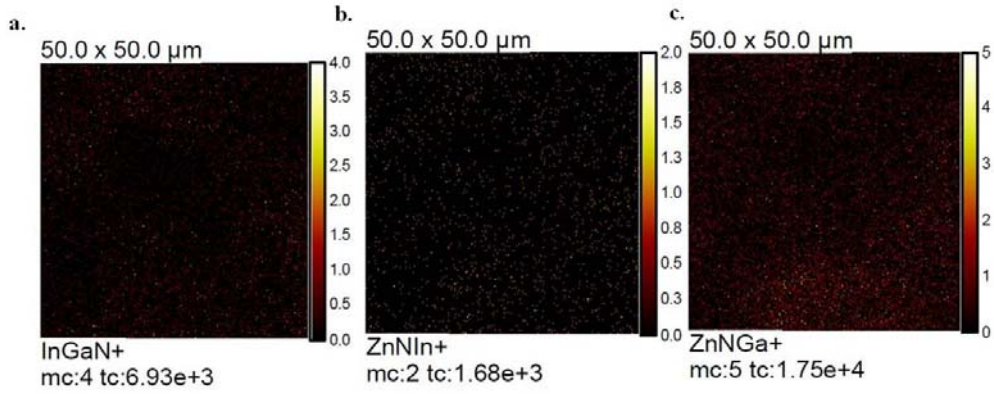

Figure 4.8 Microstructural integration of InGaN quantum dots with ZnO has been demonstrated through SIMS fragment mapping of I2G2 of critical masses of InGaN, ZnNIn and ZnNGa.

4.2.2. Electronic Integration Aspects

N 1s core level of InGaN@ZnO was analysed using XPS and the results are shown in Figure 4.9a. Single sharp peak at 397.1 eV is obtained for N 1s core level for all compositions of InGaN@ZnO and its intensity

generally increases with the increment in In + Ga content. This peak is assigned to nitride (N^{3-}) present in the InGaN@ZnO material and it is in good correspondence with the literature reports.[33a, b] No other N 1s peak was observed highlights that nitrogen is present exclusively as nitride; whereas, N-doping in ZnO shows N-atoms similar to that of ammonia or amines, which is not present in InGaN@ZnO. On $Zn_{0.92}Ga_{0.08}O_{0.88}N_{0.}$ (G8)[29], nitride also appears, in addition to the ammonia feature. This also supports that substitutional N-doping as N^{3-} can abstract the maximum electron density than any other type of nitrogen species. Further assistance in charge compensation and replacement of oxygen vacancies can be effectively accomplished by N^{3-} -type features.

Nitride components of InGaN@ZnO are identified by its characteristic vibrational frequencies from Raman spectral analysis Figure 4.9b Results are compared with Raman spectra of ZnO, UZ5 and

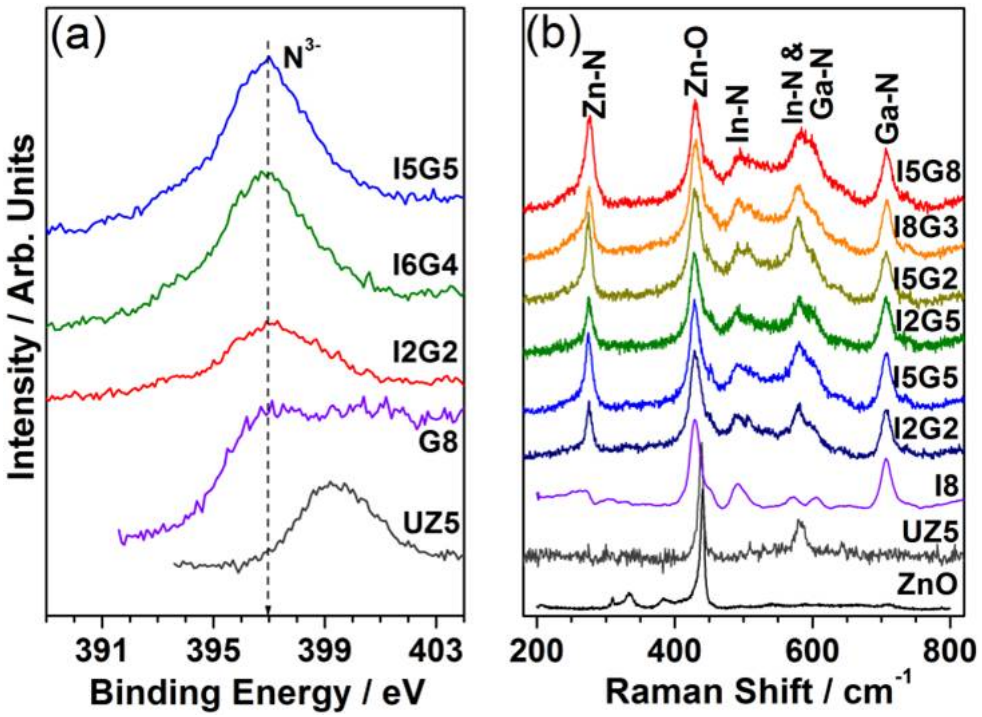

Figure 4.9 Electronic integration of InGaN quantum dots with ZnO. (a) XPS of N 1s core level, and (b) Raman spectra of InGaN@ZnO materials with different compositions, and compared with reference materials. Note the observation of nitride formation with all InGaN@ZnO in XPS and Raman results.

$Zn_{0.92}In_{0.08}O_{0.85}N_{0.15}$ (I8). Prominent E_2(high) feature was observed at 437 cm^{-1} for ZnO and UZ5, which is characteristic for Wurtzite phase; however, InN or InGaN introduction shifts this feature to 430 cm^{-1} with peak broadening. Characteristic E_2(high) of InN(490 cm^{-1})[34] and GaN(579 cm^{-1}) [35] demonstrates the presence of both components in InGaN@ZnO.

In addition, a broad feature centred between 575 and 600 cm^{-1} corresponds to typical metal nitrides, especially A_1LO of In-rich $In_xGa_{1-x}N$.[36] A sharp feature at 708 cm^{-1} confirms the presence of Wurtzite In-N (A_1LO and E_1LO mode of InN). Local vibration modes of Zn-N was observed at 273 cm^{-1},[37] and this was not observed with G8 or I8.[29, 30] Zn-N feature and A_1LO of In-rich InGaN suggests the electronic integration of InGaN and ZnO and nitride feature is likely to be at the interface. The fact of homogeneous distribution of incorporated elements is strongly supported by elemental mapping images displayed Figure 4.10a and b (up and below) for two different compositions namely I5G5 and I5G2 are compared.

The elements are represented in different colors for clear identification. The images illustrate the uniform distribution and chemical identification of incorporated In, Ga, N elements. The images also demonstrate the change in the surface composition as well as surface structure with the changes in the content of incorporation. As the nitride components are structurally integrated, the influence of incorporation over the surface is expected.

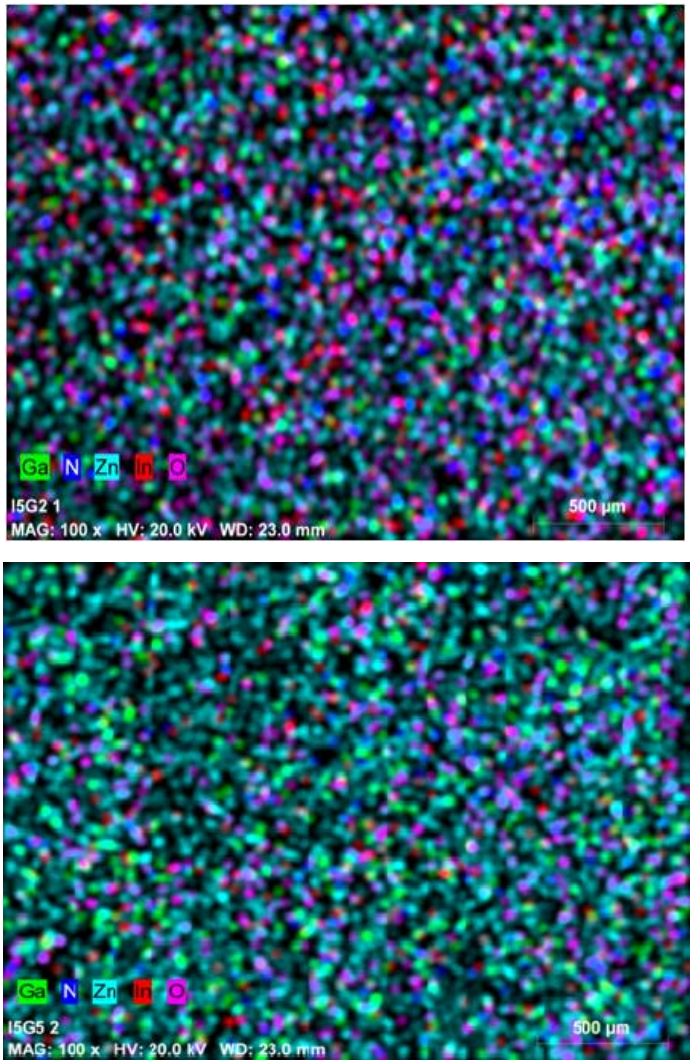

Figure 4.10 Elemental mapping of compositions of I5G2 of upper all the elements: Zn, O, N, In, Ga and below without Zn and O.

4.2.3. Absorption and Emission Studies

Figure 4.11 displays absorption spectra of InGaN@ZnO and reference materials. Onset of visible light absorption between 650 and 700 nm is observed with all InGaN@ZnO compositions; absorption coefficient increases with increase in In and Ga contents. Although G8 absorbs visible light up to 550 nm, a marked increase in absorption with I1G1 up to orange region with extended absorption up to 650 nm highlights the importance of InGaN QD as light harvesting antennas. I2G2 shows absorption upto 700 nm. I5G2 and other compositions shows enhanced absorption compared to

I2G2 at all wave lengths in visible light as well as into near IR regime. A comparison of solar spectrum with the absorption spectra of InGaN@ZnO suggests the maximum overlap in absorption from violet to green (~550 nm) region highlighting the possibility of absorption of high flux visible light photons of solar spectrum. As the material absorption spans from UV to visible regime, the minimum criteria for working in rainbow solar cell is fulfilled by InGaN@ZnO.[38] The absorption spectra of InGaN@ZnO is continuous suggesting the structural compatibility with electronic integration of the individual components, and completely eliminating the chances of being a physical mixture of individual components. Inset in Figure 4.12a shows a photograph for colour associated with InGaN@ZnO and fully supports the reduction in optical band gap to 1.8 eV.

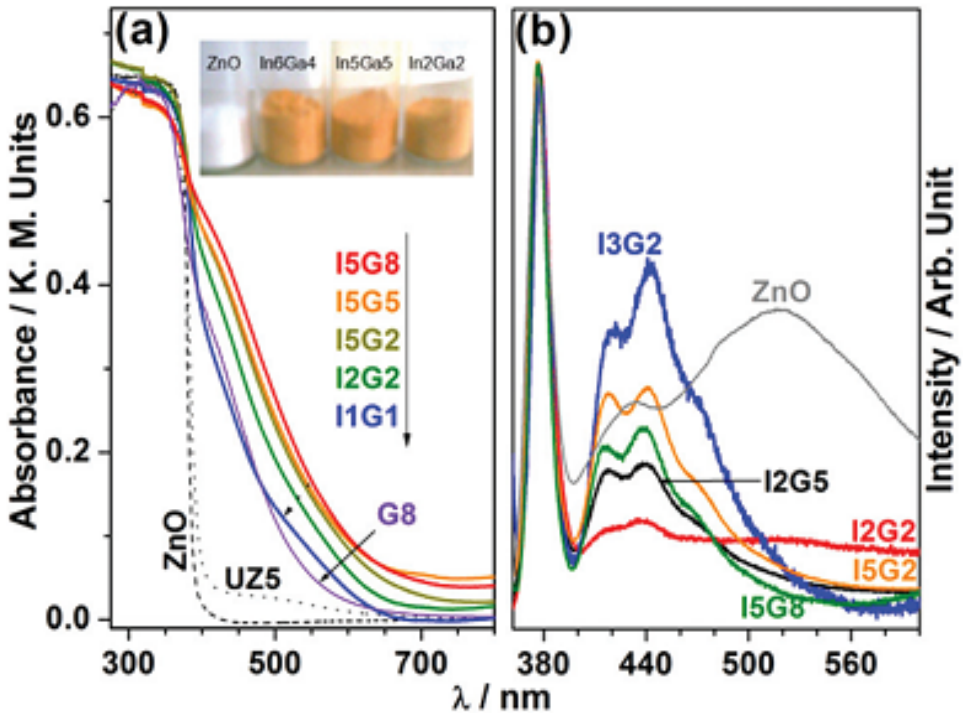

Figure 4.11. UV-Visible absorption (a) and photoluminescence emission spectra (b) of IxGy series with different compositions. Absorption and emission spectrum of ZnO is also included for comparison. Note the significant visible light absorption at 700 nm (in a), and no green emission feature at 540 nm (in b), corresponding to oxygen vacancies, observed for InGaN@ZnO whereas it was observed in bulk ZnO as reference.

Consideration of absorption spectrum of UZ5 suggests the visible light absorption is exclusively due to nitride features in InGaN@ZnO. Indeed, N 2p states of N^{3-} decreases the optical band gap indicating the broadening of valence band (VB) in InGaN@ZnO. N^{3-} doping is reported to be essential for the formation of shallow acceptor levels arising p-type conductivity in ZnO.[39] Theoretical and experimental findings on the formation of shallow electronic levels due to nitride postulate favourable overlapping of 2p bands of N and O,[40] and as a result optical band gap reduction occurs in InGaN@ZnO.

To further understand the electronic structure of InGaN@ZnO, emission spectra were recorded with excitation wave length at 325 nm Figure 4.11b. Near band edge emission is observed at 380 nm for InGaN@ZnO as in ZnO.[41] Room temperature PL result of reference ZnO is also given in Figure 4.11b. Note the entirely different emission features for ZnO and InGaN@ZnO. Similar emission features is observed for all InGaN@ZnO compositions with two sharp features at 420 and 440 nm and a shoulder at 480 nm, and these features are assigned to InGaN.[42] As the new emission features appear at higher λ than ZnO band edge emission, formation of new bands are suggested to be just above the VB. Indeed, extended visible light absorption up to 700 nm fully supports the broadening of VB in InGaN@ZnO. Further support available from emission peak observed around 740-770 nm in Figure 4.12 due to InGaN in InGaN@ZnO. An important feature to be underscored is the absence of green emission around 520 nm from InGaN@ZnO, which is prominently observed for ZnO, mainly due to O-vacancies.[43] Oxygen vacancies and nitrogen vacancies are noted as trap states in ZnO and nitride materials, respectively. In general, emission from such trap states are characteristically broad in nature.[44] In fact, O-vacancies are principally responsible for photocorrosion by leaching Zn^{2+}, and absence of broad green emission addresses anti-photocorrosion[45] nature of InGaN@ZnO. The intriguing phenomenon of suppression of O-vacancies is likely due to the effective nitride substitution at the expense of O-vacancies during the Zn_xO_y clusters growth under combustion conditions.

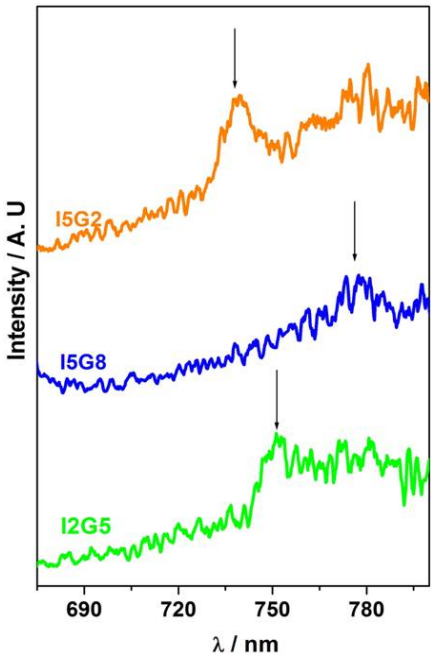

Figure 4.12 Room temperature Photoluminescence Spectra of InGaN@ZnO of varying compositions indicated with respective codes. Excitation wavelength employed was 550 nm. An emission feature is observed between 735 and 775 nm. Above emission is attributed to the emission of InGaN QDs

4.2.4. Studies on Material Stability

a. ICP analysis: Photostability

The photostability of the material is further experimentally verified by continuous strong UV irradiation studies carried out using 400 watts mercury vapour lamp for 48 hours. The materials are suspended in methanol aqueous mixture so as to simulate the reactant conditions and irradiated under UV for 48 hours. Then solution is filtered and subjected to ICP analysis for detecting Zn ion concentration that expelled out from the material due to light exposure. The results on leached ion concentration from the photocatalysts upon light irradiation are tabulated in Table 1. When one compared with ZnO leaching analysis for which 185 ppm concentration of Zn ion in 6 hours of irradiation is leached out, analysis on the solid solution with embedded quantum dots produces significantly suppressed leaching of Zn ion concentration of 1.5 ppm for 48 hours of irradiation. Similar suppressed values of leaching are obtained in other compositions of solid

solutions also. The suppression of Zn ion concentration is more than 2 orders of magnitude in solid solutions ensuring extreme photostability of the new material. For further substantiation, absorption of the spent sample is also studied by UV-Visible spectroscopy and the spectrum is given in Figure 4.13b. The absorption of spent InGaN:ZnO is retained as that of fresh sample. These results clearly demonstrate material photostability which is the utmost demanding requirement for ZnO based photocatalysts.

Table 1. ICP analysis for leaching Zn^{2+} ion estimation from the filtrated solution

Material Code	Zn^{2+} Estimated after UV irradiation (in ppm)
I3G5	1.77
I2G5	1.96
I5G5	1.39
I5G8	1.31
ZnO*	186

ZnO* was irradiated for 6 hours

b. Thermal Stability

Thermal stability of the material is also concerned for sustainable performance in many applications. In that viewpoint, the material I5G5 was subjected to TG/DTA and high temperature calcinations treatments for several hours. Figure 4.13a shows TG/DTA analysis in which sharp feature for weight loss is observed. It supports high degree of crystalline nature of the materials in corroboration with sharp diffraction pattern in XRD result. Initial stages of weight loss correspond to the loss of surface adsorbed species followed by weight gain around 700 ^{0}C. The weight gain is due to oxidation of InGaN to oxide components, such as In_2O_3, Ga_2O_3. This is the indication of the loss of nitride components from the material underscoring its stability up to 700 ^{0}C. Fresh material I5G5 is calcined in open atmosphere at 500 ^{0}C for 12 hours and the calcined sample is subjected to UV-Visible analysis and the results are displayed in Figure 4.13b. The absorption of calcined material (at 500 ^{0}C), indicated in blue solid line, shows only

marginal difference with that of fresh sample. The materials retain absorption even after calcinations at 500 ^{0}C; however, calcination at 800 ^{0}C, oxidizes nitrides.

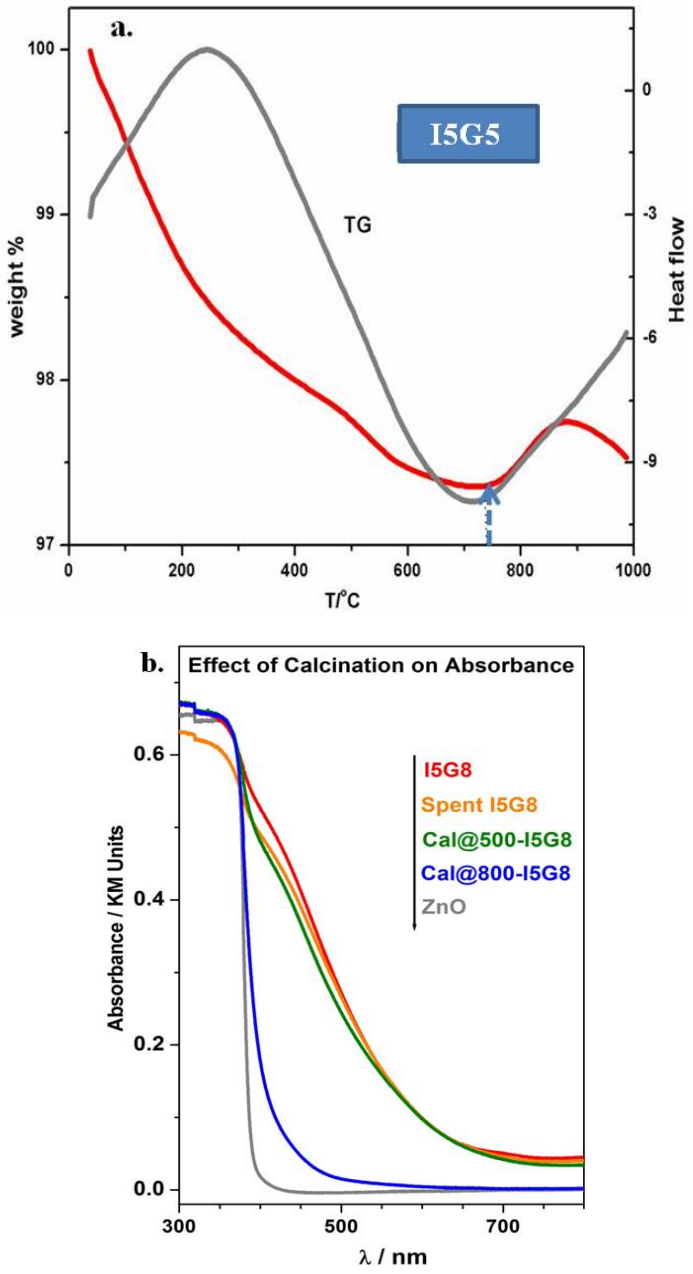

Figure 4.13 TGA of I5G5 shows the gain in weight after 750 ^{o}C with marking dotted line (a) and UV-Visible spectra (b) recorded for standard ZnO, InGa8 material, spent I5G8 extracted out from reaction after continuous irradiation of 12 hours, calcined materials at 500 ^{0}C and calcined materials at 800 ^{0}C.

Though nitrides are prone to oxidation and volatilization, stability of InGaN in this case is achieved mainly by structural and electronic integration with ZnO lattice. As the preparation condition is maintained at 500 ^{0}C, the stability of the material at that temperature is feasibly attained. When the calcination temperature rises to 800^{0}C for 3 hours, the material loses it reddish yellow colour and becomes pale white colour. The absorption after calcination at 800^{0}C reduces dramatically and the absorption edge is blue shifted to 400 nm. This result illustrates material stability above 500^{0}C but below 800^{0}C coinciding with TG/DTA result which explains that the loss of nitride at 800^{0}C leads to the loss of material colour. In the perspective of enhanced visible light absorption for new solid solutions, this result strongly supports the sole responsibility of integrated InGaN quantum dots for bringing visible light absorption. Owing to withstanding thermal stability, high photostability, InGaN quantum dots integrated ZnO as single photocatalyst system can be suitable for sustainable solar photocatalysis.

4.3 Photocatalytic Applications

4.3.1. Photocurrent Generation

Figure 4.14a displays linear sweep voltammograms of InGaN@ZnO recorded under visible light irradiation (λ=400-770 nm) and pH was maintained neutral pH throughout the reactions. ZnO furnishes <1 μA/cm^2, mainly due to absorption by O-defects. However, InGaN@ZnO exhibits a dramatic increase in photocurrent generation and the response increases up to 50 μA/cm^2 at 0 V with a gradual increase in In + Ga content; similarly, photocurrent increase from 25 to 60 μA/cm^2 at 0.5 V. Photoresponse of InGaN@ZnO lies in the fact of enhanced visible light absorption with notable absorbance values. Hence the visible light photoresponse is solely attributed to InGaN QDs due to the above factors. We observed two orders of magnitude enhancement in visible light photocurrent generation at 0 V with InGaN@ZnO than ZnO. Considering ZnO, which is only UV active material, the enhancement in photocurrent for InGaN@ZnO under visible light irradiation at zero voltage (0 V) condition is noteworthy.[45] According to

literature reports, the aspect of visible light absorption by InGaN alone does not show significant photoresponse implying intrinsic nature of poor charge utilization by InGaN.[24] Structurally integrated InGaN with ZnO brings the electronic coupling of light harvesters with fast conducting ZnO. The enhancement is attributed to the fact of synergistic operation of visible light harvesting by InGaN QDs and charge carrier conduction by ZnO. Incident photon conversion efficiency (IPCE) calculated for I5G8 varies from 7.5 % (VBP), 2.23 % (455 nm), 0.75 % (510 nm) and 0.52 % (610 nm) with different cut off wavelengths given in parenthesis (Table 2). The values obatined for each sample with the range of incident wavelengths is given in Table 2. Linear sweep voltammogram of I5G5 and I5G8 materials exhibit increment in both cathodic and anodic current implying p-type as well as n-type conductivity.[46] It is also to be underscored here that neither solid solution of GaN in ZnO or InN in ZnO produces more than 2-3 $\mu A/cm^2$ under the above conditions.

This fact is further confirmed by chronoamperometry measurements at 0 V, with different cut-off filters including AM1.5, visible band pass, 455 nm, 610 nm Figure 4.14b. Table 2 furnishes the incident photon efficiency for the selected compositions of InGaN@ZnO series for the mentioned cut-off filter wavelengths. Among the series, the composition I5G8 gives the highest efficiency value for incident wvwlength 380 nm. Although the magnitude of photocurrent is small at 610 nm filter, it indicates the effective absorption of high wavelength light underscoring the In-rich nature of InGaN@ZnO. Indeed, this broad-band absorption and efficienct conversion of light energy into current highlights the potential nature of the materials to act as rainbow solar cells.

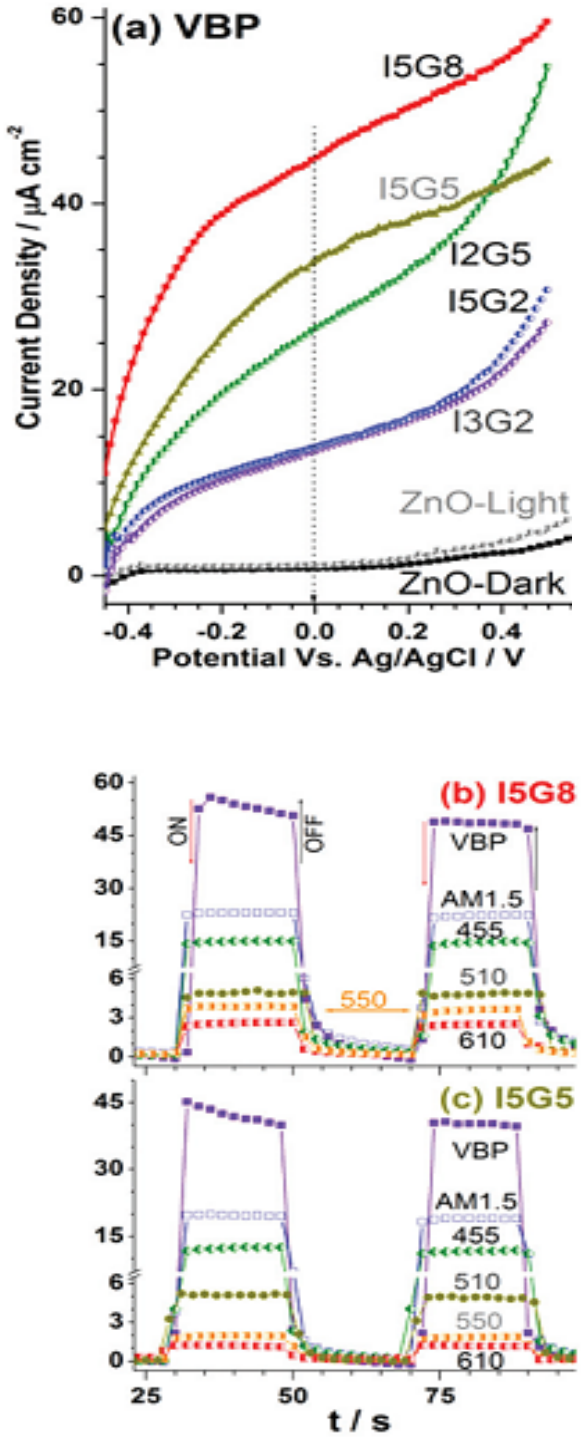

Figure 4.14 a) Linear sweep voltammograms of InGaN@ZnO and ZnO under 20 mW cm^{-2} irradiation (λ=380–770 nm) and dark scan of ZnO at the scan rate of 10 mV s−1in the sweeping potential range from −0.5 to 0.5 eV. Chronoamperometry measurements carried out under 0 V and the results given for representative materials in (b) I5G8, and (c) I5G5 with different cut-off λ filters and the cut-off (λ) is given in the figure.

Table 2. Photocurrent generation efficiency from different InGaN@ZnO compositions with different cut-off filters

InGaN@ZnO	380 nm	455 nm	510 nm	610 nm
I5G8	7.5	2.1	0.75	0.5
I5G5	6.0	1.8	0.63	0.35
I2G5	3.8	1.2	0.57	0.34
ZnO	0.03	0.0	0.0	0.0

4.3.2. Photocatalytic Studies

i. Photocatalytic Dehydrogenation of 2-butanol into Ethyl methyl ketone

Ethyl methyl ketone is one of the industrially important raw materials for many valuable organic chemicals, perfume industry and as a solvent in dry erase makers. The commercial synthesis of ethyl methyl ketone requires two step processes involving high temperature process and valuable n-butylene petrochemical as raw material. ZnO is conventionally known catalyst for dehydration and dehydrogenation reactions by its strong tendency towards alcoholic –OH species adsorption. As the new materials are being ZnO based bounded with visible light response, they open up the chances to explore dehydrogenation of 2-butanol into ethyl methyl ketone.

For the first time we successfully attempted photocatalytic dehydrogenation of 2-butanol into ethyl methyl ketone at ambient conditions under visible light irradiation using $NaNO_2$ filter for allowing only visible light wavelength above 420 nm. Figure 4.15c displays the yield of ethyl methyl ketone with high selectivity observed for six different (higher and lower) compositions. The highest yield around 56 % is achieved for the composition designated as I5G8. Standard ZnO shows negligible yield due to its poor visible light response despite its strong adsorption of reactants. On completion of irradiation time of 2.5 hours, so formed immiscible organic phase in water medium is separated and analyzed by IR and UV experiments given in Figure 4.15.a and b. The formation of ethyl methyl ketone is confirmed by characteristic peak for aliphatic C=O stretching frequency at

1746 cm^{-1} in IR spectra and in conjunction to characteristic absorption peak of ethyl methyl ketone at 270 nm in UV spectra. Recyclability test is done for six cycles for the material I5G8.

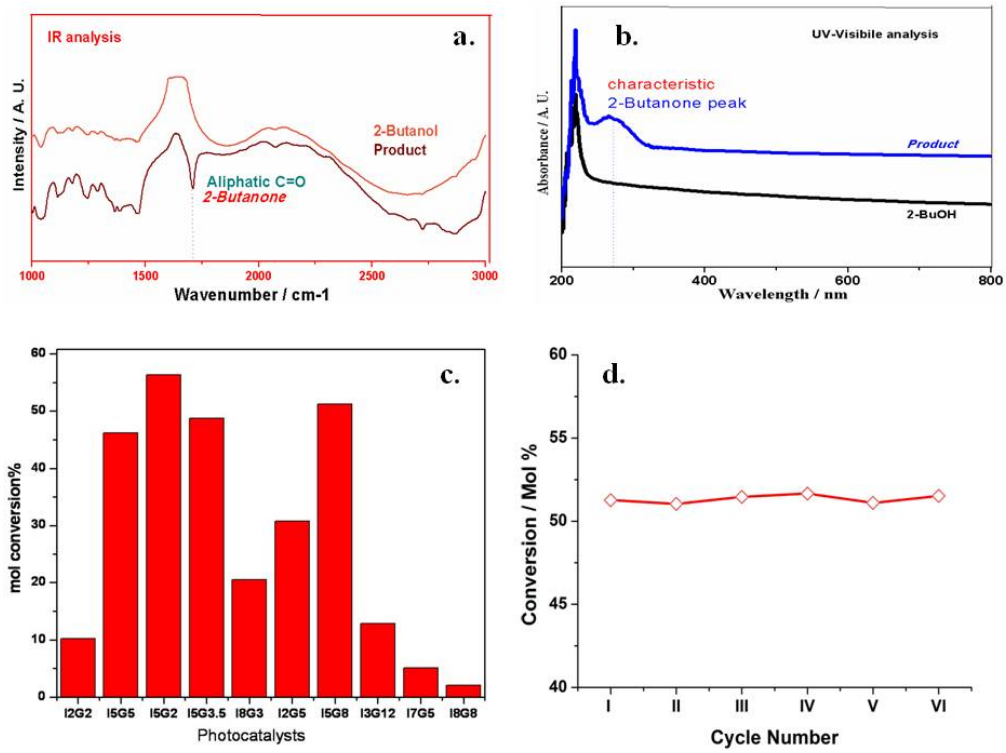

Figure 4.15 a. UV-Visible spectra, b. IR spectra of the 2-butanol reactant and reactant mixture after 3 hours of irradiation. The dotted line indicates characteristic absorption peak or carbonyl stretching for Ethyl methyl ketone confirming the formation of product, c. Conversion yield percentage of 2-butanone from visible light photocatalytic dehydrogenation of 2-butanol plotted as the function of the catalyst with varying compositions of In and Ga and d. Recyclability analysis carried out for visible light induced dehydrogenation of 2-butanol in 6 cycles with 3 hours of irradiation. The mol conversion % of 2-butanol into ethyl methyl ketone in each cycle is plotted.

The result is given in Figure 4.15.d which shows the retention of mol conversion% in all cycles. Synthesis of ethyl methyl ketone through simple one step process at ambient conditions using visible light source acclaims the current strategy. Standard ZnO shows negligible activity and group III

nitrides are reported to be catalytically inactive. When on embedding InGaN quantum dots in ZnO, photocatalytic yield multiples to several fold higher than the individual precursors. This supports the synergetic operation of quantum dot as light harvesting components and ZnO catalytically active components integrated in single lattice.

ii. Photocatalytic Hydrogen Generation

Photocatalytic hydrogen generation results from water splitting with methanol as sacrificial agent is shown: Visible light induced photocatalytic Hydrogen generation from water source attracts research interest towards future energy crisis issue. Reports on quantum dots assisted viable powder photocatalysis are scarce till date. Here we demonstrate the use of InGaN@ZnO in powder semiconductor photocatalysis. Aforementioned salient properties of the materials such as enhanced visible light absorption, synergetic operation of the components for catalytic activity, photostabiliity and high crystallinity accompanied with perfect ordering of the particles satisfy the demanding requirements for a photocatalyst. Therefore the materials are evaluated for the photocatalytic hydrogen generation under visible light irradiation in different categories: with sacrificial agent, pH adjusted without sacrificial agent and effect of electrolytes. It is to be emphasized here that the results shown in is without using any cocatalyst and underscores the importance of the present invention. On comparing with similar solid solution, oxynitride cases[21, 23, 47] showing negligible hydrogen yield, without using noble metal cocatalyst, the material achieved promising activity towards water splitting.

a. Effect of sacrificial agent using methanol

The use of sacrificial agent is advantageous for suppressing recombination of electron/hole carriers and effective charge carrier utilization. The sacrificial agents involve in the scavenging either electron or hole based on their redox potential. To improve hydrogen evolution and oxygen evolution rate, methanol and silver nitrate are used as sacrificial agents respectively. Methanol is the lowest alcohol which scavenges the

holes and further was oxidized into CO_2 and H_2O. The bar graph presentation in Figure 4.16 gives the hydrogen evolution rate for the selected compositions of InGaN(QD)@ZnO.

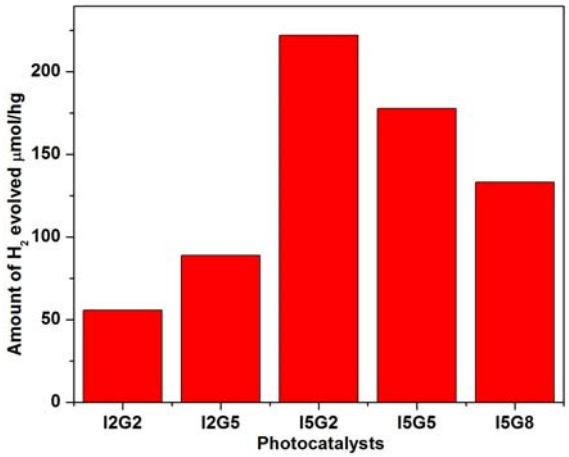

Figure 4.16 The hydrogen evolution with different compositions of In and Ga under visible light irradiation, with sacrificial agent

b. Effect of pH adjustment

The pH of the reactant solution is adjusted to 4.5 by adding mineral acid; sulphuric acid. The other mineral acids such as nitric acid, hydrochloric acid are having the chances in competing with the hydrogen reduction reactions. The increment in pH will shift the CB potential towards more negative and thus the free energy for water reduction increases. The hydrogen evolution increases and there is no need of sacrificial agents. The results are given in Table 3 for the selected compositions of InGaN(QD)@ZnO.

Table 3. Visible light ($\lambda \geq 420$ nm) photocatalysis results for conversion of 2-butanol to 2-butanone, and H_2 yield with different InGaN@ZnO compositions

InGaN@ZnO	H_2 µmol/h g
I2G2	17
I2G5	35
I5G2	48
I5G5	66
I5G8	56
I3G2	23

c. Effect of incident wavelength

The photocatalyst is expected to be efficient enough to generate the charge carriers with the absorption of visible light photon. Therefore the incident wavelength is changed by using different cut-off filters in the path of irradiation. The best working catalyst among the above the catalyst was analyzed and corresponding results are tabulated in Table 4.

Table 4. Effect of incident wavelength: The rate of hydrogen evolution is given in μmol/h g.

InGaN@ZnO	370 nm	400 nm	455 nm	515 nm	550 nm
I2G5	38	34	19	7	2

4.4 Conclusion

The first attempt on synthesis of single phase InGaN QDs integrated with ZnO by solid state synthesis through solution combustion method was successful. On associating the findings in XRD, RAMAN, XPS, SIMS and HRTEM, the presence of InGaN quantum dots embedded in ZnO forming homogeneous solid solution is confirmed. Plausible mechanism for the formation of the new solid solution is elucidated by the following explanation. During the combustion of the homogenous reactant mixture at 500^0C, plenty of in-situ ammonia is produced from urea decomposition. In-situ generated ammonia interacts with available gaseous state In and Ga atoms in the environment. Feasible nitrogen incorporation from ammonia source in such type nascent ZnO clusters at the expense of oxygen vacancies is already well reported. The difficulty in forming InGaN has been overcome by the formation of Zn-N bonds in near neighbour sites and distribution in ZnO whose lattice parameters are comparable with that of both InN and GaN. This is likely to compensate lattice distortion for stabilizing and connecting InGaN directly to ZnO units through Zn-N bonds. As evident from elemental mapping and bulk SIMS analysis the quantum dots are distributed throughout the surface and in the bulk. Hence flux of visible light

photons can be concentrated by the quantum dots on the surface and the photons can make several passes into the bulk also by the distribution of InGaN quantum dots. Structural and electronic integration in InGaN@ZnO leads to synergistic operation that is exploited for visible light driven photocatalysis without any cocatalyst.

4.5 References

1.M. King Hubbert, *Science,* 1949, **109**, 103.

2. M. S. Dresselhaus, I. L. Thomas, *Nature,* 2001,**414**, 332.

3. P. V. Kamat, *J. Phys. Chem. C* 2007,**111***,* 2834.

4. M. Bowker, *Green Chem.,* 2011, **13**, 2235.

5. A. Kubacha, M. F. Garia andG. Colon, *Chem. Rev*. 2012,**112,** 1555.

6. U.Maitra, S. R. Lingampalli andC. N. R. Rao, *Curr. Sci.,* 2014, **106***,* 518.

7. A. Kudo andY. Miseki, *Chem. Soc. Rev.*2009,**38**, 253.

8. DOE's website: energy.gov/science-innovation/energy-sources.

9. V. I. Klimov, A. A. Mikhailovsky, S. Xu, A. Malko, J. A. Hollingsworth, C. A. Leatherdale, H. J. Eisler andM. G. Bawendi, *Science,* 2000, **290**, 314.

10.(a) K. Sivaranjani, S. Raja Ambal, T. Das, K. Roy, S. Bhattacharyya, C.S. Gopinath, *ChemCatChem,* 2014, **6**, 522. (b) C. Ratanatawanate, Y. Tao,andK. J. Balkus.*J. Phys. Chem. C* 2009, **113**, 10755.

11. J. M. Caruge, J. E. Halpert, V. Wood, V. BulovicandM. G. Bawendi, *Nature Photon.* 2008, **2**, 247.

12. E. M. Barea, M. Shalom, S. Gimenez, I. Hod, I. Mora-Sero, A. Zaban and J. Bisquer, *J. Am. Chem. Soc.,* 2010, **132,** 6834.

13. M. C. Beard, J. M. Luther, O. E. Semonin andA. J. Nozik, *Acc. Chem. Res.*2013, **46**, 1252.

14. S. Nakamura, *Science,* 1998, **281**, 956.

15. O. Ambacher, *J. Phys. D: Appl. Phys.*1998, **31**, 2653.

16. F. A. Ponce and D. P. Bour, *Nature* 1997, **386**, 351.

17. C. W. Hsu, A. Ganguly, C. H. Liang, Y. T. Hung, C. T. Wu, G. M. Hsu, Y. F. Chen, C. C. Chen, K. H. Chen andL. C. Chen, *Adv. Funct. Mater.* 2008, **18**, 938.

18. P. Chen, A. Chen, S. J. Chua,J. N. Tan, *Adv. Mater.,* 2007, **19**, 1707.

19. C. W. Hsu, A. Lundskog, K. F. Karlsson, U. Forsberg, E. Janzen andP. O. Holtz, *Nano Lett.* 2011, **11**, 2415.

20. T. Kuykendall, P. Ulrich, S. Aloni andP. Yang, *Nature Mater.,* 2007*,* **6**, 951.

21.Y. H. Ko, J. H. Kim, L. H. Jin, S. M. Ko, B. J. Kwon, J. Kim, J. Kim andY. H. Cho, *Adv. Mater.,* 2011, **23**, 5364.

22. G. B. Stringfellow, *J. Cryst. Growth.,* 2010, **312**, 735.

23. M. G. Kibria, H. P. T. Nguyen, K. Cui, S. Zhao, D. Liu, H. Guo, M. L. Trudeau, S.Paradis, A. R. Hakima and Z. Mi, *ACS Nano,* 2013, 7, 7886.

24. B. N. Pantha, A. Sedhain, J. Li, J. Y. Lin andH. X. Jiang, *Appl. Phys. Lett*. 2009, **95**, 261904.

25. H. M. Chen, C. K. Chen, Y. C. Chang, C. W. Tsai, R. S. Liu, S. F. Hu, W. S. Chang andK. H. Chen, *Angew. Chem. Int. Ed.,* 2010, **49,** 5966.

26. (a) K. Maeda, T. Takata, M. Hara, N. Saito, Y. Inoue, H. Kobayashi and K. Domen, *J. Am. Chem. Soc.*2005, **127**, 8286. (b) K. Maeda, H.

Hashiguchi, H. Masuda, R. Abe and K. Domen, *J. Phys. Chem. C* 2008, **112**, 3447.

27. (a) M. Mapa andC. S. Gopinath, *Chem. Mater.*2009, **21**, 351. (b) M. Mapa, S. Raja Ambal and C. S. Gopinath, *Trans. Mater. Res. Soc. Jpn*. 2013, **38**, 145.
28. (a) K. Maeda and K. Domen. K. *J. Phys. Chem. C*2007, **111**, 7851. (b) K. Maeda and K. Domen. *Chem. Mater*., 2010, **22**, 612.
29. M. Mapa, K. S.Thushara, B. Saha, P. Chakraborty, C. M. Janet, R. P. Viswanath, C. M. Nair, K. V. G. K. Murty andC. S. Gopinath,*Chem. Mater.* 2009, **21**, 2973.
30. (a) M. Mapa, K. Sivaranjani, D. S. Bhange, B. Saha, P. Chakraborty, A. K. Viswanath and C. S. Gopinath, *Chem. Mater*. 2010, **22**, 565. (b) B. Murugan, A. V. Ramaswamy, D. Srinivas, C. S. Gopinath and V. Ramaswamy, *Chem. Mater*., 2005, **17**, 3983.
31. (a) J. Tang, K. W. Kemp, S. Hoogland, K. S. Jeong, H. Liu, L. Levina, M. Furukawa, X. Wang, R. Debnath, D. Cha, K. W. Chou, A. Fischer, A. Amassian, J. B. Asbury andE.H. Sargent, *Nature Mater.,* 2011, **10**, 765. (b) T. Trindade, P. O'Brien andN. L. Pickett, *Chem. Mater.,* 2001, **13**, 3843.
32. (a) B. Naik, K. M. Parida, C. S. Gopinath, *J. Phys. Chem. C* 2010, **114**, 19473. (b) K. Sivaranjani, S. Agarkar, S. B. Ogale and C. S. Gopinath, *J. Phys. Chem. C* 2012, **116**, 2581. (c) K. Sivaranjani and C. S. Gopinath, *J. Mater. Chem.* 2011, **21**, 2639. (d) M. Satish, R. P. Viswanath and C. S. Gopinath, *J. Nanosci. Nanotech.,* 2009, **9**, 423. (e) M. Satish, B. Viswanathan, R. P. Viswanath and C. S. Gopinath, *Chem. Mater.* 2005,

17, 6349. (f) C. S. Gopinath, *J. Phys. Chem. B* 2006, **110**, 7079. (g) D. G. Kulkarni, A. Vadivel Murugan, A. Kasi Viswanath and C. S. Gopinath, *J. Nanosci. Nanotech*., 2009, **9**, 371.

33. (a) K. Roy, C. P. Vinod and C. S. Gopinath, *J. Phys. Chem. C*2013, **117**, 4717. (b) K. Roy and C. S. Gopinath, *Anal. Chem.* 2014, **86**, 3683. (c) XPS reference website: http://srdata.nist.gov/xps/.
34. V. M. Naik, R. Naik, D. B. Haddad, J. S. Thakur, G. W. Auner, H. Lu andW. Schaff, *Appl. Phys. Lett.,* 2005, **86**, 201913.
35. E. V. Konenkova, Yu. V. Zhilyaev, V. A. Fedirko andD. R. T. Zahn, *Appl. Phys. Lett.* 2003, **83**, 629.
36. S. R. Hernandez, C. D. Pastor, L. Artús, K. P. O'Donnell, R. W. Martin, I. M. Watson, Y. Nanishi andE. Calleja, *J. Appl. Phys.*2005, **98**, 013511.
37. A. Kaschner, U. Haboeck, M. Strassburg, M. Strassburg, G. Kaczmarczyk, A. Hoffmann, C. Thomsen, A. Zeuner, H. R. Alves, D. M. Hofman andB. K. Meyer, *Appl. Phys. Lett.,* 2002, **80**, 1909.
38. P. V. Kamat, *J. Phys. Chem. C* 2008, **112**, 18737.
39. C. H. Park, S. B. Zhang and S. H. Wei, *Phys. Rev. B* 2002,**66**, 073202.
40. W. J. Chun, A. Ishikawa, H. Fujisawa, T. Takata, J. N. Kondo, M. Hara, M. Kawai, Y. Matsumoto and K. Domen, *J. Phys. Chem. B* 2003, **107**, 1798.
41. V. A. Fonoberov, K. A. Alim, A. A. Balandin, F. Xiu andJ. Liu, *Phys. Rev. B* 2006,**73**, 165317.
42. P. Chen, S. J. Chua and J. N. Tan, *Appl. Phys. Lett.,* 2006, **89,** 023114.
43. K. Vanheusden, W. L. Warren, C. H. Seager, D. R. Tallant, J. A. Voigt andB. E. Gnade, *J. Appl. Phys.,*1996, **79**, 7983.

44. Z. Chen N. Zhang andY. J. Xu, *CrystEngComm.,* 2013*,* **15***,* 3022**.**

45. K. Maeda, M. Higashi, D. Lu, R. Abe and K. Domen, *J. Am. Chem. Soc.*2005, **127**, 8286.

46. L. Mandal, M. Deo, A.Yengantiwar, A. Banpurkar, J. Jog andS. B. Ogale, *Adv. Mater.,* 2012, ***24***, 3686.

47. K. Maeda, K. Teramura, D. Lu, N. Saito, Y. Inoue andK. Domen, *Angew. Chem., Int. Ed.,* 2006, **45**, 7806.

Solar Light Active Quantum Dot Integrated ZnO Based Composites

5.1 Introduction

ZnO is well known wide band gap semiconductor with high exciton energy of 3.37 eV even at room temperature.[1] This native property of ZnO affords the advantage of fast conduction of charge carrier which is one of the key aspects in the context of solar harvesting.[2] The structure of ZnO consists of polar planes that enable the formation of diverse nanostructures such as nanorods,[3] hexagonal crystals,[4] triangular structures[5] and nanoflowers.[6] These nanostructures are highly acclaimed for charge transport and surface adsorption activities. On the other hand, the wide band gap nature limits the absorption of ZnO only under UV light. The sunlight that reaches the earth spans the entire visible light regime in major proportion. Therefore, materials that absorb entire visible light regime is highly expected to act as a better photocatalyst.[7]

To harvest visible light absorption in wide band gap metal oxides, doping of size compatible anions or cations is generally practiced.[8] Mapa et al prepared N-doped ZnO with triangular shape morphology through solution combustion method.[9] N-doped ZnO material exhibited visible light absorption around 480 nm but the activity is limited to UV light absorption. The method of band gap engineering[10] which had been discussed in previous sections, had successfully imparted visible light absorption in ZnO based materials. However the materials are associated with difficulties due to lattice defect densities.[11] To alleviate the aforementioned problems, composites of nanostructures of ZnO combined with quantum dots (QD) as visible light harvesters[12-14] have been designed for solar harvesting applications.

QDs are highly acclaimed for high absorption cross section, multiple exciton generation, fast charge transfer kinetics and photostability.[15] Deposition of quantum dots on the surface of ZnO, ZnO nanowires increase the true efficiency for water splitting to several fold of activity than bare ZnO nanowires.[16] InGaN quantum dots are known for its wide range of visible light regime and supreme defect tolerance nature.[17] Composites that

are designed with both visible light harvesting component (InGaN) and charge carrier conducting component (ZnO) can be a potential candidate to meet the aspects of solar light harvesting. In chapter 4, we have described InGaN(QD)@ZnO component for solar light harvesting applications.[18] Considering the absorption features of InGaN QDs, we had selected InGaN(QD)@ZnO as one of the component in the composite structure. Generally, QDs are connected with wide band gap semiconductor through covalently bonded bilinkers.[19] In such cases, there are chances of losing charge carriers when they are transported through non-conductive linkers. When the QDs are deposited on the surface, the difficulties may arise in hopping of charge carriers from one component to another component and also stability issues arise upon annealing conditions.[7] Therefore, the aspect of structural and electronic integration of component A: ZnO and component B: InGaN(QD)@ZnO is being highly essential for easy conversion of light energy into charge carriers.[18] The features of similar crystal structure and common ZnO moiety in the chemical structure between the components are the main advantages of this design to achieve dispersion of InGaN QD throughout the ZnO matrix.

In this work, we prepared ZnO using biocompatible template assisted method and the integrated composite of InGaN(QD)@ZnO/ZnO is prepared through simple incipient wet impregnation method. The materials are characterized using XRD, UV-Visible absorption studies, SEM to understand structural, microstructural and photophysical features. The new composites of InGaN(QD)@ZnO/ZnO are evaluated for solar harvesting applications.

5.2. Results and Discussion

5.2.1 XRD Analysis

To understand the structure of the composites, XRD analysis was perfomed. The composites comprise two major chemical entities. Both are referred as component A that is ZnO and component B that is InGaN(QD)@ZnO in the discussion. In the figures, the codes are given as ZnO-Gly for component A and IxGy for the component B. The variable x and y representing the composition of In and Ga respectively. The

composites are denoted as ZnO/IxGy followed by the percentage of loading wherever necessary. Details on the method of preparation are explained in chapter 2, experimental section 2.2. The composite that is prepared with 50% loading of component B on A that is A and B in 1:1 equivalent weight % are used for XRD and surface area analysis. XRD pattern of the new composites, along with bulk ZnO and individual components for the comparison purpose are given in Figure 5.1.

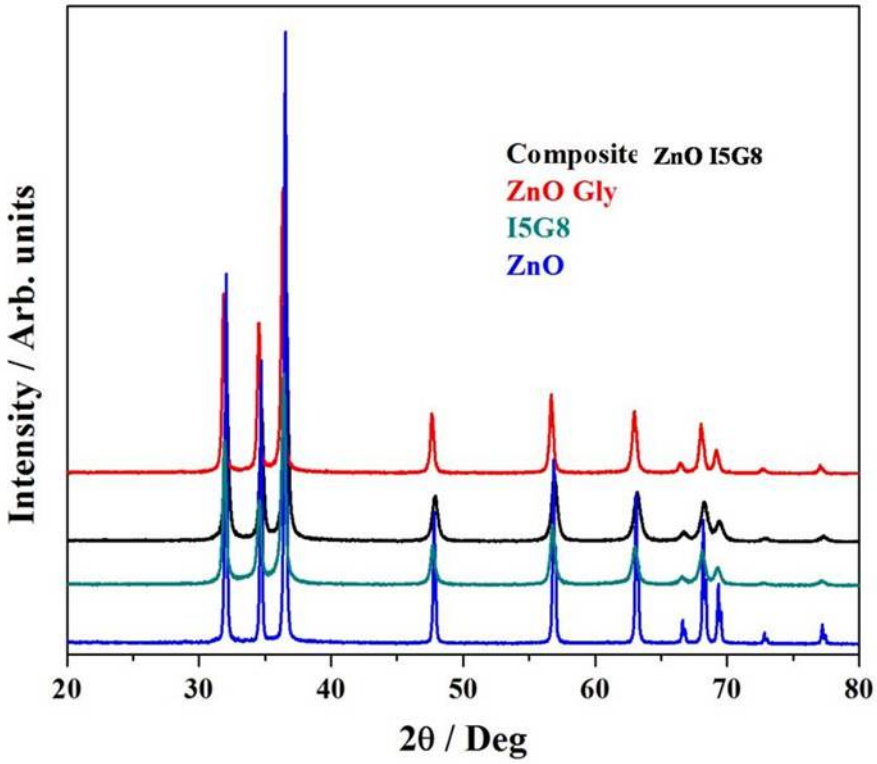

Figure 5.1 XRD patterns of glycerol assisted ZnO, Composite of ZnO/I5G8, I5G8 and bulk ZnO as reference. Inset shows the enlarged version of critical diffraction features.

There is retention of wurtzite structure in the component A as well as in the composites without any other new peak corresponding for possible impure phases such as zinc carbonate and oxides of In and Ga. Attainment of single phase structure underscores the structural integration of the composite and also emphasizes on the efficacy of the preparation method. The growth of nascent zinc oxo clusters of the component A is nucleated in the presence of component B: InGaN(QD)@ZnO. Therefore, the structural integration in the

composite becomes possible. As the thermal stability of InGaN(QD)@ZnO is extremely high,[18] there is no oxidation of In and Ga during calcinations condition at 300 ^{0}C. This is further supported by XRD and no impurity phases are observed. However, the peak of the composite shows broadening indicative of the presence of nanoclusters in the composite.

5.2.2 Surface Area Analysis:

The surface area of the material is one of the governing factors for adsorption of the reactants. Generally, ZnO compounds are crystalline in nature and surface area for reference material is 40 m^2/g.[20] When the surface area of the material is increased, the active sites can be increased and thus making surface of the material would be more available for adsorption of the reactants such as alcohol and water.[21] The component A that is glycerol assisted ZnO shows two fold higher surface area than bulk ZnO material and four-fold higher surface area than IxGy series. Due to the high surface area of the component A, composite also shows similar range of surface area. Corresponding values of surface area of the composite, individual components, bulk ZnO as reference are tabulated in Table 1.

Table 1. BET Surface Area of Composites

Material Code	Surface area m^2 / g
I5G8	22
ZnO bulk	40
ZnO Gly	85
ZnO/I5G8	90

The higher value of surface area than bulk ZnO indicating the better chances of adsorption of reactants: water or methanol in sacrificial water splitting reactions.

5.2.3 Light Absorption Study:

The design of the composite is mainly targeted for solar harvesting application and so absorption features of the composites are analyzed using UV-Visible absorption studies at room temperature. Two different composites with two different loadings of component B; 10% and 50% with respect component A are prepared and corresponding UV-Visible absorption of the composites along with reference ZnO are given in Figure 5.2. ZnO bulk has shown the absorption edge onset around 370 nm in the UV regime. In similar fashion, component A: ZnO (blue trace in Fig. 5.2) assisted has shown the absorption edge onset around 420 nm with marginal visible light absorption.[22] The composite ZnO/IxGy shows very good extent of visible light absorption onset around 680 nm; in fact uniform reddish color associated with the above composite (see inset in Fig. 5.2) suggesting the integration of components A and B into one composite

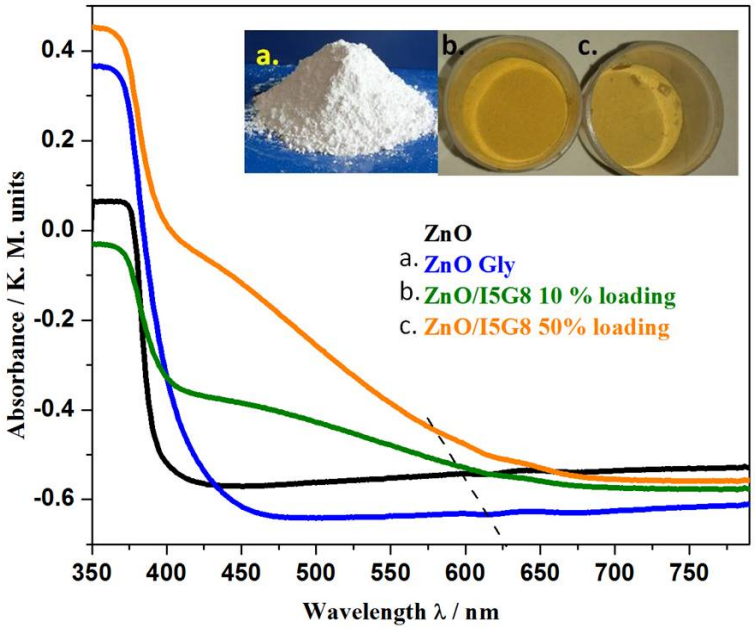

Figure 5.2 UV-Visible absorption of the composite with 10 %, 50 % loading of component B, component A: ZnO and bulk ZnO as reference. Inset shows the photograph of ZnO-Gly and ZnO/I5G8 composite with different loadings of I5G8.

The visible light absorption of the composite extended into visible light regime that is attributed to light harvesting property of InGaN QDs of component B. QDs can serve as light harvesting antennas.[23]

The amount of loading also determines the intensity of the absorbance flux. When the amount of loading of component B increases from 10 % to 50 %, the absorbance value of the composite also increases linearly. This is because of the fact of more availability of InGaN QDs throughout the composite and thus, we had fixed the 50% of loading of component B for all the composites in the harvesting applications.

Figure 5.3 shows the absorption spectra of the composites containing different compositions of IxGy series. As composition of In and Ga content changes, the absorption of the composite also varies accordingly.

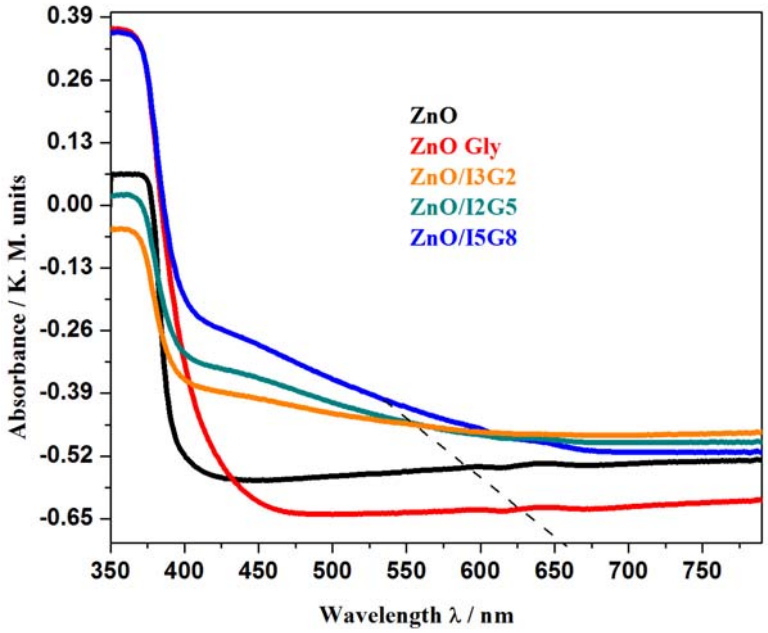

Figure 5.3 UV-Visible absorption of composite as the function of x and y variables of IxGy series along with bulk ZnO for the comparison purpose.

When the content increases, the absorption of the composite also increases with the similar trend of the absorption of IxGy series. The absorption of the composite is being tuneable with the function of composition of IxGy which could be an advantage to develop rainbow type of solar cells.[17] The fashion of continuous visible light absorption without the

appearance of any abrupt peaks for individual components is observed. This fact is attributed to the structural integration of both the components with similar structure. The component B may be dispersed throughout the composite structure that enhances the flux of absorption of visible light photons through scattering process. In the next section, morphology of the composite is explored to deduce the underlying microstructural integration factors for extensive visible light absorption of the composite of ZnO/IxGy.

5.2.4 Morphology Studies:

In first place, the morphology of the component A: ZnO which is prepared using glycerol assisted method, is analyzed and the corresponding SEM image is given in Figure 5.4. The particles of ZnO show triangular shape with rounded corner and the size falls in the 50-100 nm size regimes. Nanoparticles of ZnO are in contact with each other at the edges exhibiting good connectivity rather than agglomerated. This type of connectivity will assist in charge transport from particle to particle.[24] The morphology of the component B: IxGy is hexagonal nanocrystal and it is extensively explored in chapter 4, section 4.2. To avoid repetition, those images are not given in this section.

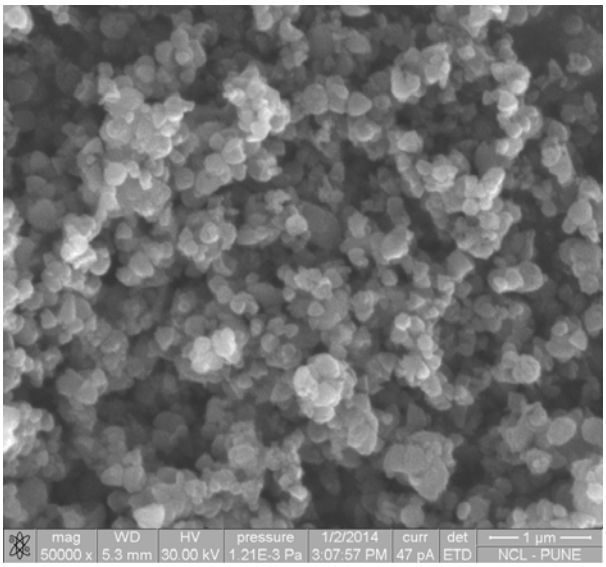

Figure 5.4 SEM image of component A: ZnO Gly powders after calcination treatment.

The composite containing 50 % loading of the component B with the composition I5G8 which shows the maximum visible light absorption, is selected for studying morphological features. There are two different modes of preparation of the composite as follows; a. integrating method and b. the impregnating method so as to understand the aspect of integration.

a. Integrating method: During the growth of Zinc oxo nanoclusters, component B is also present and corresponding result is given in Figure 5.5. A full detail of synthesis is available in chapter 2 (sec. 2.1.6).

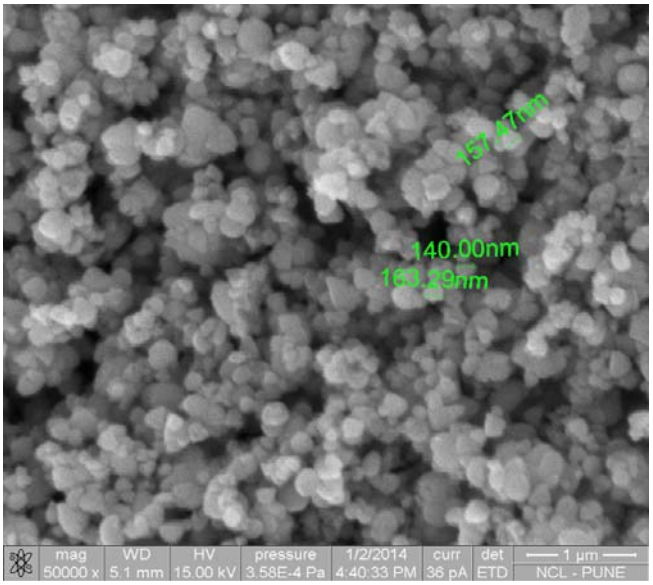

Figure 5.5 SEM image of the composite ZnO/I5G8 prepared through integration method.

The morphology of the component A is neither changed nor distorted form the triangular shape due to the loading of component B. The average size of the particle of the component A is alone increased to a higher value from 100 to 140 nm with the retention of the shape of the particle. This observation indicates the tight binding of both the components forming an integrated structure that favours easy conversion of light energy into charge carriers[18] and further transport throughout the structure. Since the addition of the component B is done at the time of nucleation of component A, the growing oxo clusters will adsorb to component B at the molecular level. The surface area of the component A which is four fold higher than bulk ZnO, also provided good chances for tight binding in forming the composite B.

The role of preparation method provide platform for integration and the same is verified changing the mode of addition of component B with component A.

b. Impregnation method: Both the components are separately prepared and physically mixed under stirring treatment in ethanol for 1 hour at 80 ^{o}C temperature. The powder material is filtered, dried and analyzed for understanding the morphology. A full detail of synthesis is available in chapter 2 (sec. 2.1.5). SEM image of intermingled composite is shown in Figure 5.6.The separate formation and physical mixing through impregnation the components in aqueous solution of isopropanol cannot provide chances for structural integration. There are two different morphological structures that could be visibly identified from the SEM image.

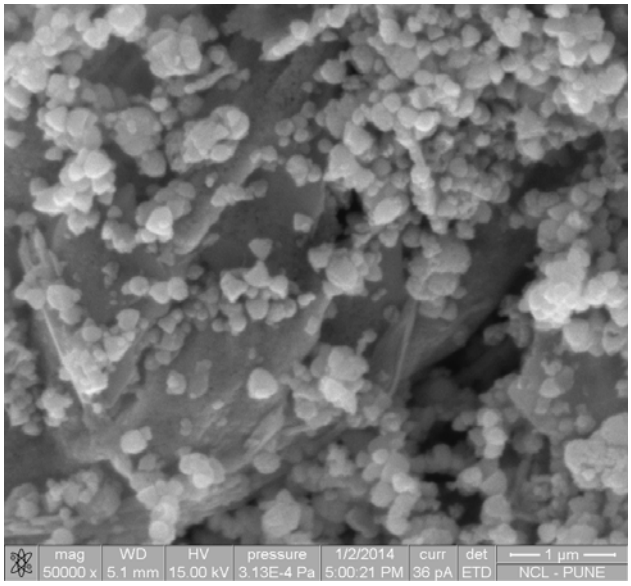

Figure 5.6. SEM image of the blended composite ZnO/I5G8.

The triangular shape particles of the component A are observed on the bulk crystals of the composite B suggesting the poor integration of the blended composite.

5.2.5 Light Harvesting Applications:

a. Photocurrent Generation:

Linear sweep voltammograms (LSV) of the composite ZnO/I5G8, component A: ZnO Gly, bulk ZnO as ZnO under visible light irradiation with the incident wavelength $\lambda \geq 420$ nm. LSV was measured at the scan rate of 10 mV/s between 0.5 and -0.5 eV at neutral pH and the results are given in Figure 5.7.

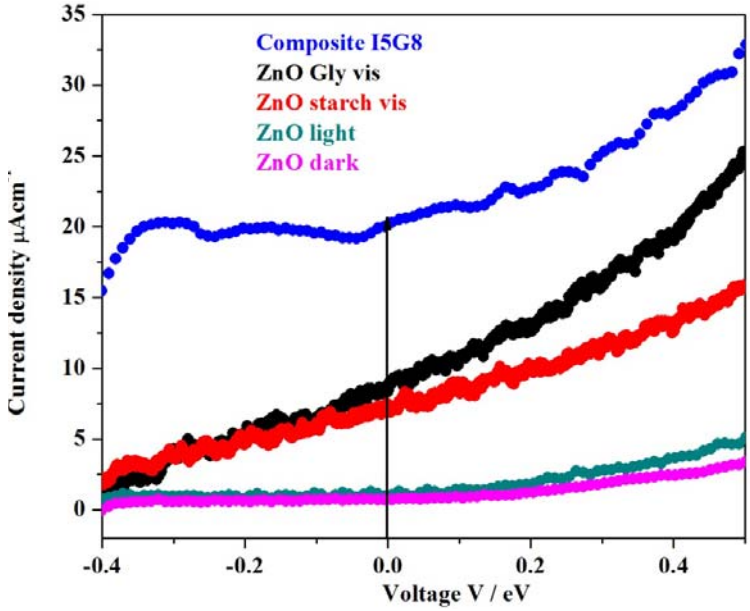

Figure 5.7 Linear sweep voltammogram of the composite, component A : ZnO Gly, ZnO starch assisted, ZnO bulk under visible irradiation at the scan rate of 10mV/s

LSV of ZnO under dark condition is also recorded for comparison purposes. The solid arrow denotes the current generation in the materials at the potential of 0 eV under light irradiation. When the current generation between light irradiation conditions and dark conditions are compared at 0 eV, there is rise in current only under light irradiation indicative of the photofunctionality of the materials. ZnO that is prepared using glycerol as template has shown higher current than reference bulk ZnO. The effect of glycerol as template is probed by comparing with the current generation of ZnO that is prepared using starch as denoted as ZnO starch. According to literature reports, templating assistance using starch leads to the formation of

agglomerated bigger size particles without any connectivity. ZnO Gly shows higher visible light generation than ZnO starch as well as bulk ZnO that is ascribed to the fact of connectivity of particles and with triangular shape supporting charge carrier transport; however, such features are absent in bulk ZnO. As expected, composite ZnO/I5G8 composition shows higher current generation than component A: ZnO under visible light irradiation due to the fact of higher degree of light harvesting by the InGaN QDs. The integrated structure of the composite brings both the components A and B in close vicinity in such a way that light harvesting component and charge transporting component are tightly bound, rather integrated, for easy conversion of light energy into charge carriers.

b. Photocatalytic Hydrogen Generation:

The composites are evaluated for photocatalytic hydrogen generation under visible light illumination $\lambda \geq 420$ nm for 3h using aqueous 20 % methanol solution with 20 mg of suspended catalyst. Corresponding results are given in Table 1. Component A was also evaluated under UV irradiation, and blended composite under visible light irradiation. There is no activity for component A under $\lambda \geq 420$ but it shows activity only under UV irradiation since it constituted only with ZnO components.

The composites exhibits higher activity than simple component A. Better H_2 generation activity is attributed to the fact of improved catalytic activity sites for hydrogen evolution with the presence of maximum content of ZnO. The rate of visible light hydrogen evolution increases with the increasing content of In and Ga in the composites. Since light harvesting is being the crucial factor, the higher the content of nitrides of In and Ga the light absorption of the composites and in turn the hydrogen evolution also increases. The impregnated composite having equivalent weight % of A and B shows negligible activity due to poor particle to particle interconnectivity leading to hindered flow of charge carriers. Apart from the above, a comparison of the results given in the above table (Table 2) and results in Table 3 (Chapter 4) provides some interesting facts. Although ZnO/IxGy shows marginally lower hydrogen yield in the above table 2, than that in

chapter 4 (table 3), it is to be noted that the percent content of IxGy is much smaller in the present chapter. Higher activity is attributed to the better dispersion of IxGy and its integration with high surface area ZnO.

Table 2: Photocatalytic Hydrogen generation under visible light using composites, ZnO Glycerol assisted, and blended composite.

Samples	H_2 μmol, 3h
ZnO Gly	1.91 [a]
ZnO Gly	nil
Impregnated composite	nil
ZnO I3G2	18.3
ZnO I2G5	38.48
ZnO I5G8	46.3

[a] under UV irradiation

5.3 InGaN(QD)@ZnO/NiO Composite

The loading of cocatalyst on the surface of the main catalyst provide additional active sites for hydrogen evolution.[25-27] Generally, the cocatalyst acts as sink for charge carriers that are photogenerated in the main catalyst. The presence of cocatalyst accelerates the diffusion of charge carriers from the bulk to the surface active sites and employs the same for redox reactions. The junction of main catalyst and cocatalyst forms the triple phase boundary at the reaction site wherein the solid phase of the catalyst, liquid phase of the reactants and gas phase of the product are being the three phases. The metals especially noble metals are dominating cocatalysts, however, the metal oxide based cocatalysts serve as cost effective solution. The metal oxide based cocatalysts provide advantages of separate active sites for hydrogen and oxygen evolution that reduces the rate of recombination of charge carriers. It is reported that loading of p-type based catalysts on n-type based catalysts forming p-n heterojunctions improves separation of charge carriers and

suppresses the rate of recombination.[28] We have illustrated role of cocatalyst in the photocatalytic hydrogen generation in Figure 5.8.

Nickel oxide is well known p-type material that is suitable for loading on ZnO based n-type material for availing the advantage of charge carrier separation. NiO is also widely used in DSSC for the purpose of creating p-type layer in forming p-n junctions.[29] The band structure of NiO shows a matching alignment with that of ZnO in such way that electron transfer from CB of InGaN@ZnO to CB of NiO is facile and helps for hydrogen generation at NiO cocatalyst sites.

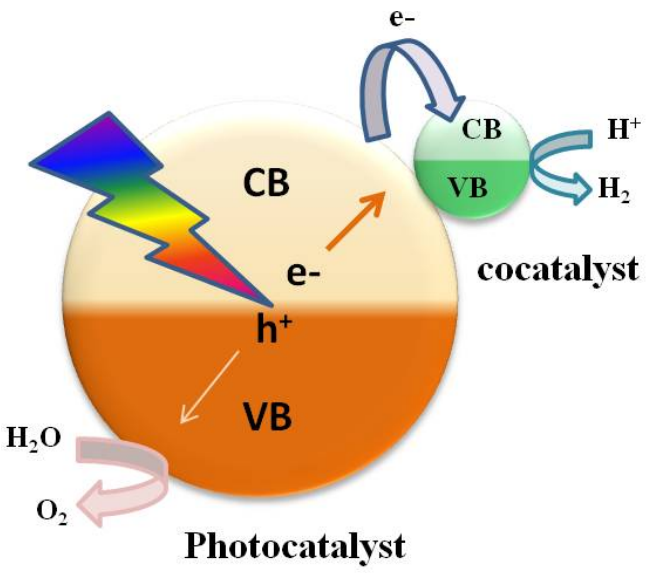

Figure 5.2.8 Role of coatalyst for photocatalytic hydrogen generation.

5.3.1 HRTEM Study

In this thesis work, we have reported composite of NiO and InGaN(QD)@ZnO which is prepared through incipient wet impregnation method. The preparation method is described in chapter 2, experimental section, 2.2 and the material code was given as IxGy/NiO z% where the x, y and z represents the contents In, Ga and wt% of NiO. Using HRTEM study, the materials are characterized for understanding the features of composite. Figure 5.9a shows the loading of 5 nm size nanoparticle on the surface of InGaN@ZnO and the formation of Ni/NiO bilayer is also identified in Figure

5.9b. The bilayer formation acts as protective coat for metal oxide core enhancing the stability. In addition, the interface at the bilayer acts as reaction site for hydrogen evolution. The presence of NiO is further confirmed from characteristic SAED pattern in Figure 5.9c. The ring pattern which is observed in Figure 5.9c is referred to the main catalyst: InGaN(QD)@ZnO which is unavoidable in the composite structure. There is good physical contact between NiO and InGaN(QD)@ZnO that allows the extraction of charge carriers from the bulk to the surface. The mixed oxide of $Rh_yCr_{2-y}O_3$ is highly acclaimed cocatalyst for the solid solution GaN:ZnO by Hisatomi et al.[30] The latter cocatalyst has attained core-shell morphology that enhances the rate of hydrogen evolution of the solid solution to several fold under visible light. This report motivates the present work of NiO bilayer loaded InGaN(QD)@ZnO.

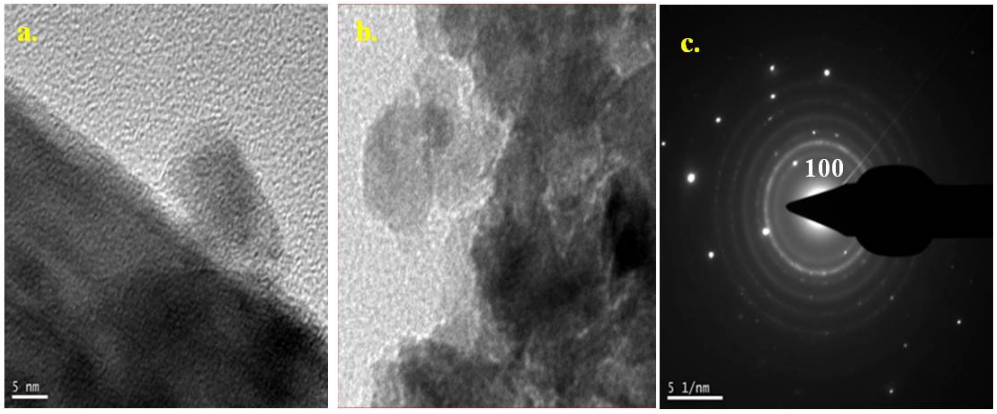

Figure 5.9 HRTEM Study of the composite I5G8/ NiO 2wt%

5.3.2 Photocatalytic Activity Study:

The composites of I xGy/NiO containing various weight percentage of NiO are evaluated for photocatalytic hydrogen evolution. The composition of I5G8 which shows maximum photocurrent generation is selected among the various compositions of InGaN(QD)@ZnO. The photocatalytic reaction is carried out under visible light $\lambda \geq 420$ nm using aqueous solution of 20% methanol. The composites are not stable under the condition of pH adjustment to 4.5 because of the fact of leaching of Ni ions from NiO

structure. Therefore, the use of methanol as sacrificial agent becomes necessary to evolve hydrogen from water using the above composite as photocatalyst and the corresponding results are tabulated in Table 2.

The rate of hydrogen evolution increases when the loading weight percentage of NiO increases from 1% to 2% that is attributed to increment of active sites by the cocatalyst loading. When the weight percentage of NiO loading increases further more from 2% to 4%, the activity decreases due to the accumulation of cocatalyst nanoparticle that arrest the light penetration through InGaN(QD)@ZnO.

Table 2. Visible light driven photocatalytic hydrogen evolution studies

Material	H_2 evolution μmol/hg
I5G8	12
I5G8/NiO 1%	25
I5G8/NiO 2%	34
I5G8/NiO 4%	10

5.4 Conclusion

The composites of InGaN(QD)@ZnO/ZnO with varying contents of In and Ga are prepared through simple impregnation method and evaluated for visible light photocatalytic applications. The component of ZnO in the composite structure InGaN(QD)@ZnO/ZnO is prepared using biocompatible template assisted approach. The composites exhibit good extent of visible light absorption and with the function of increasing In and Ga contents, the absorption of the composite also increases linearly. The connectivity and the triangular shape of the particles facilitate the transport of charge carriers throughout the composite. The integrated structure of the composite

facilitates enhanced activity compared to individual components and the impregnated composite.

The composites of InGaN(QD)@ZnO/NiO with various loading weight percentage of NiO are prepared through simple incipient wet impregnation method. HRTEM study identifies 5 nm size nanoparticle of NiO with Ni/NiO bilayer formation that enhances stability and active sites at the interface of bilayer. It is observed that there is good extent of physical contact of nanoparticles on the surface of InGaN(QD)@ZnO for easy diffusion of charge carriers from bulk to surface.

5.5 References:

1. C. Klingshirn, *Chem. Phys. Chem.,* 2007, 8, 782.
2. M. Mapa, S. Raja Ambal and C. S. Gopinath, *Trans. Mater. Res. Soc. Jpn*., 2013, **38**, 145.
3. R. Viswanatha, S. Sapra, B. Satpati, P. V. Satyam, B. N. Dev and D. D.Sarma, *J. Mater. Chem.,* 2004, **14**, 661.
4. P. X. Gao and Z. L. Wang, *Appl. Phys. Lett.,* 2004, **84**, 2883.
5. W. I. Park, D. H. Kim, S.-W. Jung and G.-C. Yi, *Appl. Phys. Lett.,* 2002, **80,** 4232.
6. B. P. Zhang, N. T. Binh, K. Wakatsuki, Y. Segawa, Y. Yamada, N. Usami, M. Kawasaki and H. Koinuma, *Appl. Phys. Lett.,* 2004, **84,** 4098.
7. A. Kubacha, M. F. Garia, and Colon, G, *Chem. Rev*., 2012, **112**, 1555.
8. Anpo, M and Takeuchi, M. *J. Catal*., 2003, **216**, 505.
9. M. Mapa and C. S. Gopinath, *Chem. Mater.,* 2009, **21**, 351.
10. M. Mapa, K. S.Thushara, B. Saha, P. Chakraborty, C. M. Janet, R. P. Viswanath, C. M. Nair, K. V. G. K. Murty andC. S. Gopinath, *Chem. Mater.* 2009, **21**, 2973.

11. K. Maeda and K. Domen, *Chem. Mater*., 2010, **22**, 612.

12. A. Kongkanand, K. Tvrdy, K. Takechi, M. Kuno, P. V. Kamat, *J. Am. Chem. Soc.*, 2008, **130**, 4007.

13. Y.L. Le e, C. Fachi, S. Lian, *Chem. Mater*., 2010, **22**, 922.

14. J. Hensel, G. Wang, Y. Li, S. Z. Zhang, *Nano Lett.*, 2010, **10**, 478.

15. A. J. Nozik, *Chem. Phys. Lett.*, 2008, **457**, 3.

16. H. M. Chen, C. K. Chen, Y.-C. Chang, C.-W. Tsai, R.-S. Liu, S.-F. Hu, W.-S. Chang and K.-H. Chen, *Angew. Chem. Int. Ed.,* 2010, **49**, 5966.

17. T. Kuykendall, P. Ulrich, S. Aloni, and P. Yang, *Nature Mater.,* 2007, **6**, 951.

18. S. Rajaambal, M. Mapa and C. S. Gopinath, Dalton Trans., 2014, **43**,12546.

19. T. Trindade, P. O'Brian, N. L. Pickett, *Chem. Mater.,* 2001, **13**, 3843.

20. Ü. Ozgur, Y. I. Alivov, C. Liu, A. Teke, M. A. Reshchikov, S. Dogan, V. Avrutin, S. J. Cho and H. J. Morkoc, *J. Appl. Phys.* 2005, **98**, 041301.

21. N. Serpone, E. Borgarello and M. Graetzel, *J. Chem. Soc. Chem. Commun*., 1984, **45,** 342.

22. T. Minami, H. Sato, H. Nanto and S. Takata, *Jpn. J. Appl. Phys. Part 2,* 1985*,* **24,** L781.

23. Kamat, P. V. *J. Phys. Chem. C* 2008, **112**, 18737.

24. K. Sivaranjani, S. Agarkar, S. B. Ogale and C. S. Gopinath, *J. Phys. Chem. C* 2012, **116**, 2581.

25. M. A. Khan, M. S. Akhtar, S. I. Woo, and O. B. Yang, *Catal. Commun.,* 2008, **10,** 1.

26. A. K. Agegnehu, C.-J. Pan, J. Rick, J.-Fu Lee, W.-N. Su, B.-J. Hwang *J. Mater. Chem.***,** 2012, **22**, 13849.

27. S. Feihl, et al., Chem.Commun., 2014, **50**, 11339.

28. U. Bach, Y. Tachibana, J.-E. Moser, S. A. Haque, J. R. Durrant, M. Gra□tzel and D. R. Klug *J. Am. Chem.Soc.,*1999,**121**, 7445.

29. C. J. Flynn, E. E. Oh, S. M. McCullough, R. W. Call, C. L. Donley, R. Lopez and J. F. Cahoon, *J. Phys. Chem. C* 2014, **118**, 14177.

30. T. Hisatomi, K. Maedo, K. Takanake, J. Kubota, and K. Domen, *J. Phys. Chem. C*, 2009, **113**, 21458.

Conclusion and Future Outlook

This chapter summarizes the present thesis work and the conclusions and possible future implications that can be extended from the work.

Chapter 1 enumerates the need of solar light harvesting to meet the ever increasing energy demand at global level. Heterogeneous semiconductor photocatalysis seems to be the viable solution for the conversion of solar energy into useful forms of chemical energy as well as electrical energy. Basic processes and mechanism of semiconductor photocatalysis are elaborately discussed. The special traits and suitable physicochemical properties of ZnO for solar light harvesting are listed out. The nature of wide band gap and notorious photocorrosion are prevailing limitations in the advancement of ZnO towards solar light harvesting. Band gap engineering in ZnO through nitrogen doping and codoping of nitrogen affinity elements are employed to achieve oxynitrides and solid solutions that have reduced band gap with visible light absorption. However loading of noble metal catalysts becomes necessary for achieving decent activity. The composites of ZnO constituting with visible light harvesting component such as plasmonic metal noanostructures and semiconductor nanostructures are also described. Development of visible light absorption solid solutions that span entire visible regime of solar spectrum and shows virgin catalytic activity is emphasized as one of the objective of the thesis. Understanding the local structure of solid solution in order to explore the minor but deleterious impurities is targeted. The formation of ZnO based new composites with integrated structure and p-n junctions for improved charge carrier generation are also aimed in the thesis work.

Details on the synthetic procedures, reaction method of photocatalytic activity, photocatalytic reactor design and characterization techniques are presented in **chapter 2.** Simple solution combustion method is employed for the preparation of integrated quantum dots of InGaN in ZnO matrix for the first time and solid solution of ZnO rich GaN is also prepared by the same method. The composites of InGaN@ZnO/ZnO and InGaN@NiO are prepared through incipient wet impregnation method. The component of ZnO in one of the composite is prepared using biocompatible template

assisted approach. To evaluate photocatalytic activity and photon conversion efficiency, photocurrent generation studies, photocatalytic hydrogen evolution, photocatalytic selective organic conversions are carried out. The elaborate description on cut-off filters and calculation method of incident photon conversion efficiency-IPCE is also described. The structural features are characterized using powder XRD and Raman spectroscopy techniques. The embedded quantum dots of InGaN in ZnO matrix are mapped in ZnO matrix through secondary ion mass spectrometry. The chemical state of the incorporated elements is probed by photoelectron spectroscopy technique. The absorption studies are done through using UV-Visible spectroscopy. The origin of visible light absorption with understanding on electronic structure is demonstrated using photoluminescence spectroscopy. The local structure studies are carried out using EXAFS study having the source from synchrotron radiation. The analysis and quantification of the products are done using relevant techniques.

Chapter 3 deals with the understanding on the structure property relationship of photocatalysts and origin of visible light absorption. The solid solutions of ZnO rich GaN with varying contents of Ga are prepared through solution combustion method. The nitrate salts are used as starting materials in order to avoid the oxidation of Ga into gallium oxide when on dissolving Ga metal in nitric acid. The local structure study of the solid solutions clearly identifies typical GaN phase without any minor impurities of gallium oxide and zinc carbonate species. The formation of GaN phase is suitable for formation of continuous bands structure with the overlapping of N_{2P} orbital to O_{2P} orbital resulting VB broadening. The band gap reduction affords visible light absorption and accompanied suppression of defect densities results in visible light virgin photocatalytic activity.

This work emphasizes the role of preparation method and starting materials for the generation of active structure. Compared to mere replacement of atoms, formation of phases with similar crystal structure is more advantages in band gap engineering and also to develop the solid solutions with virgin catalytic activity.

Chapter 4 elaborates physicochemical features and properties of the materials InGaN(QD)@ZnO with varying concentrations of In and Ga contents. The new materials exhibit wurtzite structure as that of ZnO and good extent of visible light absorption onset around 700 nm with band gap reduced to 1.85 eV. There is formation of quantum dots of InGaN that are structurally and electronically integrated with ZnO lattice. The nitride components are effectively incorporated in such a way that the oxygen vacancies are significantly suppressed in the materials that favours extreme photostability as well as thermal stability. The materials show high photocurrent generation under visible light irradiation and also at longer wavelengths. The maximum of 7.25 % of IPCE is obtained under AM1.5 simulated irradiation at 0 eV.

These materials provide scope of developing quantum dot sensitized solar cell-QDSSC replacing costly and poorly stable dyes. The leaching of dye under annealing conditions remains as significant challenge in DSSC. The application of integrated quantum dots can afford light harvesting antennas with enhanced stability for sustainable performance. The simple method of preparation and the design that makes use of common crystal structure will motivate future development of integrated quantum dot structures. The nanojunctions that are observed at the interconnecting regions of ZnO and InGaN can attract research interests towards the developments p-n junctions based diodes and devices. Taking the advantage of integrated structure for easy flow of charge carriers, these materials could serve as solid electrolytes and it is worth exploring this aspect.

InGaN preparation is still considered as a difficult task and at present InGaN is being prepared by sophisticated thin film deposition methods, such as CVD. This is mainly due to lattice stress and complications in optimizing synthesis conditions, due to very different vaporization regimes of In and Ga. Nonetheless, In-rich InGaN has been demonstrated to be a suitable solar harvesting material due to tuneable band gap. Further, it is also integrated with ZnO due to the structural similarity. This is also the first solid state method to synthesize QD embedded in a matrix and integrated too. However,

same method could be extended to prepare InGaN QD in other matrices, including Wurtzite lattice. In our opinion, this type of synthesis could be extended to other classes of applied materials such as InP. By tuning the composition of InGaN, it is also possible to explore the applications in the area of white light emission. We believe, the present work has shown one potential procedure to make this complex material in a rather simple procedure. Nonetheless, the synthesis procedure may suitably modified to produce the materials in a significantly controlled manner would improve its applicability to many other materials too. Research efforts are required in this direction to make it more adaptable for variety of applications.

Chapter 5 comprises the results of composites of InGaN(QD)@ZnO/ZnO and InGaN(QD)@ZnO/NiO through simple incipient wet impregnation method. One of the composite component, ZnO has been prepared through glycerol assisted method that affords particle to particle connectivity and also triangular shape particles for charge carrier transport. The composite has shown good visible light absorption due to the fact of InGaN quantum dots and exhibit higher activity for photocatalytic hydrogen generation than the individual components. NiO is an emerged p-type semiconductor in DSSC applications. HRTEM study on the composite InGaN(QD)@ZnO/NiO identifies 5 nm size NiO nanoparticles are in good physical contact with InGaN(QD)@ZnO. There is fine dispersion of nanoparticles that allow the light penetration and scattering. The bilayer formation of Ni/NiO improves active sites at the interface and also stability of the nanoparticles. The work of InGaN(QD)@ZnO/ZnO implies the essentiality of integrated structure of the composite for facile conversion of light energy and reduction of recombination sites. NiO The design of the composites with integrated structure can be extended to the development of tandem solar cells.

List of Publications, Patents and Awards

1. M. Mapa, **S. RajaAmbal** and C. S. Gopinath, *Trans. Mater. Res. Soc. Jpn*., 2013, **38**, 145.

2. **S. Rajaambal**, M. Mapa, and C. S. Gopinath, *Dalton Trans*., 2014, **43**, 12546.

3. **S. RajaAmbal**, A. K. Yadav, S. N. Jha, D. Bhattacharyya and C. S. Gopinath, *Phys. Chem. Chem. Phys*., 2014, **16**, 23654.

4. K. Sivaranjani, **S. Raja Ambal**, T. Das, K. Roy, S. Bhattacharyya and C. S. Gopinath, *ChemCatChem*, 2014, **6**, 522.

5. **S. Rajaambal**, K. Sivaranjani, and C. S. Gopinath, *J. Chem. Sci*., 2015, **127**, 33.

6. **S. RajaAmbal**, and C. S. Gopinath, Role of quantum dot integrated material in developing ZnO based composites. *Manuscript under preparation.*

Patent Published

1. Photostable composite of indium gallium nitride in zinc oxide useful as light harvester for production of hydrogen from water splitting, comprises indium, gallium, nitrogen and zinc oxide in specific amounts. Patent number: **WO2014195974-A1**, Patent Assigne: CSIR, India. **Inventors**: Gopinath C.S; **Sivaraman Raja Ambal.**

Awards

1) **Oral presentation** on the National Catalysis Symposium held at IIT-Madras in 2010.

2) **Best Poster award** on the Science Day Celebration at CSIR-NCL, 2011.